DTU Wind

Techno-economic comparison of grid reinforcement and battery-buffered electric vehicle fast charging stations

Amay Boudellal

DTU Wind Energy-M-0723
February 2024

Author:
Amay Boudellal

Title:
Techno-economic comparison of grid reinforcement and battery-buffered electric vehicle fast charging stations

DTU Wind Energy-M-0723
February 2024

Project period:
August 2023 - February 2024

ECTS: 35

Education: Master of Science

Supervisors:

Mattia Marinelli
Charalampos Ziras
DTU Wind & Energy Systems

Emil Mahler Larsen
Utiligize

Remarks:
This report is submitted as partial fulfillment of the requirements for graduation in the above education at the Technical University of Denmark.

Technical University of Denmark
Department of Wind Energy
Frederiksborgvej 399
4000 Roskilde
Denmark
www.vindenergi.dtu.dk

Approval

This thesis has been prepared over six months at the Section for E-mobility and Prosumer Integration, Department of Wind and Energy Systems, at the Technical University of Denmark, DTU, in partial fulfilment for the degree Master of Science in Sustainable Energy, Electric Energy Systems.

It is assumed that the reader has a basic knowledge in the areas of electrical engineering, power systems, the electric grid and electric vehicles.

Amay Boudellal - s213396

Amay Boudellal

Signature

February 1st, 2024

Date

Abstract

Connecting fast charging stations to the electric grid usually requires an upgrade to accommodate the higher loading. This upgrade takes place in the form of investments in conventional assets such as building new transformer stations and laying new cables. Battery-based solutions are sometimes chosen by the charge point operator to reduce these connection costs or perform energy arbitrage. These batteries, however, could be operated following different control objectives and support the grid to reduce the investment need in conventional assets. A grid planning algorithm is developed in several steps to compare these two options and assess their technical benefits and drawbacks as well as their economic impact.

The first part of the analysis assesses the impact of the rollout of distributed energy resources on the grid of an urban Danish distribution system operator of 18,552 end customers. The additional load and production capacity due to the development of electric vehicles, heat pumps and PV results in a total ”green-transition” investment need of 79MDKK until 2045, with 92% of these costs caused by issues in the low voltage grid. Undervoltages and overvoltages are partly solved through reactive power control of the PVs' inverters and remain the most critical and cost-heavy issues to solve, representing 66% of the total investment. In the second stage, fast charging stations are connected to the grid. The additional loading is not critical in most cases and results in an investment need of 2MDKK to solve thermal overloads and 18MDKK of connection costs to build new transformer stations and lay new cables. The increased loading is experienced in the medium voltage grid.

Once the fast charging stations' impact and upgrade needs have been assessed, batteries are considered as an alternative to new transformer stations. These batteries are sized by an optimisation algorithm based on a fast charging station load profile. The range of battery capacities spreads out between 461kWh and 1,010kWh due to the different profiles and charging power. Due to their higher capital costs and energy losses than transformers, the battery-based alternative costs between 7% and 1,109% more than a conventional grid extension. Different battery connection topologies are tested to allow batteries to provide active and reactive power support to mitigate grid thermal overloads and voltage issues. This support, reducing the need to invest in conventional assets due to the distributed energy resources rollout, results in a cost reduction of batteries between 3% and 65%. In some edge cases under a low battery price and a high conventional asset price development scenario, the battery-buffered fast charging station has lower yearly costs than the conventional one. However, the conventional grid upgrade solution remains the most cost-efficient in 89% of all investigated cases under different price scenarios and battery topologies. The combination of a transformer and a battery with both smaller ratings than the ones used in the conventional or battery-based upgrade yields the best results, with reduced costs of 61% on average compared to the conventional upgrade.

Acknowledgements

Mattia Marinelli, Head of section & Associate Professor, DTU Wind & Energy Systems, and **Charalampos Ziras**, Assistant Professor, DTU Wind & Energy Systems
for their supervision and support, advice and feedback given during the process on my research methods and writing as well as interesting discussions about the subject of this thesis.

Emil Mahler Larsen, CTO & Co-Founder, Utiligize
for making the framework and data for this thesis available and for his time and support during the process, discussing the methods employed and the results, as well as proofreading.

I would also like to express my gratitude towards all my colleagues at Utiligize, who supported me and provided me with the time and space to focus on this thesis.

Contents

1 Introduction

Electrification is the chosen path to decarbonise our society and mitigate climate change impacts. Transport and heating are historically fossil-fuel-dominated sectors that are in transition towards electricity-based technologies. The electric grid will have to face higher loads and new consumption patterns as well as changes in power flow with the development of generation in the low voltage part of the grid.

Electric vehicles represent an additional challenge due to the different charging modes users can benefit from. Especially fast charging stations, requiring high power with no flexibility as the users expect their car to charge immediately can cause severe issues in distribution grids not dimensioned for these power levels and patterns.

The conventional grid upgrade, i.e. adding additional capacity through new cables and transformers or replacing existing ones with higher ratings, is the preferred method to accommodate higher loads. The use of batteries as peak storage and an asset to participate in regulation markets is starting to develop at a commercial scale. The combination of these batteries with fast charging stations is experimented with by charge point operators, as it can reduce grid connection costs and time as well as energy costs by charging the battery based on spot price signals. These batteries, however, could also be used to support the grid and handle situations with critical thermal loadings or voltage issues. In this operation mode, the batteries could reduce the grid extension need for fast charging stations as well as reduce the investment costs on assets experiencing thermal overloads and voltage issues. The technical impact of the combined operation mode of these batteries needs to be economically assessed in comparison to a conventional grid upgrade.

To assess whether a conventional grid upgrade or a battery-buffered solution is best suited to accommodate fast charging stations, an algorithm to compare these is developed. This algorithm is tested on the grid of the Danish urban distribution system operator NKE-Elnet on which the impact of the rollout of distributed energy resources is assessed in the first stage and the connection of fast charging stations in the second stage. The induced thermal overloads and voltage issues are economically and technically analysed and the upgrade requirements are calculated. Some of these upgrades are then rolled back as batteries are connected.

Different operation modes of these batteries where they support the grid through active and reactive power regulation are investigated. The technical and economical most suited option is determined by running cost-benefit analyses. The grid planning algorithm can then be used by grid planners to identify which solution is best suited in each case, or if a general rule can be applied to their grid.

2 Literature review

With the increasing penetration of electric vehicles, the need for a properly designed charging infrastructure and the resulting strain the latter can have on the grid, there has been research focus on the use of batteries in combination with electric vehicle charging stations. The impact of fast charging stations and batteries on distribution grids has also been extensively researched and key findings are presented in the following sections.

2.1 Battery-buffered fast charging stations

Regarding the design of fast charging stations with a battery buffer, [1] proposes an electrical design where a grid connection of 22kW is used and 173kW is delivered to the charging vehicle using a lithium-iron-phosphate battery. Such a design is built as a demonstration model in a laboratory in [2], where a 16kWh battery is used to support the grid connection to supply a 50kW charging station. The results of the experiment show that the battery, in combination with the control system, has good peak-shaving performance and does not overload the grid connection.

In [3], a reconfigurable battery topology is proposed to allocate strings to different microgrid units. The system is composed of a grid connection of 43kW in combination with a 61kW photovoltaic (PV) installation and three batteries with a capacity of 104kWh each, used to supply two charging points of 175kW each. Here, in addition to the objective of delivering a power output higher than the grid connection, increasing self-sufficiency is another control objective. With an enhanced control strategy, a self-sufficiency of 87.3% is reached during the summer, significantly reducing the exchanges with the grid.

Heavy-duty electric vehicles such as buses and trucks also require charging stations that fit their user's needs. For this, [4] formulates the optimisation problem for the sizing of batteries for an electric bus fast charging station with six spots of 450kW each. The energy storage system reduces the transformer and feeder capacity from 1478kW to 626kW or 641kW based on which battery type is used. Investment costs are reduced by 22.85%, with an additional 1.65% when performing energy arbitrage.

These findings outline the technical viability of combining battery systems with fast charging stations to reduce overload in the grid and investment costs, both in simulations and laboratory experiments.

2.2 Impact of fast charging stations on the distribution grid

The impact of fast-charging stations on the distribution grid in terms of voltage deviation and harmonics is investigated in [5]. To mitigate the negative effects, next to smart charging and switching control strategies for converters, the integration of energy storage is proposed with the additional benefit of reducing losses.

Another method of reducing harmonics and transients is a DC-bus-based (Direct Current) fast charging station developed in [6]. Coupled with an energy management system, the use of local renewable energy sources can be optimised and additional profits can be earned. There is also a positive impact on the loss reduction. The dynamics of a battery-based fast charging station are also investigated in [7] both in grid-connected and islanded mode, where the results show that a battery system with a control architecture is able to decouple the internal dynamics in the station from the grid.

Based on real grid data, the impact of a 50kW fast charger in the city of Cuenca (Ecuador) on a distribution feeder is assessed in [8]. The apparent power load increase is 23.85% on the line directly connected to the charging station and between 0 and 3.27% on the rest of the lines. An additional voltage drop of up to 0.5% is observed. Using Swedish data, the authors in [9] observe a transformer station (2x40MVA) load increase of 9% when connecting 3 fast charging stations with 4 spots of 250kW each, an additional voltage drop of 0.017 p.u. (dropping below 0.95 p.u.) and voltage flicker of up to 2%.

The combined impact of slow and fast charging (up to 100kW) on a Belgian residential grid is investigated in [10]. With a 40% penetration rate of electric vehicles (EVs), the impact of uncoordinated home charging is almost 10 times worse than the fast charging one (up to 2.1MW vs. 260kW).

The reviewed articles show that fast charging stations have negative effects on distribution grids. These are not in the same order of magnitude as the impact of home charging e.g. [10], yet they add stress to the distribution grid.

2.3 Grid service oriented battery systems

In terms of battery energy storage systems for grid services, [11] investigates the different applications of these devices. The authors mention that these systems are used to mitigate the overloading of transformers and to accommodate an increasing number of loads such as EVs. [12] also outlines that these systems can reduce the impact of the green transition on distribution grids. Both publications insist on the need to properly size battery systems to avoid an unnecessary increase in investment and operating costs, accelerated ageing and low efficiency.

Using reference network models, [13] investigates the technical and cost impact on transformer substations when installing batteries of different capacities. Under consideration of demand growth in the grid, the authors found that investment savings in the range of 20-25% in an urban area with a battery storage of 200kWh can be reached. However, at the time this article was published (2015), batteries were not economically viable for this solution yet. In [14], the same lead author uses a similar approach to calculate that based on the battery size, demand growth and grid area (rural, semi-urban and urban), battery prices between 16€/kWh (10kWh, 2% demand growth and rural grid) and 150€/kWh (10kWh, 2.5% demand growth and urban grid) would result in a cheaper option than a classic grid reinforcement with a transformer upgrade. Similarly, in [15] the authors perform a cost-benefit analysis between a conventional upgrade (adding a second parallel transformer in a station) or a battery-based one. Different types of batteries and penetration of EVs are assessed, and the battery-based grid upgrade gives a higher benefit-cost ratio for a high number of EVs and battery cycles (more than 140 cars per day and 25,000 cycles per year) compared to a conventional one.

A software suite to compare conventional and battery-based grid reinforcement is presented in [16]. The findings show that battery systems are a viable solution from a technical point of view. The authors only consider charging power of up to 50kW, and no economic assessment is made.

Based on the reviewed literature, battery systems for grid applications are a technically viable solution as highlighted in section 2.1. They have the ability to reduce conventional reinforcement costs, yet the economic advantage of installing and operating such a system is closely tied to the technology type and usage, which doesn't make it a suitable solution in every case.

2.4 Research gap and objectives

In the reviewed literature, it has been proven that installing stationary batteries in combination with fast-charging stations reduces loading and stress on grid components such as transformers [1, 3, 11, 12]. Moreover, investment savings can be reached [4, 13, 14], with battery prices being the critical factor. The impact of fast charging stations on the electric grid is assessed and the resulting effects are an increase in losses, loading and voltage drops, though not as critical as conventional charging e.g. [6, 8, 9, 10].

The reviewed articles consider only the connected transformer station and not the rest of the grid, particularly at a higher voltage level [8, 10, 13, 14]. Moreover, not all consider the load increase in the grid due to the development of other distributed energy resources [8, 9, 10, 15], and those who do use a general percentual load increase, not considering new peaks [13, 14]. Finally, the ones who consider a load increase base their model on standard IEEE grid models and standard load profiles [13, 14], whereas real-life grid and smart meter data are used here. The size of the battery storage is also critical for optimal operation [11, 12] and will be assessed based on current and future needs, in combination with using the battery to reduce not fast-charger-related grid investments.

The main objectives of this work will be to:

- Analyse the combined impact of EV fast charging stations and other distributed energy resources (DERs) on a distribution grid in future scenarios.
- Develop an optimisation algorithm for battery sizing based on fast charging station load profiles.
- Compare a conventional and a battery-based grid upgrade for fast charging stations.
- Perform a cost-benefit analysis to assess the economic viability of battery-buffered fast charging stations from a distribution grid operator perspective.
- Develop a grid planning algorithm to automatize this techno-economic analysis.

3 Methodology

The methodology presented in this chapter aims to develop a grid planning algorithm which takes inputs from multiple data sources and investigates both the impact of a high DER penetration and fast charging stations. A conventional and a battery-based grid upgrade method are investigated and technically and economically compared.

3.1 Overview

The flowchart in figure 3.1 summarizes the main steps of the methodology of the grid planning algorithm presented in this chapter.

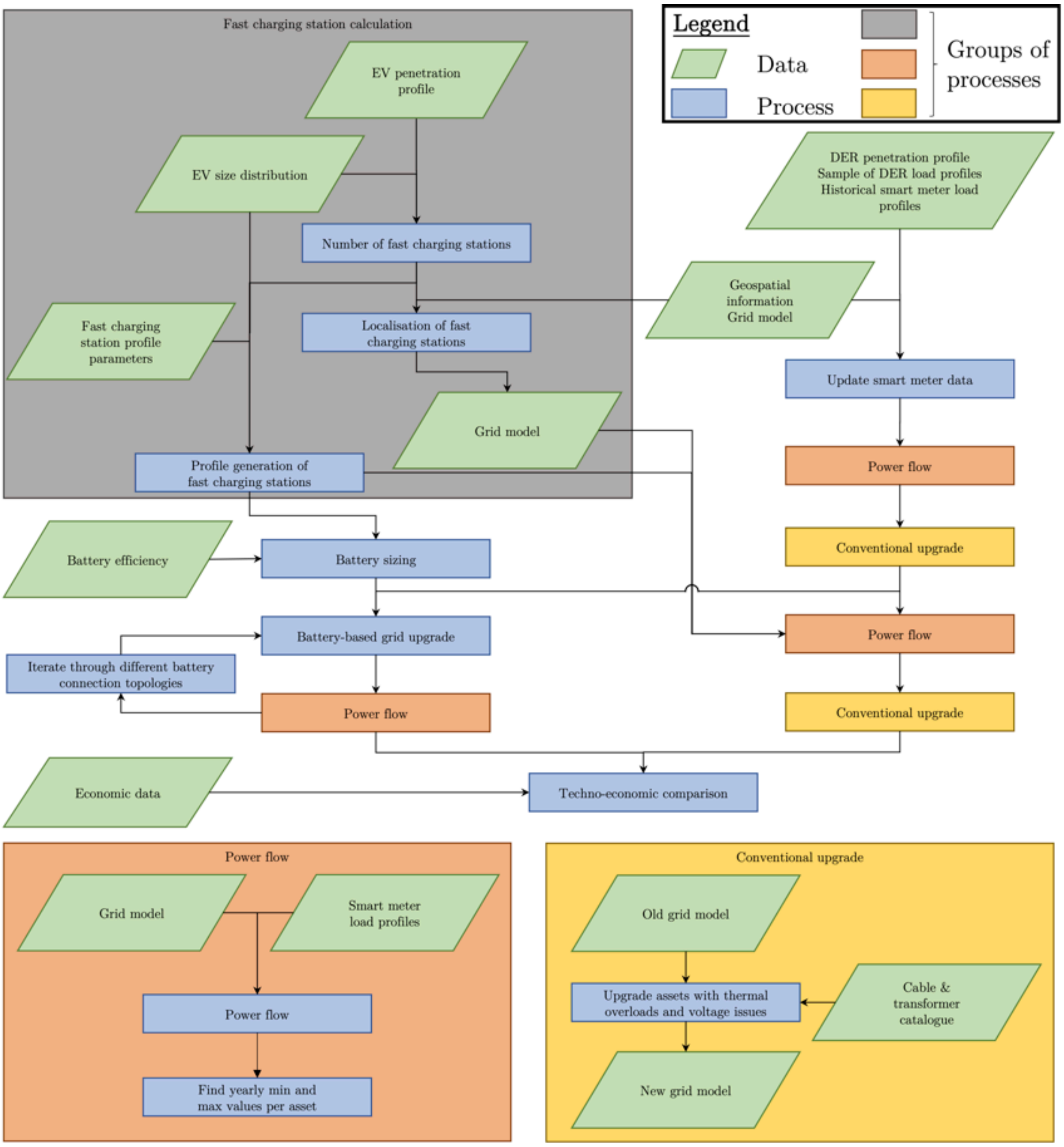

Figure 3.1: Overview of the grid planning algorithm

The input data can be summarized in the following categories: historical grid model and smart meter data, penetration and load profiles of new distributed energy resources (DERs) and fast charging stations, location of these fast charging stations, economic data and electrical parameters of grid assets and batteries. The increasing penetration of DERs (electric vehicles (EV), heat pumps (HP) and photovoltaics (PV)) is modelled based on scenarios and input data presented in sections 3.5.6 and 3.5.7. Every year, a certain number of new loads or production sites are connected to the current grid and the historical meter data is updated with the selected profiles. The power flow is run with the pandapower solver. Pandapower is an open-source, Python-based loadflow simulation tool developed by the Fraunhofer Institute and the University of Kassel in Germany [17]. For the thermal loading and the voltage results, yearly summary values are selected for each asset as described in the following sections. For assets violating certain constraints, an upgrade process is run and the grid model is updated accordingly.

A second power flow simulation and the same summary and upgrade process are run after connecting fast charging stations. The resulting technical and economic impact on the grid is assessed and in parallel batteries are connected to replace the second conventional upgrade. The costs of these solutions are compared, and different battery connection topologies are investigated to reduce the number of measures taken in the first conventional upgrade, therefore extending the batteries' range of action and reducing their cost impact.

3.2 Conventional grid upgrade model

Due to the rollout of DERs, the loading of the grid components is expected to increase and both thermal overloads and voltage violations are expected to appear. The way to handle these issues is to upgrade cables and transformers to assets with higher ratings that can operate within certain thresholds. These thresholds are presented in table 3.6 and the grid upgrade model for the two previously mentioned issues is presented in the following sections.

3.2.1 Thermal overload

To identify assets that get overloaded during power flow simulations and with which asset type they should be replaced, the following method is used. The asset loading in percent is calculated by pandapower using the following formulas, for each timestamp of the simulation:

$$\mathrm{L} = \frac{\mathrm{I}}{\mathrm{I_{max}} \cdot \mathrm{d} \cdot \mathrm{n}} \cdot 100 \tag{3.1}$$

$$\mathrm{L} = \max\left(\frac{\mathrm{I_{hv}} \cdot \mathrm{V_{hv}}}{\mathrm{S}}, \frac{\mathrm{I_{lv}} \cdot \mathrm{V_{lv}}}{\mathrm{S}}\right) \cdot 100 \tag{3.2}$$

with equation 3.1 being the loading formula for cables with L the thermal loading in percent, I the current flowing through the cable at each timestamp and $\mathrm{I_{max}}$ the maximum cable current based on its electrical parameters both in kA, d the derating factor set to one and n the number of parallel cables. Equation 3.2 is the loading formula for transformers with L the thermal loading in percent, $\mathrm{I_{hv}}$ and $\mathrm{I_{lv}}$ the high and low voltage side current flowing through the transformer in kA, $\mathrm{V_{hv}}$ and $\mathrm{V_{lv}}$ the high and low voltage side calculated voltage in kV, and S the rated apparent power of the transformer in MVA [17].

For each asset and for every year, the maximum value (corresponding to the 99.9^{th} percentile, i.e. the largest 0.1% values are discarded to remove outliers, corresponding to nine hour per year) is found across all timesteps. If this value exceeds a certain threshold, the asset needs to be replaced.

The last year before the maximum loading exceeds the threshold is the replacement year. To identify the dimension of the future asset, the loading of the last simulation year (i.e. 2045) is taken and the new required capacity is calculated as the following:

$$\mathrm{C_{new}} = \frac{\mathrm{C_{old}} \cdot \mathrm{n_{old}} \cdot \mathrm{L_{2045}}}{\mathrm{n_{new}}} \tag{3.3}$$

with $\mathrm{C_{new}}$ and $\mathrm{C_{old}}$ the new and current capacity as the rated current for cables in kA and rated power for transformers in kVA, $\mathrm{L_{2045}}$ the asset loading in 2045 in percent, $\mathrm{n_{old}}$ and $\mathrm{n_{new}}$ the number of old and new parallel assets. The smallest asset from tables E.1 and E.2 that validates this minimum new rated current/power is the future type. The number of parallel assets starts at one and is increased if no asset has enough capacity until the new capacity can distribute the required amount of current/power.

The electrical parameters of cables and transformers can be found in tables E.1 and E.2. They are provided by Utiligize and are based on equipment manufacturer catalogues.

3.2.2 Voltage violations

The voltage violations are identified at the customer connection, i.e. at the cabinet level. After each yearly power flow and the thermal overload-related upgrades (since this reduces the number and severity of voltage-related issues), the maximum and minimum voltages (corresponding to the 99.9$^{\text{th}}$ percentile of the maximum and minimum voltages) for each cabinet across all timesteps of each year are analysed, and the cabinets laying outside of the limits specified in table 3.6 are selected for an upgrade. For each of the cabinets with a voltage violation, a graph algorithm finds the path to the closest secondary substation and all the cables it goes through are registered.

First, the tap changer use of primary and secondary transformers is investigated. An algorithm that minimises the number of cabinets experiencing voltage issues by finding the optimal combination of tap changers through a unique change (i.e. changing the tap position the year before a voltage issue is identified and not changing it afterwards, due to the lack of on-load dynamic tap changers in this case) of primary and secondary substations is used. This method can solve issues for undervoltages or overvoltages, but not both. Due to the large spread between minimum and maximum voltage over the course of a day (mostly due to the high PV penetration), an on-load tap changer system controlled remotely or automatically and based on sensors would be necessary to switch the position of the tap changers, from a positive position in the morning when the load is high to a negative position at midday when the load is low and the PV installations are injecting in the grid, back to a positive position in the evening the load is high again. The transformers are not equipped with such a system, so the tap changer position is not changed and a cable upgrade is used instead.

Upgrading to a cable with a larger dimension reduces the internal resistance and therefore the voltage drop. The required upgrade is estimated by distributing the maximum allowed voltage drop at each cable on the cabinet path to the secondary substation as:

$$\Delta \mathrm{V_{max}} = \begin{cases} \dfrac{\mathrm{V_{TR,\ LV}} - \mathrm{V_{min}}}{\mathrm{n}} & \text{if } \mathrm{V_c} < \mathrm{V_{min}}, \quad (3.4) \\[2ex] \dfrac{\mathrm{V_{max}} - \mathrm{V_{TR,\ LV}}}{\mathrm{n}} & \text{if } \mathrm{V_c} > \mathrm{V_{max}} \quad (3.5) \end{cases}$$

with $V_{TR,\ LV}$ the voltage at the low voltage bus of the secondary substation, V_{min} and V_{max} the voltage boundaries defined in table 3.6, V_c the voltage at the cabinet laying outside of the limits and n the number of cables between the cabinet and the primary substation. From there, the new resistance for each of these cables is calculated as:

$$R_{new} = \frac{\Delta V_{old} \cdot \frac{R_{old}}{n_{old}}}{\Delta V_{max}} \cdot n_{new} \tag{3.6}$$

with ΔV_{old}, R_{old} and V_{old} the original voltage drop, resistance and number of parallel cables, ΔV_{max} the previously calculated maximum voltage drop allowed and n_{new} the new number of parallel cables. The closest cable from table E.1 with a smaller resistance is then looked for to match this new parameter, and if none exists the new number of parallel cables, starting at one, is increased until a cable is found.

The cable upgrade is, similar to the tap changer method, not able to solve all overvoltages by itself either. The chosen solution which doesn't involve installing new assets such as reactive power compensation banks is the ability to set the power factor of the inverter for all newly installed PV installations to 0.95 leading (in generator convention). Therefore, the inverters consume reactive power proportionally to the injection of active power, which helps to reduce the voltage. This method, in combination with cable upgrades, can remove all voltage issues experienced in the grid.

3.2.3 Fast charging stations extension

When installing new assets for future fast charging stations, the same approach as the one currently used by urban Danish DSOs is used. A 10kV cable with a 150mm^2 dimension is connected to the HV-side of the closest existing 10/0.4kV transformer station, under the assumption that there is space for this connection. A new transformer station of 800kVA is installed next to the fast charging station. The cable length is calculated as a straight line using a geographical analysis in QGIS and the resulting distance will be multiplied by two to account for the need to avoid buildings and follow roads, existing cables and other infrastructure. The cable between the new transformer station's LV side and the fast charging station port is ignored. A fast charger efficiency of 95% is used [18].

3.3 Battery-based grid upgrade model

A parallel path in the algorithm to the conventional grid upgrade based on assets with larger capacities is to add battery storage systems to the grid. The approach in this algorithm is to size these battery systems based on the fast charging station demand and to use the remaining capacity to resolve grid loading and voltage issues. Therefore, the first upgrade operation (regarding thermal overloads and voltage issues caused by DERs) is always performed as a conventional upgrade. Batteries intervene when connecting fast charging stations to remove the upgrade requirements caused by these new loads. In a second iteration, the use of batteries to remove some of the issues caused by DERs is investigated.

3.3.1 Optimisation problem

The goal of the battery-based grid upgrade model is to size a battery with the smallest possible charging power (to reduce the grid loading) and capacity (to reduce costs and space requirements). For this, an optimisation problem with as main input a generated yearly fast charging station profile described in section 3.5.7 is formulated. The profiles used are generated based on the EV penetration expected in 2045, which is the most critical scenario year. Because each profile is stochastic and involves a part of uncertainty, a large enough number of these profiles needs to be generated and used as inputs of the optimisation algorithm, in this case, one profile per future fast charging station. The resulting largest battery can then be considered satisfying in most cases.

The different technical parameters of a lithium-ion battery used here are shown in table 3.1. The same fast charger efficiency of 95% as in the case without batteries is used [18].

Battery one-way efficiency [%]	**Depth of discharge [%]**	**Power electronics one-way efficiency [%]**	**Initial SOC [%]**
90	80	95	50

Table 3.1: Battery and power electronics parameters [19]

The charging power is limited to 800kVA as it is the transformer's rating used to supply the existing fast charging station and will be used for future ones. Therefore, the goal is to reduce this number. The battery's capacity upper bound is set to 5,000kWh due to the size of the distribution grid.

The battery's operational principle is that it supplies power to the fast charger when the demand is higher than its maximal charging power from the grid. Otherwise, the power is directly supplied from the grid to the fast charger to avoid losses and unnecessary battery usage. E.g., if the battery has a maximum charging power from the grid of 100kW and the fast charger demand is 50kW, then this power is directly supplied from the grid and the battery can charge up to 50kW. If the fast charger demand is 150kW, then 100kW will be supplied from the grid and 50kW from the battery.

The resulting optimisation problem is the following, given:

- T: Total number of timesteps (a 15-minute resolution, so 35,040 timesteps per year. This resolution is also the reason why the charging and discharging power are divided by four to get energy values),
- $P_{\text{charged, max}}$: Maximum power charged (supplied to the battery) across all timesteps in kW,
- P_{max}: Maximum charging power of 800kW,
- Q: Battery capacity in kWh,
- Q_{max}: Maximum capacity of 5,000kWh,
- w_P: Weight on the charging power between 0.1 and 0.9,
- w_Q: Weight on the capacity, complementary to the one on the charging power, between 0.1 and 0.9,
- $P_{\text{charged, }t}$: Power charged (supplied to the battery) at timestep t in kW,
- $P_{\text{discharged, }t}$: Power discharged (supplied to the fast charger) at timestep t in kW,
- SOC_t: Battery state of charge at timestep t in kW,
- η_b: Battery one-way efficiency in percent,
- η_{pe}: Power electronics one-way efficiency in percent,
- η_{fc}: Fast charger efficiency in percent,

- DOD: Maximum depth of discharge in percent.

Additionally, three variables help to constrain the charging power:

- b_t: binary variable to indicate whether the fast charger demand is higher or lower than the maximum charging power at timestep t,
- M: big-M variable to enforce conditional constraints,
- ϵ: tolerance to simulate a strict inequality constraint.

$$\min_{\mathrm{P_{charged,\ max}},\ \mathrm{Q}} \frac{\mathrm{P_{charged,\ max}}}{\mathrm{P_{max}}} \cdot \mathrm{w_P} + \frac{\mathrm{Q}}{\mathrm{Q_{max}}} \cdot \mathrm{w_Q} \tag{3.7}$$

subject to

$$0 \leq \mathrm{P_{charged,}}_{\ t} \leq \mathrm{P_{max}} \qquad \forall\, t = \{1, ..., \mathrm{T}\} \tag{3.8}$$

$$0 \leq \mathrm{Q} \leq \mathrm{Q_{max}} \tag{3.9}$$

$$\epsilon = 0.0001 \tag{3.10}$$

$$\mathrm{M} = \mathrm{Q_{max}} + \epsilon \tag{3.11}$$

$$\mathrm{Q} \cdot (1 - \mathrm{DOD}) \leq \mathrm{SOC}_t \leq \mathrm{Q} \qquad \forall\, t = \{1, ..., \mathrm{T}\} \tag{3.12}$$

$$\mathrm{P_{charged,\ max}} \geq \frac{\mathrm{P_{discharged,}}_{\ t}}{\eta_{\mathrm{fc}}} + \epsilon - \mathrm{M} \cdot (1 - \mathrm{b}_t) \qquad \forall\, t = \{1, ..., \mathrm{T}\} \tag{3.13}$$

$$\mathrm{P_{charged,\ max}} \leq \frac{\mathrm{P_{discharged,}}_{\ t}}{\eta_{\mathrm{fc}}} + \mathrm{M} \cdot \mathrm{b}_t \qquad \forall\, t = \{1, ..., \mathrm{T}\} \tag{3.14}$$

$$\mathrm{b}_t = 1 \implies$$

$$\mathrm{P_{charged,}}_{\ t} \leq \mathrm{P_{max}} - \frac{\mathrm{P_{discharged,}}_{\ t}}{\eta_{\mathrm{fc}}} \qquad \forall\, t = \{1, ..., \mathrm{T}\} \tag{3.15}$$

$$\mathrm{SOC}_t = 0.5 \cdot \mathrm{Q} + \frac{\mathrm{P_{charged,}}_{\ t} \cdot \eta_{\mathrm{b}} \cdot \eta_{\mathrm{pe}}}{4} \qquad \forall\, t = \{1\} \tag{3.16}$$

$$\mathrm{SOC}_t = \mathrm{SOC}_{t-1} + \frac{\mathrm{P_{charged,}}_{\ t} \cdot \eta_{\mathrm{b}} \cdot \eta_{\mathrm{pe}}}{4} \qquad \forall\, t = \{2, ..., \mathrm{T}\} \tag{3.17}$$

$$\mathrm{b}_t = 0 \implies$$

$$\mathrm{P_{charged,}}_{\ t} = 0 \qquad \forall\, t = \{1, ..., \mathrm{T}\} \tag{3.18}$$

$$\mathrm{SOC}_t = 0.5 \cdot \mathrm{Q} - \frac{\mathrm{P_{discharged,}}_{\ t} - \mathrm{P_{max}}}{4 \cdot \eta_{\mathrm{b}} \cdot \eta_{\mathrm{pe}} \cdot \eta_{\mathrm{fc}}} \qquad \forall\, t = \{1\} \tag{3.19}$$

$$\mathrm{SOC}_t = \mathrm{SOC}_{t-1} \cdot \mathrm{Q} - \frac{\mathrm{P_{discharged,}}_{\ t} - \mathrm{P_{max}}}{4 \cdot \eta_{\mathrm{b}} \cdot \eta_{\mathrm{pe}} \cdot \eta_{\mathrm{fc}}} \qquad \forall\, t = \{2, ..., \mathrm{T}\} \tag{3.20}$$

The objective function in equation 3.7 minimizes both the maximum charging power and the capacity. Both terms are divided by their maximum value so that each parameter ends up being a value without a unit between zero and one, allowing to sum them without scaling issues, as the capacity tends to be a larger number than the charging power. Weight parameters are also implemented in the objective functions to be able to change the importance of each variable. The charging power at each timestep and the capacity are constrained between zero and their upper bound values in equations 3.8 and 3.9. In equations 3.10 and 3.11, the auxiliary variables are constrained to be just large enough to trigger the state change of the binary variable b_t. Equation 3.12 sets the constraint for the SOC to always lay between the battery capacity and the capacity at the lowest discharged point as specified by the depth of discharge parameter.

The next two equations 3.13 and 3.14 are used as conditional statements to determine the state of b_t. In 3.13, if the maximum charging power is greater or equal to the power discharged, i.e. delivered to the fast charger, divided by its efficiency, then b_t is set to 1. It means that the fast charger is not using all the grid connection power and that the battery can charge with the remaining power. In 3.14, if the maximum charging power is less or equal to the power discharged, then b_t is set to 0. In that case, the demand at the fast charger is higher than the power the grid connection can directly provide and the battery needs to supply the missing power.

In the first case, the charging power of the battery is set to be less or equal to the difference between the maximum power and power consumed by the fast charger in 3.15. Equations 3.16 and 3.17 update the SOC, with the first equation being used in the first timestep where the SOC is initialised to 50% of the capacity and the second being used in all other timesteps where the previous SOC is taken. Because it is a situation where the battery is being charged, the SOC is increased with the charged power multiplied by the battery and power electronics efficiency, representing the actual power stored in the battery, divided by four due to the 15-minute resolution.

In the second case, the charged power is set to zero in equation 3.18 as more than the grid connection power is required. Similarly to the previous case, the SOC is updated with either the initial or the previous value in equations 3.19 and 3.20. The SOC decreases by the difference between the power required by the fast charger and the power supplied by the grid divided by the battery, power electronics and fast charger efficiencies as well as four because of the time resolution.

3.3.2 Battery topology

Three different topology types are investigated to compare the additional thermal loading and voltage issues minimisation the batteries can provide and their economic impacts.

Conventional-like topology

The first topology to be investigated is the one based on the way fast charging stations are conventionally connected to the grid as described in section 3.2.3. In this configuration, the closest transformer station to each new fast charging station is identified through a nearest neighbour analysis in the QGIS software. The pandapower net object is then updated and a 10kV cable is installed from the high voltage (HV) bus of the closest transformer station to the bus to which both the battery and the fast charging stations are connected. This configuration implies the use of 10kV power electronics.

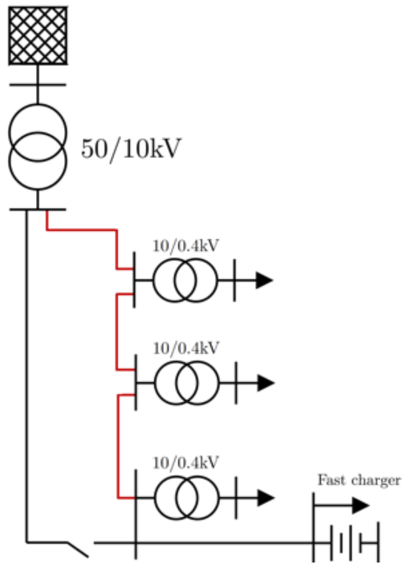

Figure 3.2: Battery connection under the conventional-like topology configuration

In this configuration, additionally to supplying energy to the fast charging station, the battery can contribute to reducing the loading in the upstream medium voltage (MV) cables, marked in red in figure 3.2. For this purpose, every MV cable connected between the primary substation and the battery is identified in a graph algorithm and their thermal loading is tracked during the simulation to identify overloads.

Transformer LV-side topology

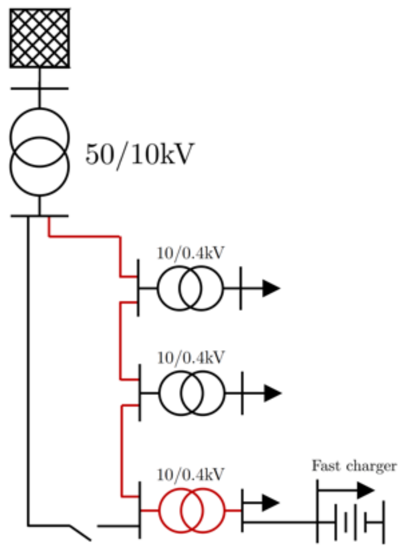

Figure 3.3: Battery connection under the transformer LV-side topology configuration

This topology is identical to the previous one, with the exception that instead of connecting the battery and fast charging station to the HV bus of the closest transformer station, the low voltage (LV) bus is chosen. This allows the use of LV power electronics and the battery can not only target thermal overloads in the upstream MV cables but also the ones happening at the secondary station, marked in red in figure 3.3. Since voltage issues are mostly present in the LV grid, the battery controller will be extended with a reactive power droop controller to mitigate voltage issues at the connected cabinets.

LV topology

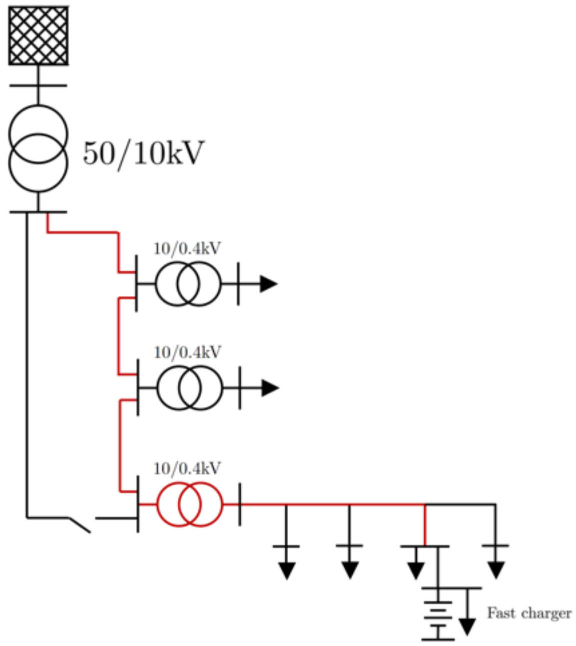

Figure 3.4: Battery connection under the LV topology configuration

The last topology configuration is different in the sense that it targets a larger grid area. Instead of connecting the battery to the closest transformer station, it is connected to the closest cabinet. Additionally to the support the battery can provide in terms of thermal overload mitigation to the upstream MV cables and secondary substation, all the LV cables between the substation and the battery get supported, as marked in red in figure 3.4. A reactive power controller will also be used to reduce voltage issues at the connected cabinets.

3.3.3 Pandapower implementation

To implement the different battery control strategies based on the grid state, a controller with three different objectives is implemented. The controller first runs a power flow with all battery setpoints (active and reactive power) set to zero. The state of the grid is then analysed and if issues are identified, the active and reactive power controllers take action. A maximum number of 10 iterations per timestep is set. Because the controller is not always able to converge (i.e. not solve all loading and voltage issues), the simulation needs to be carried on to the next timestep independently of the results. In this case, the setpoints of the last iteration are taken.

For both active and reactive power controllers, it is important to note that due to the iteration principles, the changed power outputs are summed to the previous iteration. I.e. if the battery's output is not enough to solve an issue in the first iteration, in the second one the updated grid value is the controller input and the power output is summed to the one of the previous iteration.

Active power controller

For each battery, all the assets on which it can have an influence are monitored during the simulation based on the previously presented topologies. If one of these assets violates the thermal loading constraints defined in table 3.6, the battery active power output will be recalculated based on the following formula:

$$P_{b,\ new} = P_{b,\ old} - \left(P_{a,\ max} - \frac{L_{limit} \cdot P_{a,\ max}}{L_{max}} \cdot \frac{n}{\eta_b \cdot \eta_{pe} \cdot \eta_g} \right) \tag{3.21}$$

with:

- $P_{b,\ new}$: Updated battery setpoint in kW,
- $P_{b,\ old}$: Previous battery setpoint in kW,
- $P_{a,\ max}$: Active power flowing through the asset with the highest loading in kW,
- L_{limit}: Thermal loading limit of the asset in percent,
- L_{max}: Thermal loading of the most loaded asset in percent,
- n: Number of batteries connected to that asset,
- η_b: Battery efficiency in percent,
- η_{pe}: Power electronics efficiency in percent,
- η_g: Grid efficiency, assumed at 90% to take into account losses of the different assets.

The power flowing through the asset can either be positive (i.e. from the primary substation to the cabinets) or negative (the other way around). As in the pandapower convention, positive power at a battery means charging and negative discharging, in the first case the updated battery setpoint will be positive and smaller or negative and larger than the original setpoint. In the second case (a PV injection larger than the consumption), the updated battery setpoint will be positive and larger or negative and smaller than the original one.

Reactive power controller

To control the battery's reactive power output, the voltage is calculated at each cabinet connected below the battery. These voltage values are used as the input for a droop controller that will inject reactive power into the grid in the case of an overvoltage and consume some in the case of an undervoltage. The droop curve characteristics are shown in figure 3.5, with a deadband between a voltage of 0.99 and 1.01.

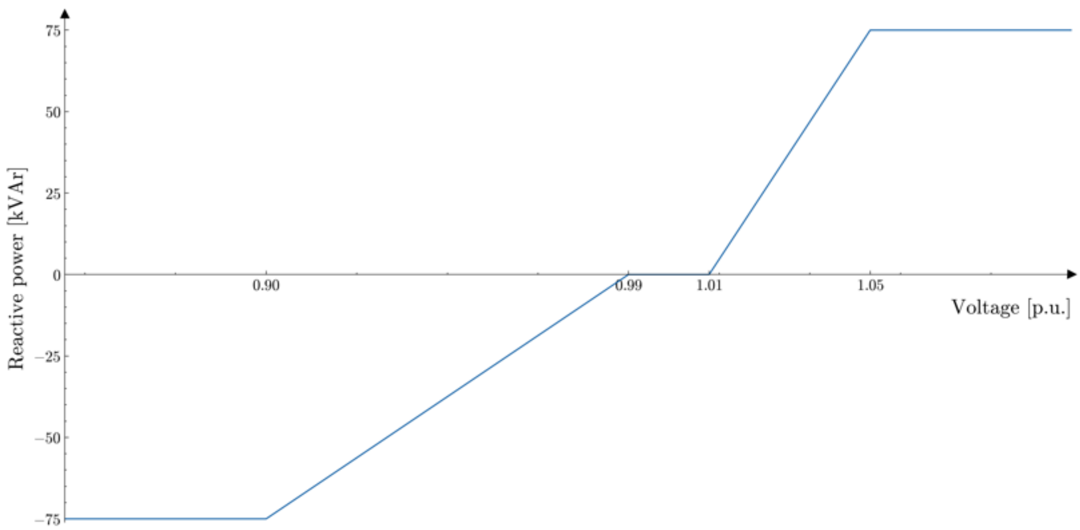

Figure 3.5: Reactive power droop curve

This tight deadband is justified as the voltage limits specified in table 3.6 lay at 0.95 p.u. and 1.025 p.u. Deadband values closer to these limits would make the controller bring the voltage back close to these values but never within. An additional control structure is a conditional statement where this controller is only triggered if the voltage values lay outside of the limits of 0.95 and 1.025. This is implemented to reduce simulation runtime, as the tight deadband limits would otherwise trigger the controller frequently, increasing simulation time up to 10 times.

SOC controller

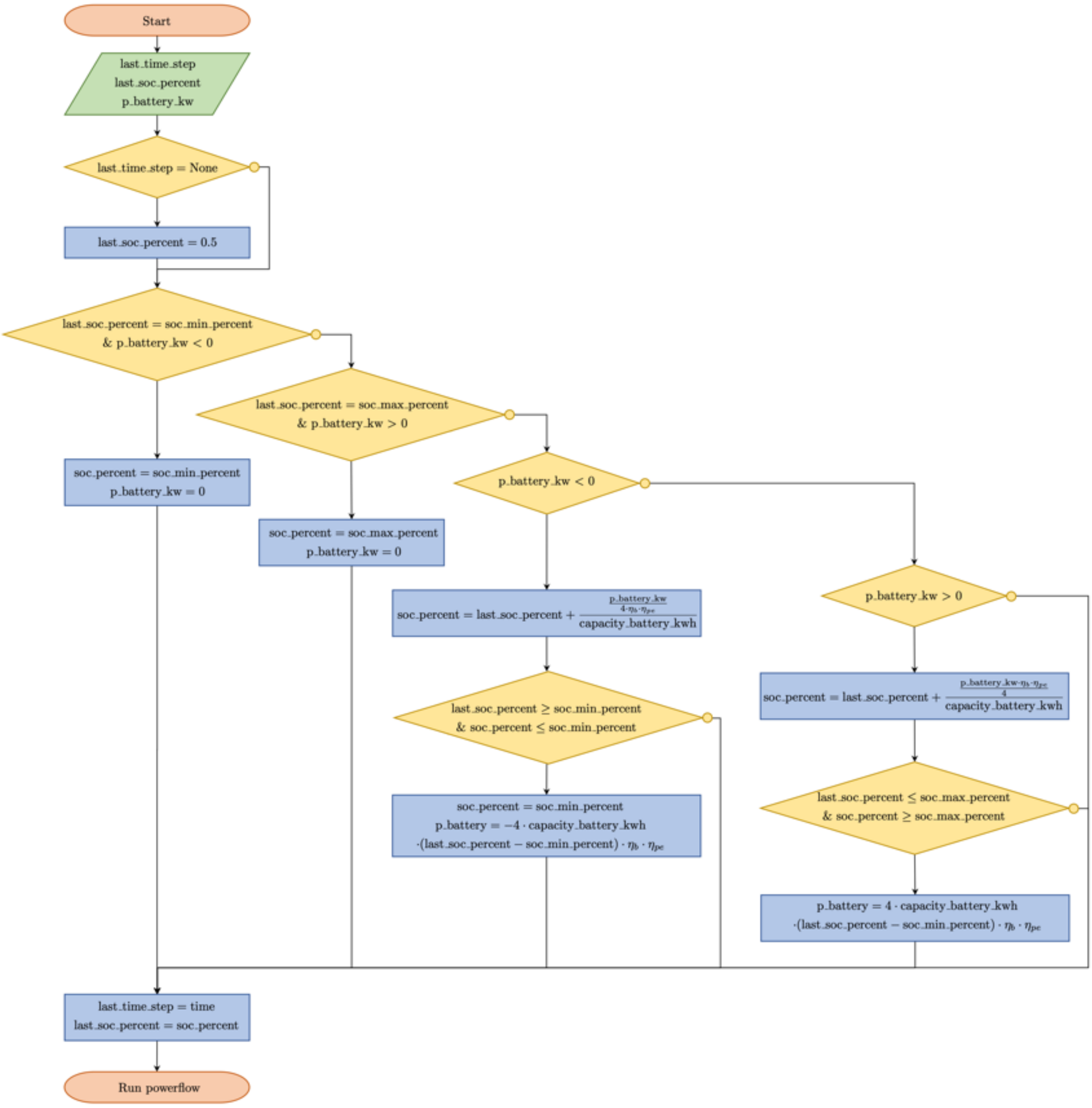

Figure 3.6: Battery SOC controller

After the active power setpoint of the battery is set, the state-of-charge (SOC) controller needs to make sure that the requested power can be delivered or charged. Even if pandapower offers a range of time series simulation functions that are used here, no battery or SOC controller is integrated with the main Python package. This is outlined as: "As pandapower is not a time dependend [*sic*] simulation tool and there is no time domain parameter in default power flow calculations, the state of charge (SOC) is not updated during any power flow calculation." [17]. A battery controller is proposed in a pandapower tutorial [17]. This Python class updates the battery's SOC by taking the SOC at the previous timestep and calculating based on the current power. However, no constraints that would actually limit the SOC are enforced, so the proposed controller is extended using the algorithm displayed in figure 3.6.

3.4 Cost comparison model

To compare the costs of conventional and battery-based grid upgrades, the capital expenditures (CAPEX) of assets will be the main component. The price of cables and transformers is fixed at the values described in tables 3.8, 3.9 and 3.10, and the price of the battery will be dependent on its size and installation year as specified in section 3.5.9.

Additionally to CAPEX, the lifetime is an important factor. For this, a transformer lifetime of 45 years and a battery lifetime of 20 years are chosen [20], where the transformer lifetime is based on how DSOs in Denmark depreciate their assets [21], and the battery lifetime based on an 80% remaining state of health. Depending on the actual use of the battery, an extended or reduced lifetime can or needs to be considered.

Operation and maintenance (O&M) costs are set at 2.6% of CAPEX costs per year for transformer and 2.5% for batteries [20, 22].

Finally, losses are the last component of the price comparison. The losses through the transformer are calculated by pandapower and the ones through the battery will be composed of a 95% power electronics and a 90% battery efficiency [18, 19]. This energy will be multiplied by the average day-ahead spot price for the DK2 bidding zone in 2021, 653.78 DKK/MWh [23]. The resulting formula is the following:

$$\mathrm{P} = \frac{\mathrm{C_{CAPEX}}}{\mathrm{L}} + \mathrm{C_{CAPEX}} \cdot \mathrm{O} + \sum_{t=0}^{35{,}040} \mathrm{E}_{\mathrm{l},\, t} \cdot \mathrm{C_{el}} \tag{3.22}$$

with P the asset price in DKK/year, $\mathrm{C_{CAPEX}}$ CAPEX costs in DKK, L lifetime in years, O the share of O&M costs from the CAPEX costs in percent, $\mathrm{E}_{\mathrm{l},\, t}$ the energy losses per timestamp in MWh and $\mathrm{C_{el}}$ the electricity spot price in DKK/MWh.

In a second iteration, the previous formula will be extended to eventual savings on other assets. If the batteries can be used to differ other investments that are not related to fast charging stations, the prices of these cables and transformers will be considered and the updated formula for the battery will then be:

$$\mathrm{P} = \frac{\mathrm{C_{CAPEX}}}{\mathrm{L}} + \mathrm{C_{CAPEX}} \cdot \mathrm{O} - \frac{\mathrm{C'_{CAPEX}}}{\mathrm{L'}} + \sum_{t=0}^{35{,}040} \mathrm{E}_{\mathrm{l},\, t} \cdot \mathrm{C_{el}} \tag{3.23}$$

with $\mathrm{C'_{CAPEX}}$ the CAPEX costs of assets that don't require an investment anymore in DKK and L' their lifetime in years.

When comparing asset costs between the power flows with and without batteries, the losses across the existing transformers to which the batteries are connected are also considered and added to the batteries' costs. The updated formula is then:

$$\mathrm{P'} = \mathrm{P} + \sum_{t=0}^{35{,}040} (\mathrm{E}_{\mathrm{l\ w/\ battery},\, t} - \mathrm{E}_{\mathrm{l\ w/o\ battery},\, t}) \cdot \mathrm{C_{el}} \tag{3.24}$$

with $E_{l\ w/\ battery,\ t}$ transformer losses per timestamp with battery, and $E_{l\ w/o\ battery,\ t}$ without battery, both in MWh.

The cost comparison of transformers or batteries only considers the costs of these assets, i.e. without building or secondary equipment-related costs (such as switches, breakers, ventilation systems e.g.). This underestimation of the total costs is assumed to not impact the comparison since the same costs are omitted for both transformers and batteries.

3.5 Input data

This section lists and presents the input data for the model: EV and other DERs penetration and load profiles, fast charging behaviour and characteristics, economic data and grid components information.

3.5.1 Geographical scope

The area supplied by NKE-Elnet A/S is shown on the map in figure 3.7 with the administrative boundaries of Næstved municipality [24] and Næstved town (postal code 4700) [25]. Because statistical data is not available for the exact area within NKE-Elnet's but usually either for Næstved municipality or Næstved town, some assumptions will be made. These will be specified in the following section.

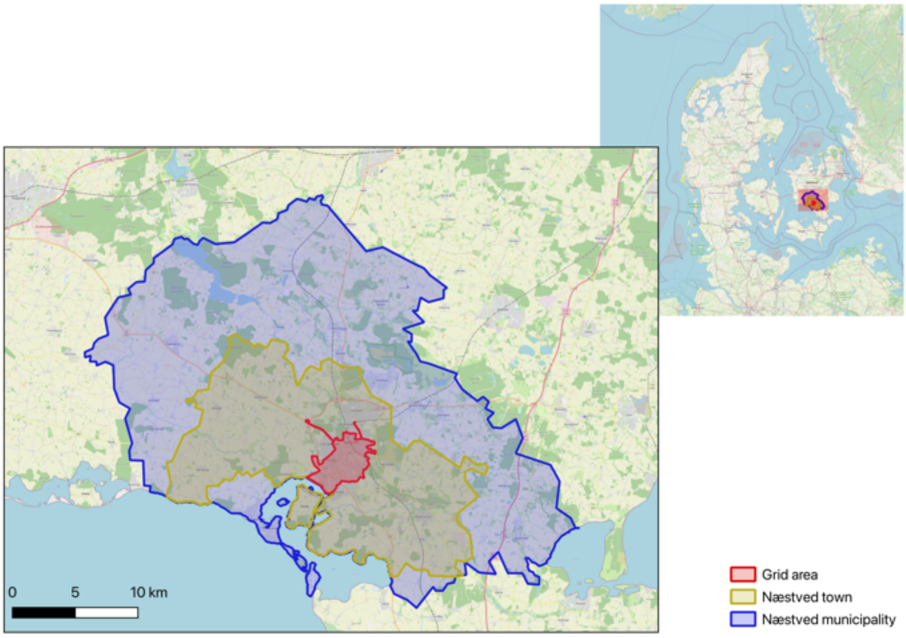

Figure 3.7: Geographical boundaries and scope of the analysis

3.5.2 EV penetration

The number of electric vehicles in the future is estimated based on the total number of vehicles expected combined with the current government's goal of making Denmark CO_2 neutral by 2045 [26]. It is expected that, by this date, 100% of vehicles will be electric.

The future number of overall vehicles is based on a linear extrapolation model based on historical data gathered on the Bilstatistik portal, collecting the import statistics from all car manufacturers [27]. The resulting graphs for Denmark and the grid area are shown in figure 3.8. It is assumed that the number of cars will develop in a similar way in Næstved town as in the rest of Denmark and that the grid area contains 56% of the town's cars. This is based on the neighbourhoods of Appenæs, Lille Næstved, Holsted and Ny Holsted being not part of the grid area, and their total population in 2023 is estimated at 25,000 people based on their surface and the surface of the similar town of Fensmark [28]. With a total population in Næstved town of 44,996, this results in a 56% share. Even if most of the population growth will probably take place by building new neighbourhoods outside of the city's current borders, transformations of areas such as those proposed in communal development plans will still bring population growth within the grid area's boundaries [29, 30].

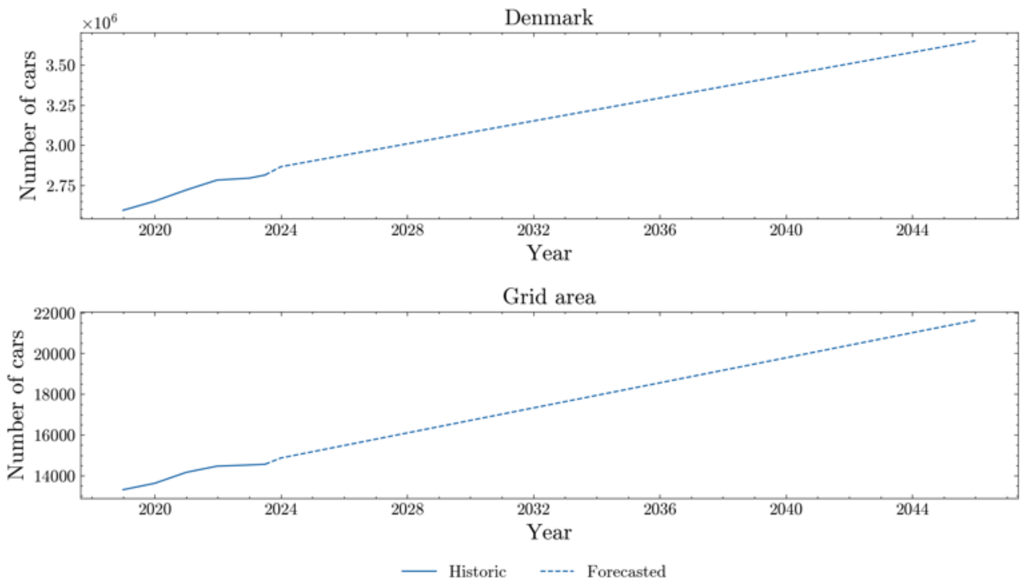

Figure 3.8: Evolution of the number of cars in Denmark and the grid area

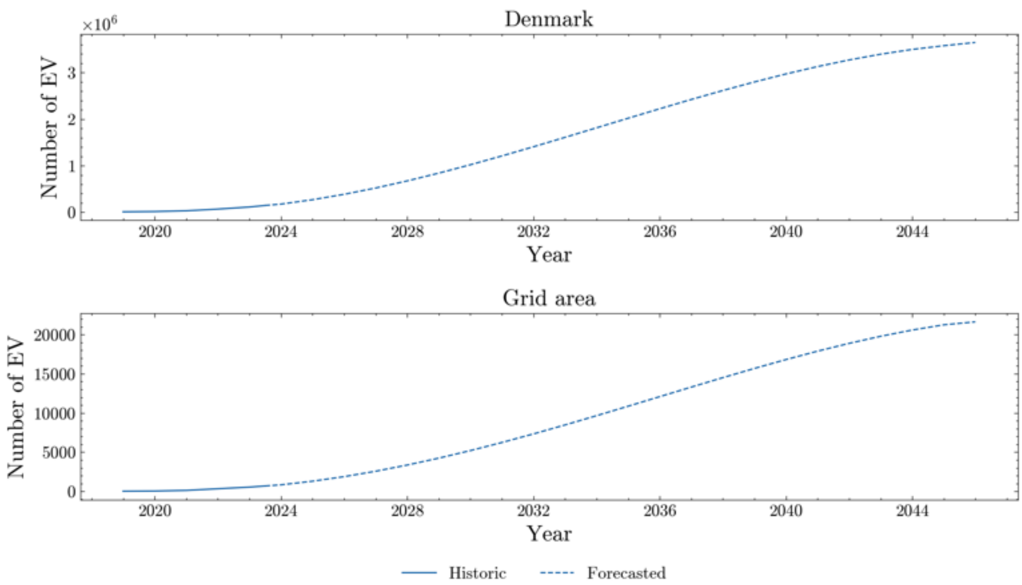

Figure 3.9: Evolution of the number of electric vehicles in Denmark and the grid area

The potential of hydrogen vehicles is neither investigated nor taken into account. The historic number of EVs is retrieved from the Bilstatistik portal [27]. By 2030, 1.2 million EVs are expected to be driving on Denmark's roads [31]. Between 2024 and 2030 and 2030 and 2045, the car numbers are interpolated to fit the expected rate of penetration of electric vehicles. The resulting graphs display the expected number of EVs in Denmark and in the grid area in figure 3.9. The evolution of the number of EVs in Næstved town follows the same trend as in Denmark.

The number of EVs is in the same order of magnitude as the latest numbers published by Energistyrelsen (the Danish Energy Agency) [32]. The published number is an energy amount for electric mobility and with the average EV efficiency described in section 3.5.4 and an average distance of 47km/car/day [31], 3.345 million EVs are expected in 2045 by Energistyrelsen versus 3.649 million calculated here, an 8% relative difference.

3.5.3 Fast charging station penetration and distribution

In this analysis, fast charging will be defined as charging taking place with a capacity above 50kW.

As of September 2023, two fast charging stations are already installed in the grid area: one with four charging spots of 300kW each placed at a gas station and one with two spots of 225kW on a public parking [33].

The number of required fast charging stations in the future is derived from DTU's and Danske E-Mobilitet's charge point calculator introduced in [31]. As most of the area of Næstved municipality is a rural area and Næstved town concentrates around half of the population, it is assumed that 75% of these fast charging stations will be placed in NKE-Elnet's grid area. The standard parameters of the charge point calculator are used, the only change is regarding the share of energy charged at fast charging stations, which is set at 10.31% based on the data discussed in section 3.5.5. The resulting evolution of the number of fast charging stations for Denmark and the grid area is shown in the graphs in figure 3.10. By 2045, it is expected to have 29 fast charging stations installed in the area. Considering the two existing stations, it means that 27 new ones will be installed [33].

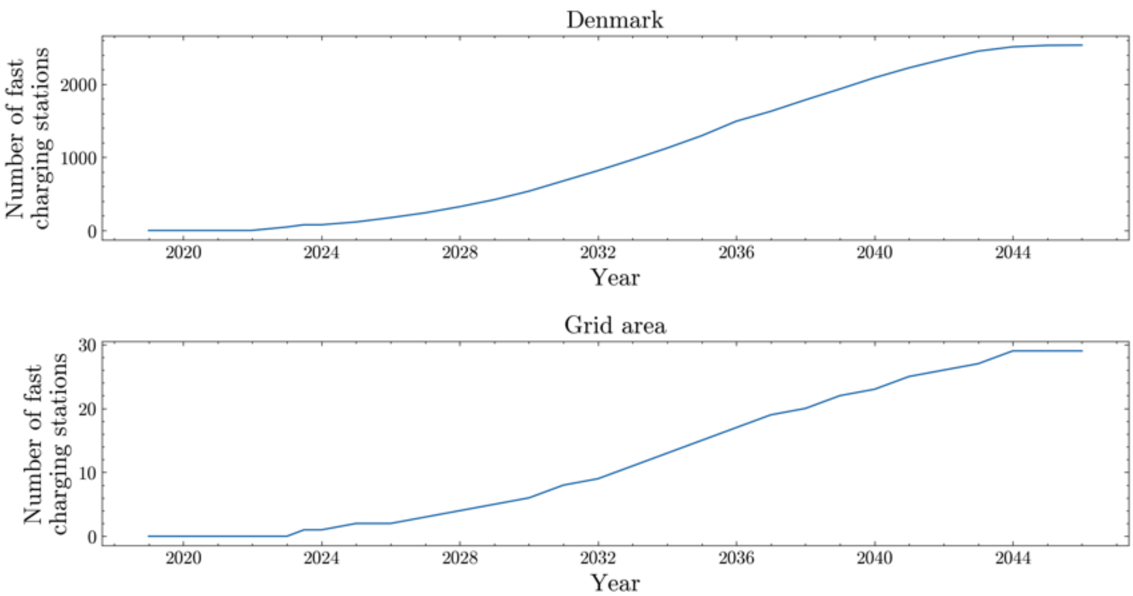

Figure 3.10: Evolution of the number of fast charging stations in Denmark and the grid area

Regarding the geographical distribution of these fast charging stations, the following method is applied. First, historical traffic data is collected as the number of cars per day measured at different locations by the Danish Road Directorate [34]. This data is used as an input in the QGIS software and a geographical interpolation is realised to estimate the traffic between two measurement points (shown in figure A.1). Then, points of interest susceptible to attracting people are collected from OpenStreetMap data [35]. These points include e.g. sports facilities, supermarkets, cinemas, restaurants and cafes, and other stores. Additionally, gas stations are located [36]. Finally, public parking locations are downloaded from [37]. These locations are shown in figure A.2.

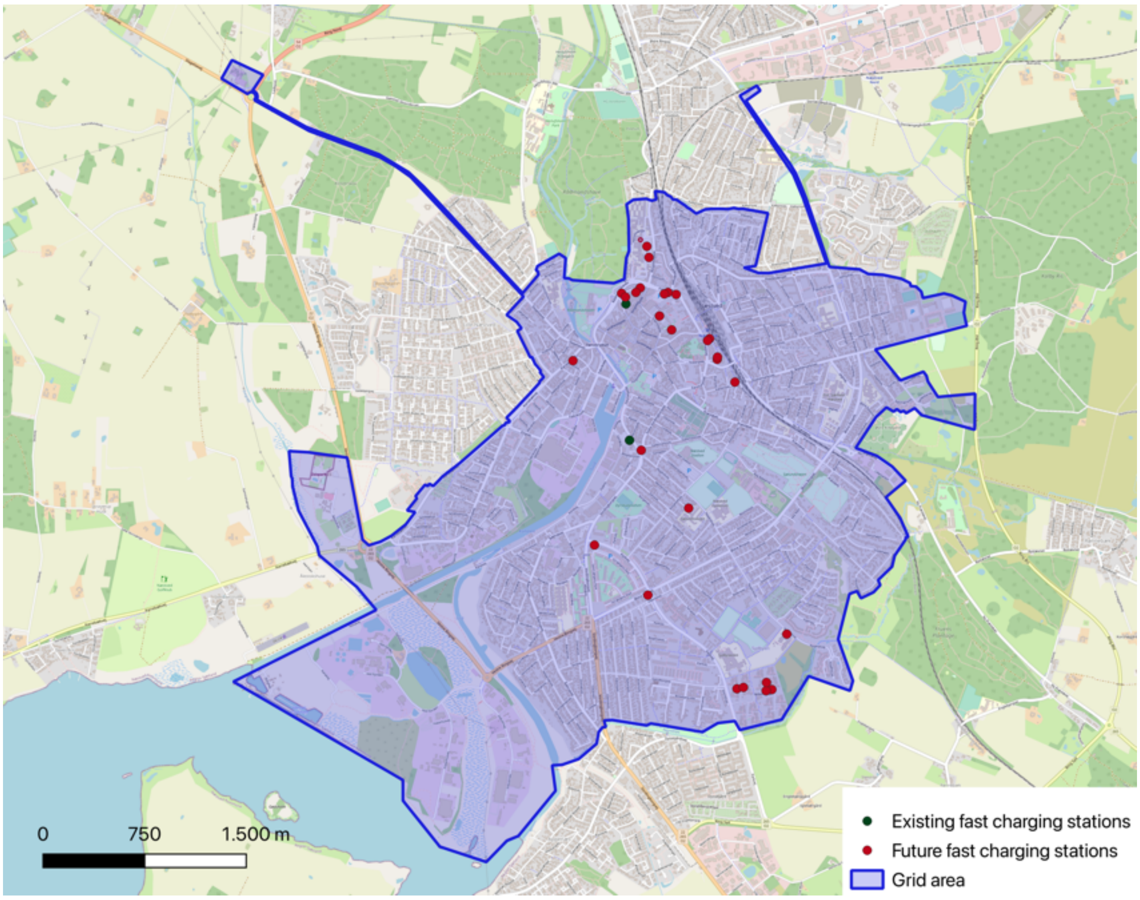

Figure 3.11: Geographical distribution of fast charging stations in the grid area in 2045

It is assumed that gas stations would be the first infrastructure providers to install fast charging stations to sustain their business model. Based on this assumption, fast charging stations are first placed on these points based on the penetration rate. For the remaining stations, the following approach using QGIS functions is used. On each public parking, a random point is placed. For each point, a weight factor is calculated based on the distance to a point of interest and the traffic intensity. The distance from the parking point to the closest point of interest lies between 33 and 511 meters, while the traffic data indicates between 256 and 12,756 cars per day depending on the closest measurement point. The resulting weight factor is calculated using the following formula:

$$\mathrm{w} = \frac{1}{2} \cdot \frac{\mathrm{d_{max}} - \mathrm{d}}{\mathrm{d_{max}}} + \frac{1}{2} \cdot \frac{\mathrm{n_{max}} - \mathrm{n}}{\mathrm{n_{max}}} \tag{3.25}$$

with w being the weight, d the distance of each potential location to the closest fast charging station and d_{max} the maximum distance of 511 meters, n the number of cars and n_{max} the maximum number of 12,756 cars. The resulting points and factors (shown in figure A.3) are then exported and further processed in a Python script. There, for each year, locations are selected stochasticly based on their weight and the number of new fast charging stations that year. The remaining potential locations are then negatively weighted based on the inverse of their average distance to other fast charging stations, and a calculation for the next year is run. The updated weight equation is the following:

$$w' = \frac{2}{3} \cdot w + \frac{1}{3} \cdot \frac{\frac{1}{d} - d_{min}}{d_{max} - d_{min}} \tag{3.26}$$

with w' the update weight, w the weight calculated in equation 3.25, d the distance of every potential location to the closest fast charging station, d_{max} and d_{min} the maximum and minimum distances to an existing fast charging station in that year's iteration.

The resulting locations of fast charging stations in 2045 are shown on the map in figure 3.11.

3.5.4 EV characteristics

The electric vehicle battery sizes and maximal charging power capacities are important factors impacting fast charging. In figure 3.12, the evolution of battery size based on the 80% most possessed models in Næstved town is plotted over time, based on EV models from [27] and battery capacity from [38]. It can be seen that the size of batteries tends to increase, with models with less than 30kWh capacity being replaced with models in the (50-70]kWh range, while the share of models with a battery larger than 70kWh stays relatively constant. The average battery capacity grew from 50 to 65kWh between 2019 and 2023.

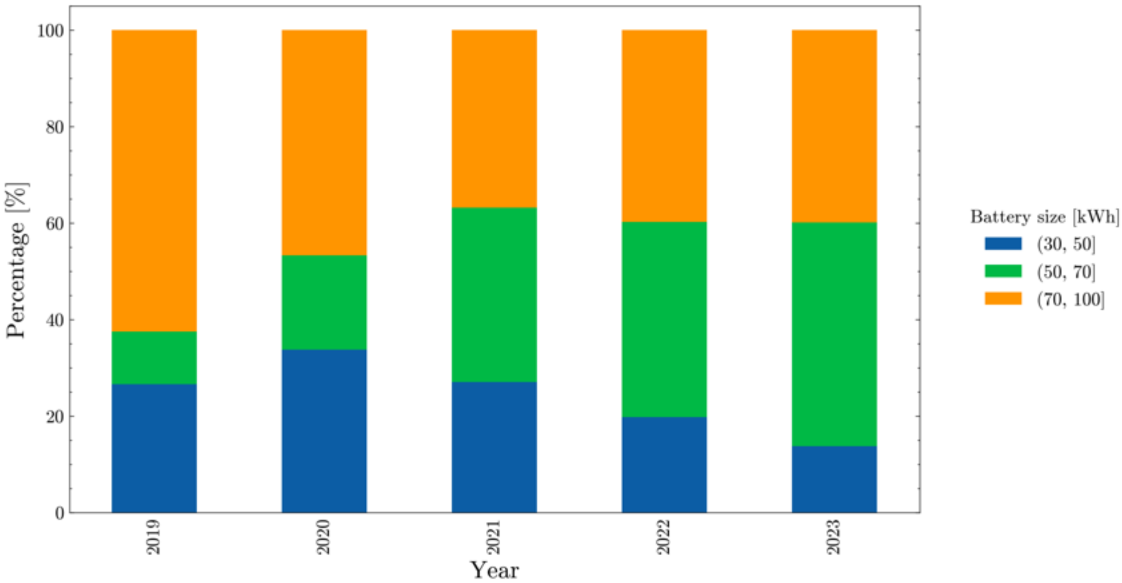

Figure 3.12: Distribution of EV battery size based on the 80% most possessed models in Næstved town

This trend can, however, not be assumed to continue in the future. When looking at the distribution of the category of cars possessed, EVs are not representative of all other fossil-fuel types, as shown in figure 3.13 [27]. Cars in the small and micro categories represent constantly around 58% of 80% of the most possessed car models (excluding EVs), whereas they are disappearing from EVs. On the other side, more than 80% of 80% of the most possessed EV models are large, medium SUV or large SUV cars, whereas this category only accounts for less than 20% of all other cars.

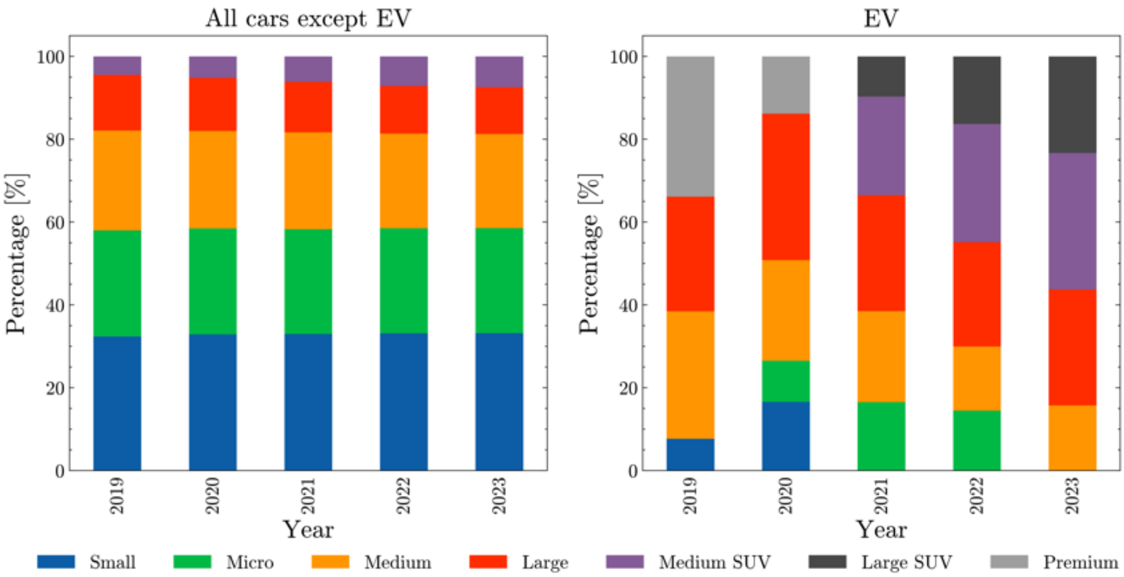

Figure 3.13: Distribution of car categories based on the 80% most possessed models in Næstved town

The historic evolution is mostly due to the fact that a majority of premium and high-end EVs have been put on the market, yet not a large number of models to replace small and micro cars has been offered to this day [27]. Based on this, it will be assumed for future scenarios that the share of vehicles with a smaller battery will increase. The future distribution of battery sizes is shown in table 3.2.

Battery capacity [kWh]	**Share of EVs [%]**
(30, 50]	58
(50, 70]	21
(70, 100]	21

Table 3.2: Battery size distribution for future scenarios

Driving efficiency is an important factor in estimating the required charging energy based on the number of kilometres driven. The evolution based on the 80% most possessed models in Næstved town is plotted over time in figure 3.14 [27, 38]. It can be observed that due to larger and heavier EVs (partly because of batteries with higher capacity), the consumption increases over time, from an average of 161Wh/km in 2019 up to 175Wh/km in 2023.

For future scenarios, a constant energy consumption of 175Wh/km will be used under the assumption that the increasing weight of EVs in the near future will be compensated by technical improvements and the medium to long-term development of small EVs.

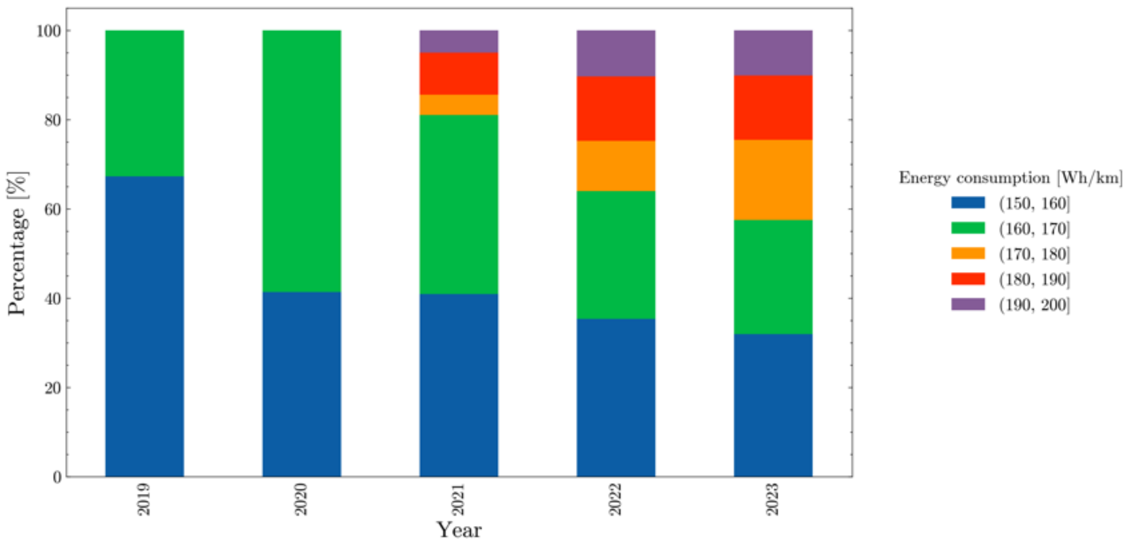

Figure 3.14: Distribution of EV energy consumption based on the 80% most possessed models in Næstved town

3.5.5 Usage of fast charging stations

Share of energy charged at fast charging stations

The usage of fast charging stations outside of its very specific application during a longer trip that can't be fulfilled with one battery charge is mostly dependent on battery size and private charging access, as demonstrated in [39]. The authors show that over the course of a day when comparing different charging types, fast charging never reached far above 10% of all charging types (including home, public, semi-public, work and fast charging). They also demonstrated an inverse relationship where the larger the battery size, the less energy was charged at a fast charging station. Moreover, car owners without private charging access were prone to use fast charging stations twice as much in comparison to owners with private charging access. In table 3.3, the share of energy charged at a fast charging station per month that will be used is shown [39], based on the distribution of battery sizes shown in section 3.5.4.

Battery capacity [kWh]	Share of energy at fast charging stations per month [%]
(30, 50]	13.0
(50, 70]	6.9
(70, 100]	6.3
Average based on battery size distribution	10.31

Table 3.3: Distribution of the share of energy charged at fast charging station based on battery size

Usage of fast charging stations from non-residents

Regarding estimating the number of EVs charging in the grid area that are not registered in Næstved, the following approach is used. From tourism-related documents, the following information has been extracted and translated: "The tourism that exists [...] is characterised by a large number of day tourists who come to Næstved to make use of the city's many shopping opportunities and other offers." and "In the vision for the future tourism efforts [...], the overall message is that tourism in Næstved must build on the municipality's existing place-based qualities and development potential - the unique nature, living cultural history and many events and shopping opportunities in Næstved town." [40].

It will be assumed in the following that these day tourists are a target group for fast charging stations. From a survey performed in 2012, numerical data regarding this number of day tourists can be used for further analyses [41]. Over the course of three days, the number of people in Næstved's town centre was counted at six different locations. Additionally, questions were asked to a selection of these people to determine where they were coming from e.g. The key findings from this survey are that 20% were coming from outside Næstved town, that 52% came by car and 86% of these parked inside an area described as the "City Ring", which will be assumed to be similar to the grid area. A map showing the origin of day tourists is shown in figure B.1. The aggregated number of people is listed in table 3.4.

Day	**Hours**	**Number of people**
Thursday	12-18	18,235
Friday	12-18	25,197
Saturday	10-14	17,367

Table 3.4: Number of people monitored in Næstved's city centre in 2012

To estimate the number of people today and in the future over a whole week, the following approach is used. First, it is assumed that the number of people in this survey followed the historical and will follow the future population development of Denmark. It is also assumed that 90% of the 20% of people coming from outside Næstved town are coming by car and that the rate of penetration of EVs in these areas is and will be similar to the one in Næstved town. Then, the number of people based on the 2012 data is extrapolated to represent a complete week as the following. Monday to Wednesday are assumed as Thursday, with an additional 20% counting for people before 12:00 and after 18:00. Friday is counted with an additional 40% for people before 12:00 and after 18:00. Saturday is doubled for the 14:00-18:00 period and an additional 20% is added to that for people after 18:00. Sunday is counted like Friday before 18:00. The resulting numbers are shown in table 3.5

Day	**Number of people**
Monday - Thursday	21,882
Friday	35,275
Saturday	41,681
Sunday	30,236

Table 3.5: Number of people monitored in Næstveds city centre, corrected for an entire week in 2012

It is further assumed that there are on average two people per car, that there is no seasonal effect (the lower population during the summer due to holidays will be compensated by tourists and bad weather in the winter is compensated by holidays and Christmas shopping), and that the share of charging sessions at fast charging stations follows the data presented in table 3.3. The resulting numbers of EVs coming outside from Næstved town and charging at fast charging stations are shown in figure 3.15.

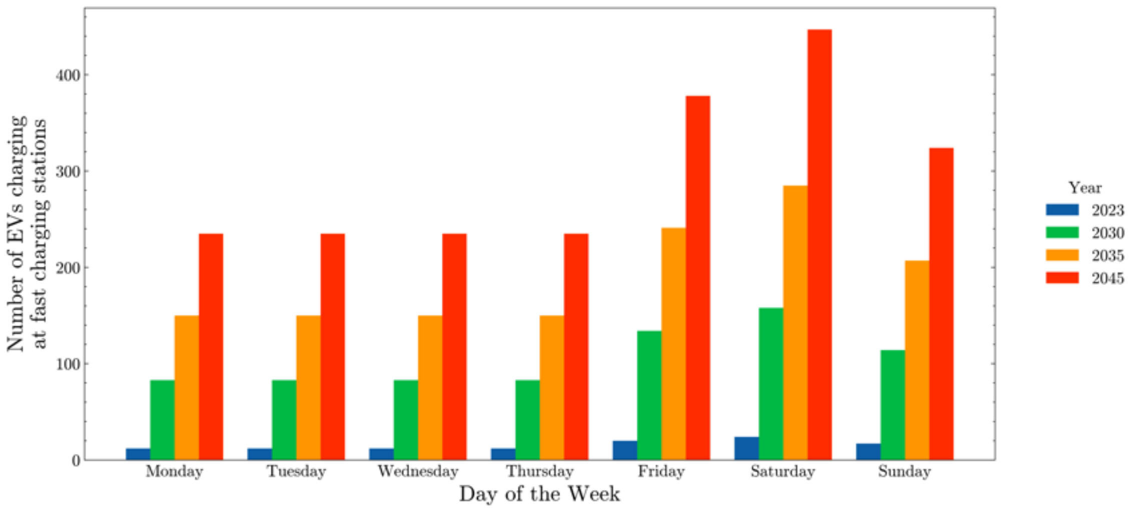

Figure 3.15: Number of EVs coming outside of Næstved town and charging at fast charging stations

3.5.6 Penetration of other DERs

EV home charging stations

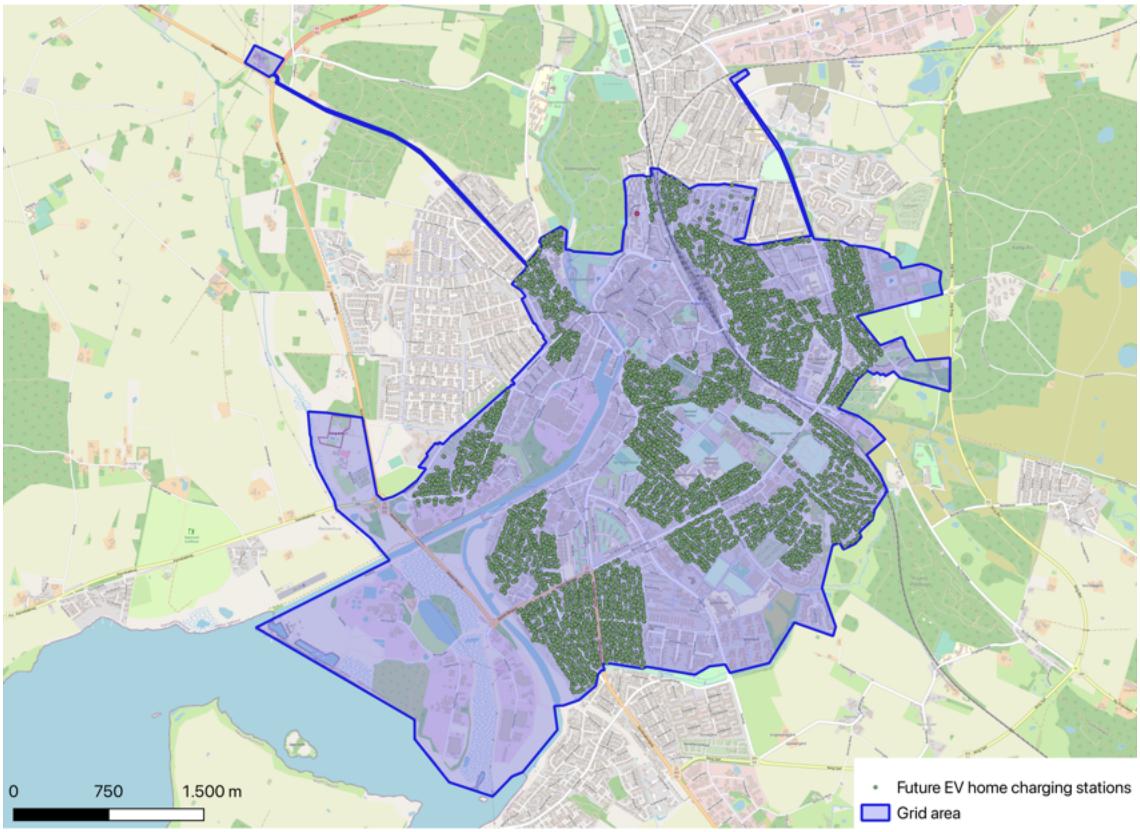

Figure 3.16: Geographical distribution of home charging stations in the grid area in 2045

The EV home charging stations are distributed by first identifying the areas with houses with private parking spots [42]. From there, it is assumed that by 2045, all these houses will be equipped with EV charging stations and two EVs per house. Following this, the yearly new charging stations are stochastically distributed following the EV penetration curve presented in section 3.5.2. The resulting installations in 2045 are shown in figure 3.16.

EV private shared charging stations

With EV shared charging stations are meant buildings with multiple households having access to private parking where not each spot is equipped with a charging station and therefore this resource is shared between the users. To identify areas where this type of charger will be placed, parking areas near larger residential buildings are identified [37, 42]. Then, the number of parking spots is estimated by assuming that 50% of each area is available for parking and that each spot is 12.5m^2 [43]. The yearly number of charging stations for each category is retrieved from DTU's and Danske E-Mobilitet's charge point calculator [31]. These charging spots are then stochastically distributed on the available parking spots. The resulting charging stations in 2045 are shown in figure 3.17.

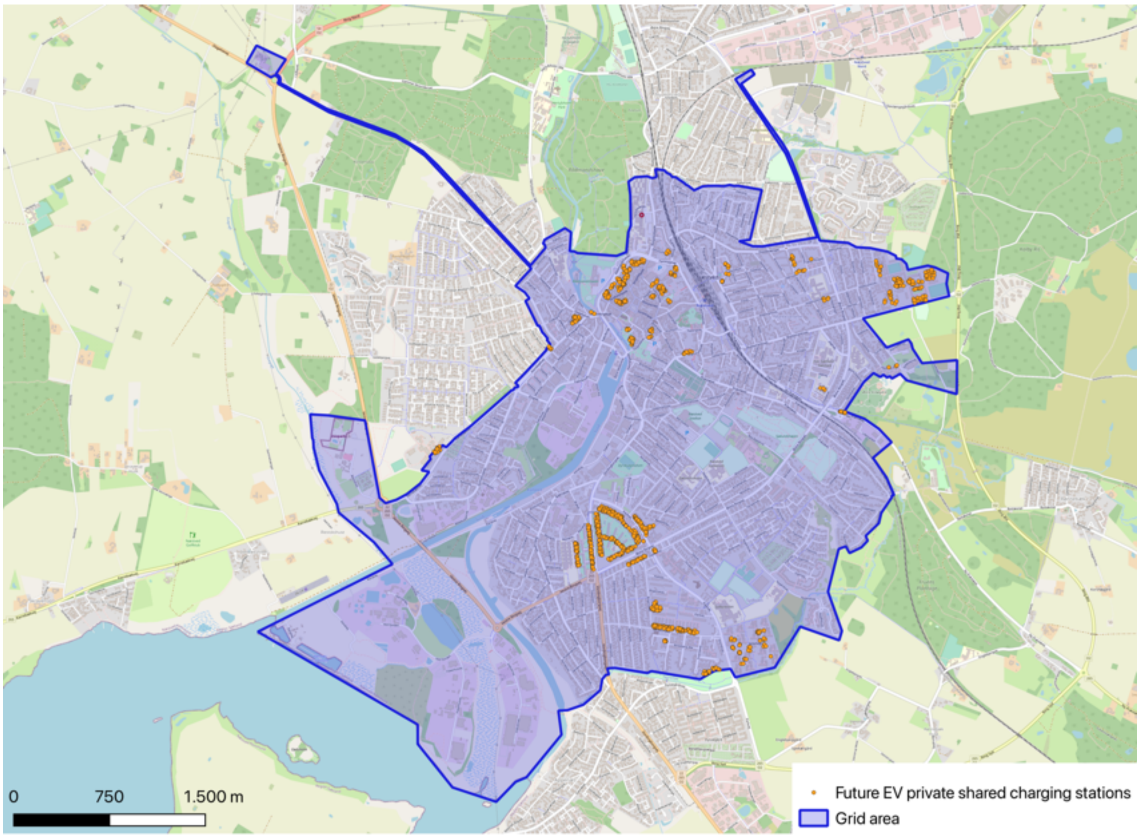

Figure 3.17: Geographical distribution of private shared charging stations in the grid area in 2045

EV normal public and workplace charging stations

For the EV normal (in this case considered as not fast, i.e. below 50kW) public and workplace charger distribution, the same approach as for private shared charging stations is used due to the lack of data regarding the parking availability around workplaces. First, all public parking areas close to areas of interest for the public or workplaces are identified [37, 42]. From there, the same method as presented in the previous section for private shared charging stations is applied. The resulting charging stations in 2045 are shown in figure 3.18.

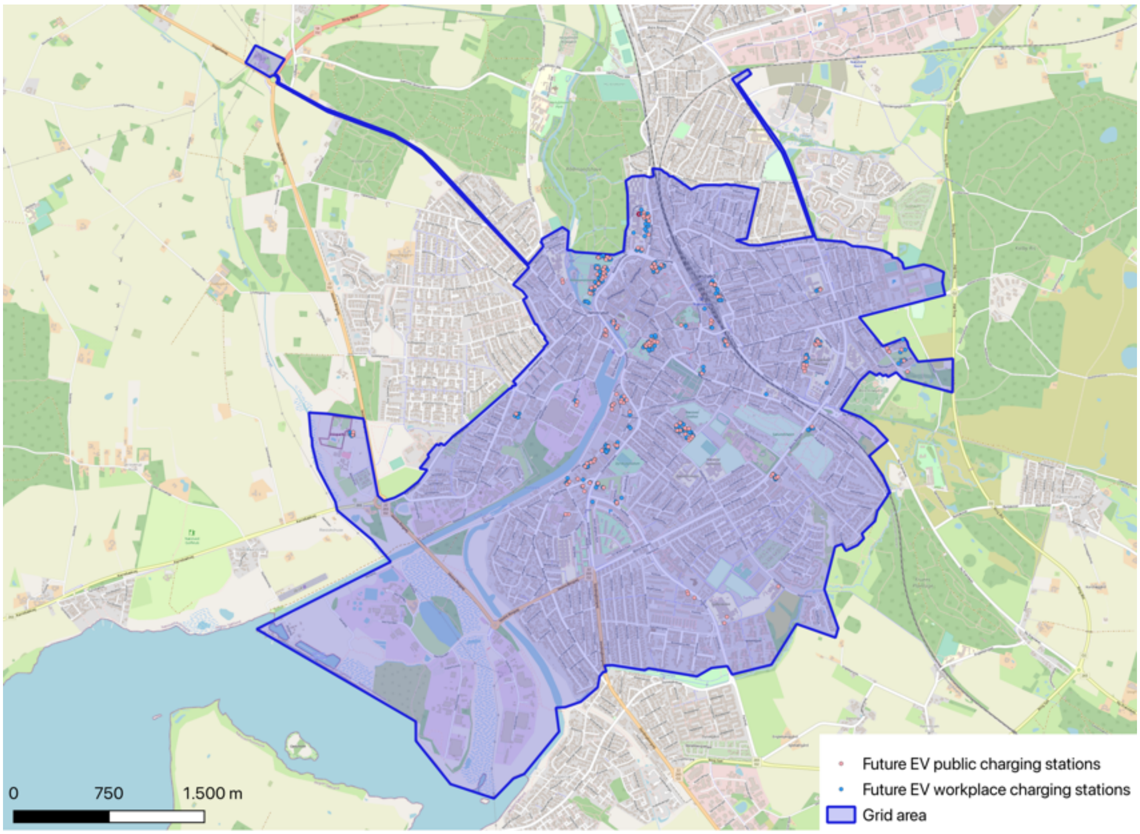

Figure 3.18: Geographical distribution of normal public and workplace charging stations in the grid area in 2045

Heat pumps

District heating is expected to play a major role in the heat supply of the grid area based on the Heating Development Plan 2030 from Næstved municipality [44]. 68% of the area is currently covered by district heating and 18% has district heating potential that might be connected until 2030. These areas are shown in figure C.1. With this data, under the consideration that all the Danish heating system is supposed to be gas-free in 2035 [45] and the current heating system of buildings coming from the BBR (Bygnings- og Boligregistret, Building and apartment register) [46], the following assumptions are made.

In areas with district heating, 1% of buildings that do not have a district heating connection or a heat pump will choose a heat pump. In areas with district heating potential, 10% of buildings will choose a heat pump, except for the industrial area located south of Næstved, where due to the proximity to a waste incineration facility, it is assumed that all buildings will be connected to a local district heating grid. In areas without district heating, all the buildings will choose a heat pump. The rate of penetration of heat pumps is set linearly between 2024 and 2035, the buildings choosing a heat pump are assigned stochastically, and the buildings with the current heating system information or coordinates missing are ignored. The resulting future heat pump locations in 2045 are shown in figure 3.19.

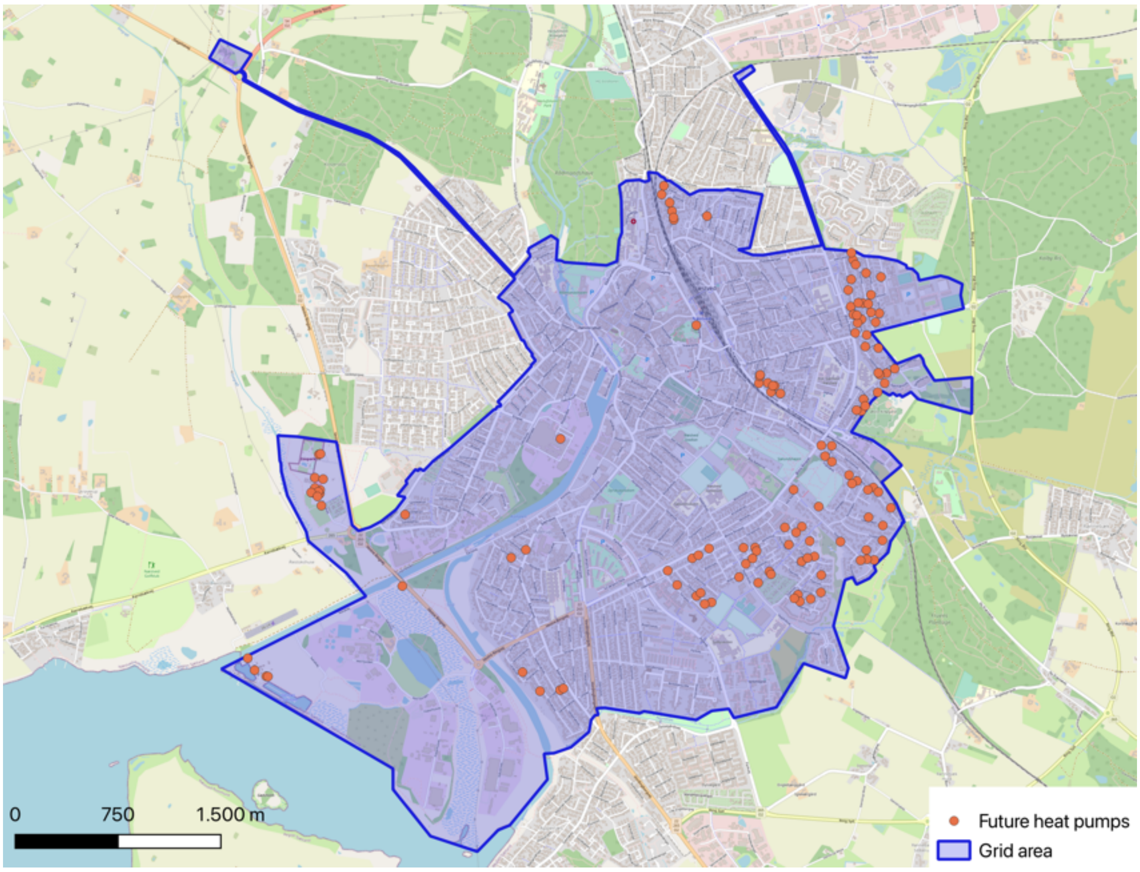

Figure 3.19: Geographical distribution of future heat pumps in the grid area in 2045

PV

In terms of the penetration of future PV installations, data for Denmark is first retrieved from an analysis from the Danish Energy Agency, where 37,588MW are expected to be installed in 2045 [32]. Based on production data from the Danish transmission system operator (TSO) Energinet from 2022 [47] and power output from the Global Solar Atlas [48], the installed capacity at that time for Næstved municipality was 60MW. The future numbers for Næstved municipality are then calculated based on the 2022 installed capacity in Denmark versus in Næstved municipality. Following solar park projects in Næstved municipality and the official development plan, it is assumed that 10% of the future capacity will be installed in the grid area, resulting in a capacity of 73MW in 2045 [49, 50]. The PV capacity evolution is shown in figure C.2.

Based on the building's sizes [51], it is assumed that buildings with an area of more than 7,000m^2 are commercial or industrial. The minimum solar installation size is set at 4kWp and with an average power density of 205Wp/m^2, it is therefore assumed that buildings with an area below 80m^2 will not qualify for an installation [52]. Finally, the available area for solar cells is calculated for every building, using 62.5% of the roof area for commercial and industrial buildings and 24.5% for residential ones [53].

This data is used as input for a Python algorithm and for each year, based on the newly connected PV capacity, a stochastic number of buildings are selected until the capacity is reached. A linear penetration rate between 2023 and 2045 is assumed. The resulting installations in 2045 are shown in figure 3.20.

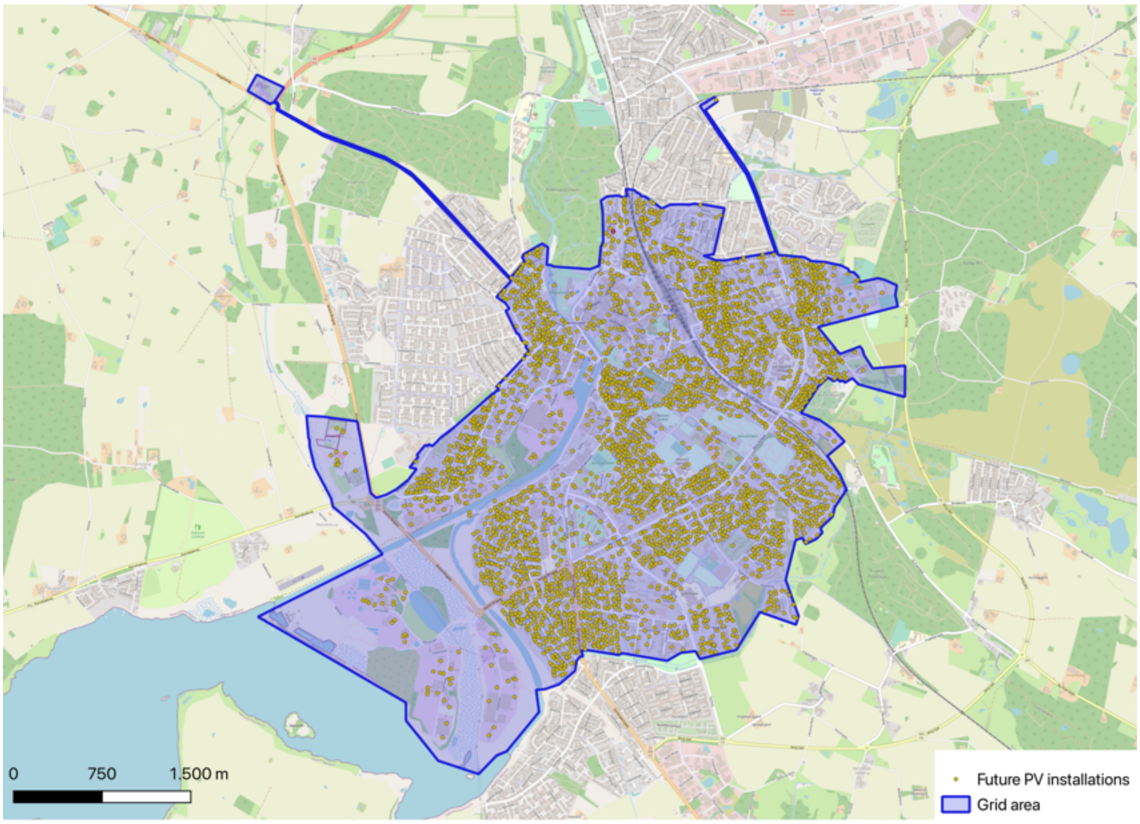

Figure 3.20: Geographical distribution of future PV installations in the grid area in 2045

3.5.7 Load profiles

For all the load profiles presented in this section (except the fast charging station ones), after the first processing step, the same method is used. The profiles retrieved from literature or data from Utiligize cover one or two years, in a 15-minute to 1-hour resolution, with the hourly one linearly interpolated into 15-minute steps. The resulting profiles are then split into weeks which are then clustered based on the seasonal behaviour, using Python's statsmodels library [54]. This creates, for each season, a dozen profiles that will be used stochastically to add uncertainty to the model and a closer-to-real-life behaviour instead of one identical profile for each DER.

EV fast charging stations

The EV fast charging station load profiles are generated using a Monte Carlo simulation based on parameters that are published in the literature [3, 55]. These parameters, shown in figure 3.21, observed at fast charging stations, give a probability distribution over the arrival time, connection time, and charged energy. The charging power is given by dividing the charged energy by the connection time.

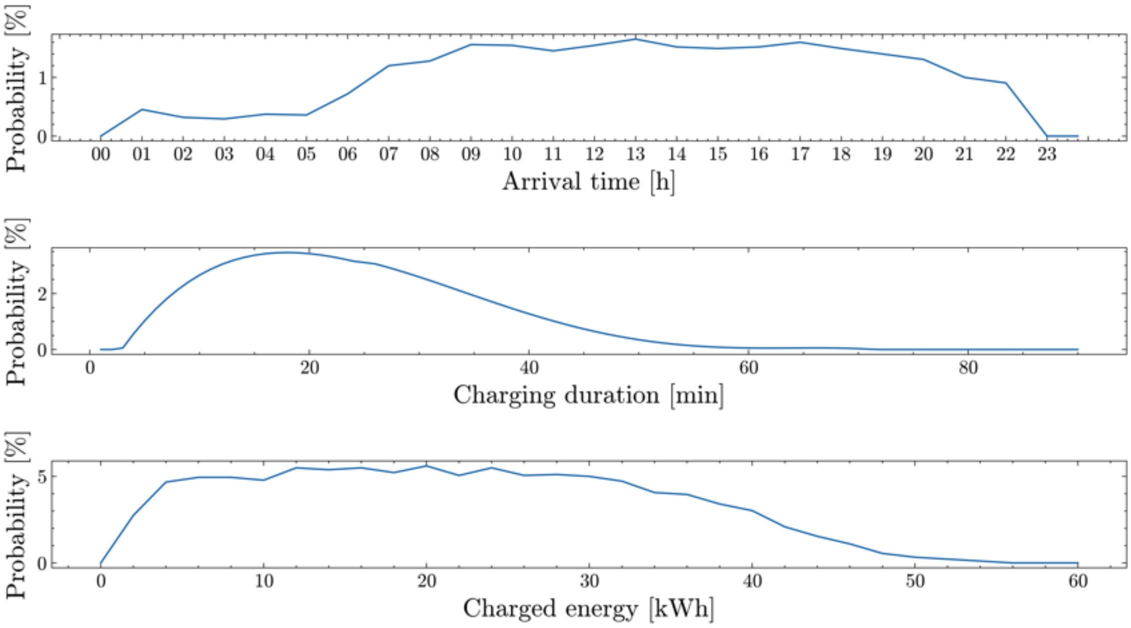

Figure 3.21: Fast charging profile parameters

To avoid generating unrealistic profiles (i.e. where the charged energy would be higher than the battery's capacity), for each charging session a battery capacity based on the distribution presented in table 3.2 and in section 3.5.4 is selected and set as a limit. Additionally, the SOC before the charging cycle is calculated with the following equation:

$$\mathrm{SOC} = \mathrm{random}(\mathrm{C} - \mathrm{E}) \tag{3.27}$$

With random a function picking a number between zero and the specified upper limit between brackets, C the battery capacity and E the charged energy, both in kWh. If the sum of the SOC before charging and the charged energy is above 80% of the capacity, then the charging session is split and the energy above 80% is charged at a 5kW power [15]. Additionally, the maximum fast charging power is set based on the previously chosen battery size. For the 80% most possessed electric vehicles in Næstved in 2023, the maximum fast charging speed is collected [27, 38]. The battery size of these vehicles is then clustered in three categories and for the battery size selected for each charging session, a maximum fast charging speed in this category is selected stochastically. These numbers can be found in table D.1. A final constraint is implemented to limit the number of simultaneous charging sessions. It is assumed that four charging spots are available per station, i.e. no more than four simultaneous charging sessions can take place.

The number of profiles generated varies each year based on the EV penetration and the share of charging sessions performed at a fast charging station as described in section 3.5.5.

To assess that the probability profiles from the literature shown in figure 3.21 are representative of the use-case behaviour, they are compared with available charging data from one of the currently two installed fast charging stations in the grid area. The data used was collected between June 11$^{\text{th}}$, 2023 and January 10$^{\text{th}}$, 2024. The smart meter data, available in 15-minute resolution, is disaggregated in single charging sessions by identifying each peak and extracting the charging session start time, duration and charged energy. The results are shown in figure 3.22, where the mean relative error between the literature and the observed arrival time is 3.9%. Differences in the charging duration can be explained by the time resolution of the measurements of 15 minutes being less precise than the minute resolution in the literature, as well as the disaggregation method employed. The observation curve skewed to longer durations might also indicate EVs with larger batteries in the grid area than in the literature. The more evenly distributed charged energy in the observation could be explained by EVs with a higher driving consumption (since the data is from 2019 and this number has been increasing since) or larger EVs due to geographical differences (the data is from the Netherlands).

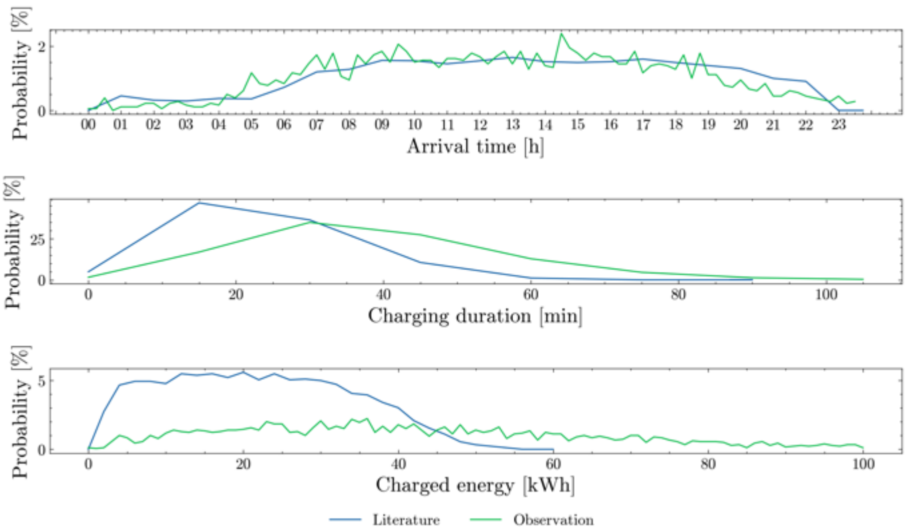

Figure 3.22: Fast charging profile parameters, literature vs. observation

EV home and private shared charging stations

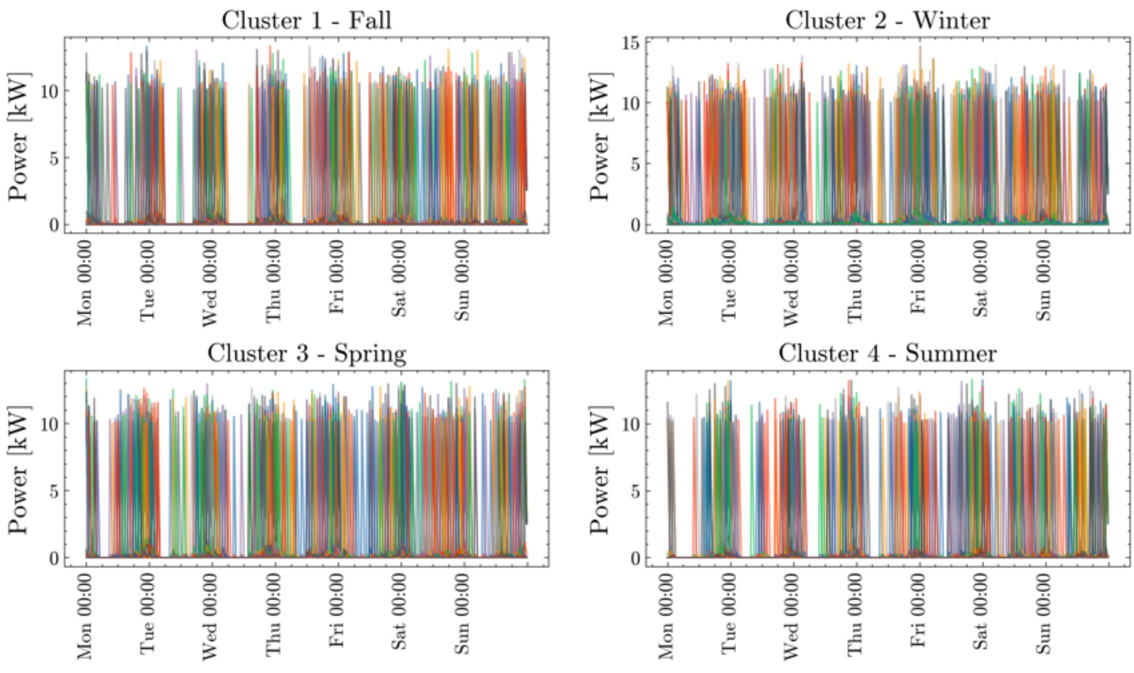

Figure 3.23: Clustered EV home and private shared charging profiles

For the home and private shared charging stations, 11.2kW profiles from EV charging in NKE-Elnet's grid area are used. These profiles are identified using Utiligize's EV charging detection algorithm, and the base load power observed before charging is removed. The resulting clustered profiles are shown in figure 3.23 and result from the observation of 45 cars over the course of a year. The data is available in a 1-hour resolution and is interpolated linearly down to a 15-minute resolution. Due to the lack of data regarding private shared charging, the same profiles are used.

EV workplace charging stations

The EV workplace charging data comes from a dataset published by NREL tracking 300 EVs over the course of four years [56]. The data selected is for 2018, the start and end charging time as well as the max charging power are logged for most of the charging events. For the missing entries, the arrival and departure times are used with a maximum charging power of 3.6kW. This data is used to create load profiles with a 15-minute resolution under the assumption that the vehicle charges at the maximum power during the whole event. The resulting clustered profiles are shown in figure 3.24.

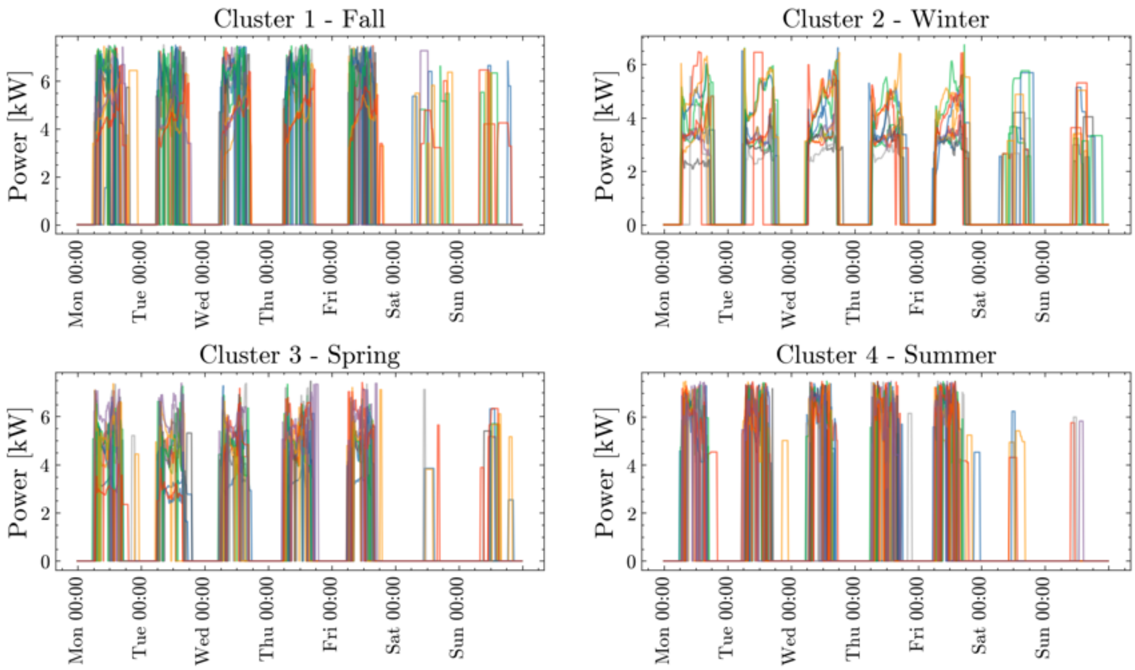

Figure 3.24: Clustered EV workplace charging profiles

EV normal public charging stations

The EV normal public charging profiles are collected from a dataset from the Netherlands, from the research centre ElaadNL [57]. This dataset registered 10,000 charging events in 2019. For each event, the transaction start time, the charge time, the total energy and the maximum power are logged. These are used to create load profiles with a 15-minute resolution under the assumption that the vehicle charges at the maximum power during the whole event. The resulting clustered profiles are shown in figure 3.25.

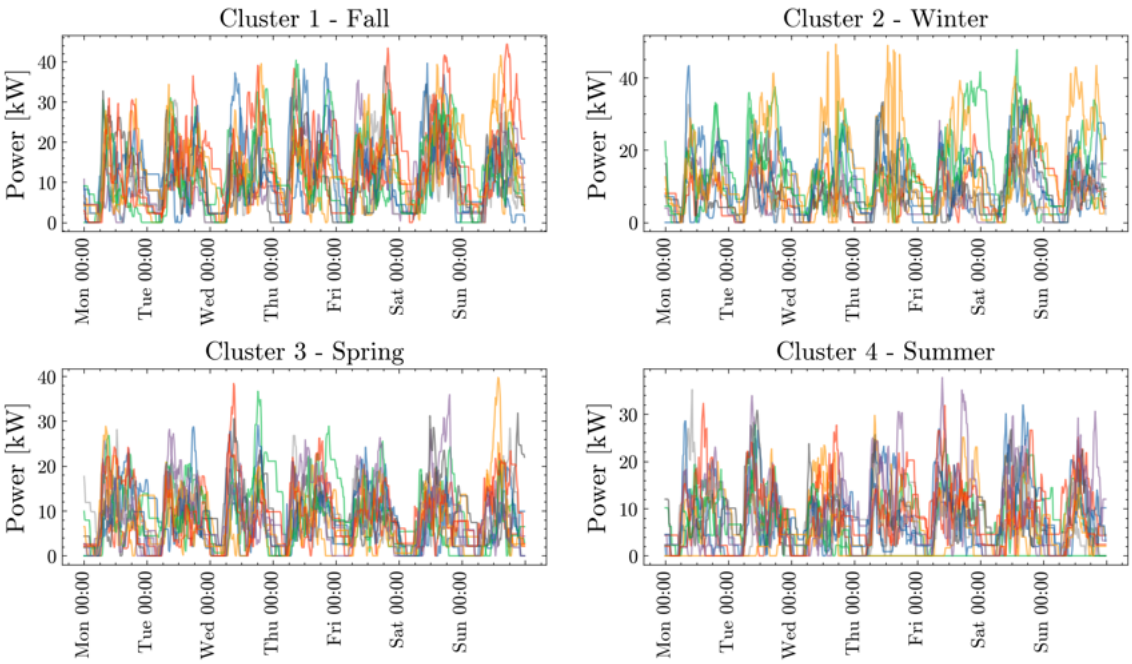

Figure 3.25: Clustered EV public charging profiles

Heat pumps

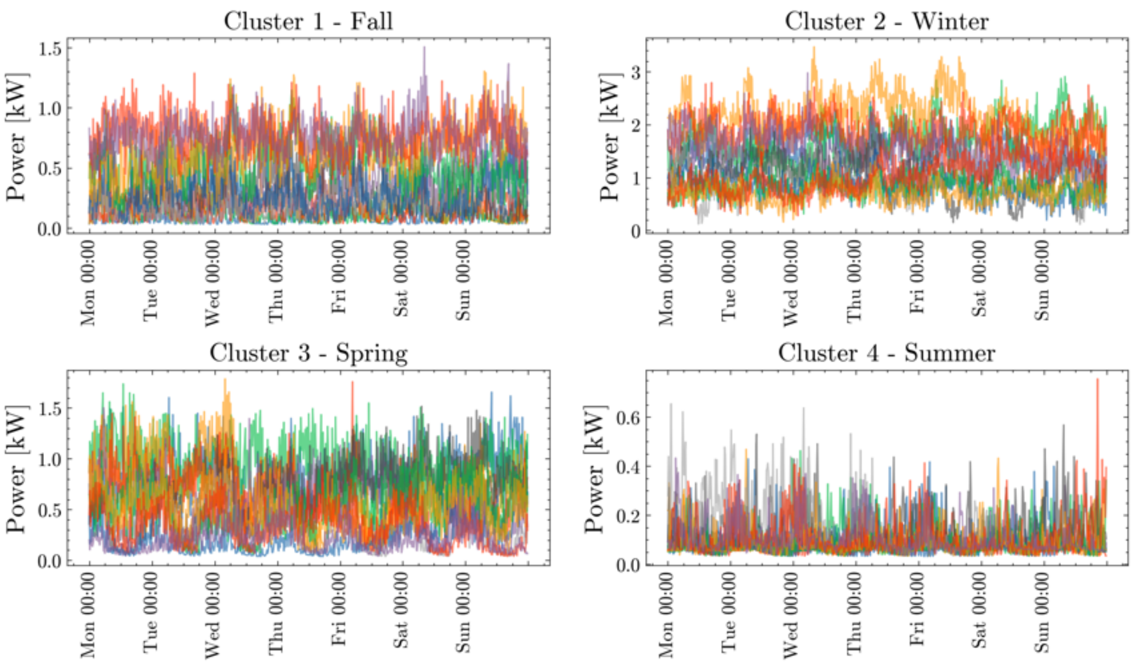

Figure 3.26: Clustered heat pump profiles

The heat pump profiles come from a dataset based on 38 single-family houses in the city of Hamelin, Germany [58]. The profiles are available in a 15-minute resolution, the selected year is 2019. To ensure that the meteorological conditions are similar to those in Næstved, the temperatures of these two locations are compared. The temperature time series for Hamelin is also available in the dataset, the temperature from Næstved is retrieved from the Danish Meteorological Institute [59]. Both temperatures follow the same trend and the mean relative error between the two locations over the year is 2.33%. Both temperature time series are shown in figure D.1. From the 38 profiles, one average year profile is created and split into weeks. The clustered profiles are shown in figure 3.26.

The average German single-family house is $157m^2$ [60]. Because these heat pumps provide only heating and not domestic hot water [58], for each building with a new heat pump, the power will be scaled to the building's area based on the information available from the BBR [46].

PV

The PV load profiles are based on the total PV production in Denmark in 2022 provided by Energinet [61]. The data, in hourly resolution, is linearly interpolated to a 15-minute resolution. The data is then normalised to percent of the PV's nominal power. Because 2022 was a year with a significant increase in PV capacity in the Danish grid with more than 1GW being newly connected [62], it is scaled to 1,664MW being 100%, so that the highest peak delivers 100% of the nominal power. The resulting graphs are shown in figure 3.27.

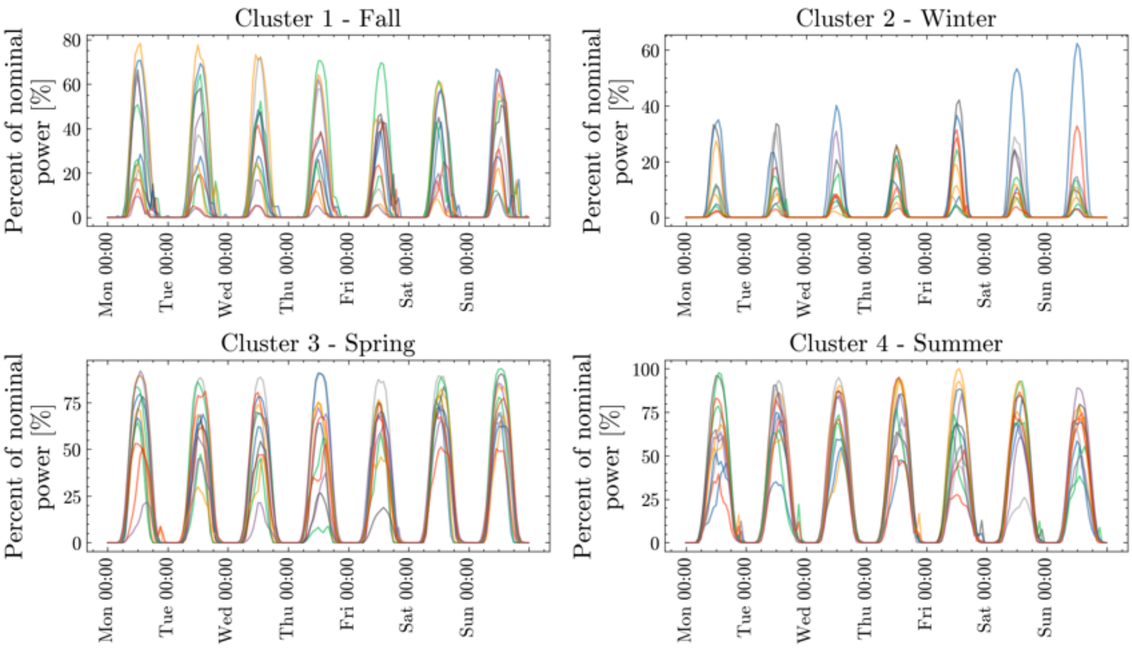

Figure 3.27: Clustered PV profiles

These profiles will then be individually scaled based on the size of each new PV installation described in section 3.5.6. Unlike the other profiles, the same profile will be applied to all installations in one simulation.

For each installation, an inverter efficiency of 97,2% is applied [63]. Regarding the fact that not all installations are placed with a 180° orientation, a stochastic factor based on a normal distribution function where the DC production is set at 100% for a 180° orientation and drops to 75% towards a 90° and 270° orientation is also applied [48], following this logic:

$$f(x) = \frac{1}{(\frac{25}{3})\sqrt{2\pi}} \exp\left(-\frac{1}{2}\left(\frac{x-100}{\frac{25}{3}}\right)^2\right) \tag{3.28}$$

$$\text{factor} = \begin{cases} \text{f(x)} & \text{if f(x)} \leq 100, \quad (3.29) \\ 100 - (\text{f(x)} - 100) & \text{otherwise.} \quad (3.30) \end{cases}$$

3.5.8 Thermal overload and voltage thresholds

The thresholds used for thermal overload and voltage violations are defined in table 3.6 and come from the TEGRA model developed by Green Power Denmark and are used by DSOs across the country [64].

	Loading [%]		Voltage [p.u.]	
	Cables	**Transformers**	**Lower bound voltage**	**Upper bound voltage**
Medium voltage	70	90	0.95	1.025
Low voltage	90	110		

Table 3.6: Loading and voltage thresholds

3.5.9 Economic data

Grid components

The grid component prices (here cables and transformers) are provided by Utiligize. They are based on data from Danish regulatory bodies and DSOs. These are specified in tables 3.7, 3.8, 3.9 and 3.10.

Rating [kVA]	16,000	20,000	25,000
Price [kDKK]	7,200	8,625	9,940

Table 3.7: 50/10kV transformer prices

Rating [kVA]	250	400	600	800	1,000	1,200	2,000
Price [kDKK]	100	130	200	250	325	380	755

Table 3.8: 10/0.4kV transformer prices

Dimension [mm^2]	95	120	150	240	300	400	500
Price [DKK/m]	1,800	1,840	1,880	2,000	2,100	2,150	2,300

Table 3.9: 10kV cables

Dimension [mm^2]	95	120	150	240	300
Price [DKK/m]	465	495	530	620	680

Table 3.10: 0.4kV cables

Grid component age

The age of grid components plays a role in the replacement costs as their value is depreciated over time. Replacing an asset before its economic end-of-life induces therefore additional costs to the grid operator. The economic lifetime of cables and transformers is set to 45 years [21].

The age distribution of assets is shown in figure 3.28. The age of 96% of all transformers is available, the missing ones are estimated as the average of all transformer ages. No age data for cables is available and therefore the age distribution of these assets is assumed to be the same as the average Danish medium and low voltage grid as published by the regulatory agency [65].

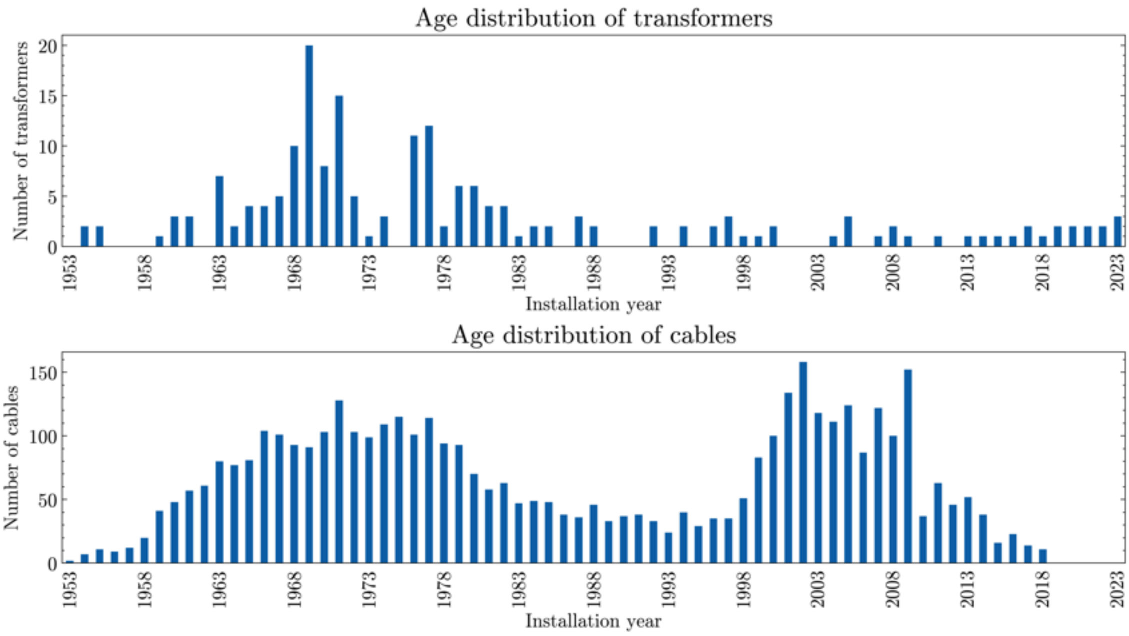

Figure 3.28: Asset age distribution

The remaining value of each asset is calculated as:

$$C_{\mathrm{remaining}} = \frac{C_{\mathrm{new}}}{L \cdot (L - A)} \tag{3.31}$$

With $C_{\mathrm{remaining}}$ the remaining and C_{new} the new asset costs in DKK, L the asset lifetime and A the age at the replacement year both in years.

Batteries

Due to the technological improvements and the increasing scale of production of batteries, these assets are expected to see their costs similarly decrease over the next decades as it happened in the past. A starting price for 2022 of 1.056MDKK/MWh is used and three price evolution profiles from NREL are used for future prices [20, 66].

These values are used as a benchmark when processing results and assessing the total costs of a classic grid reinforcement with cables and transformers with higher ratings. The different scenarios will be used for sensitivity analyses.

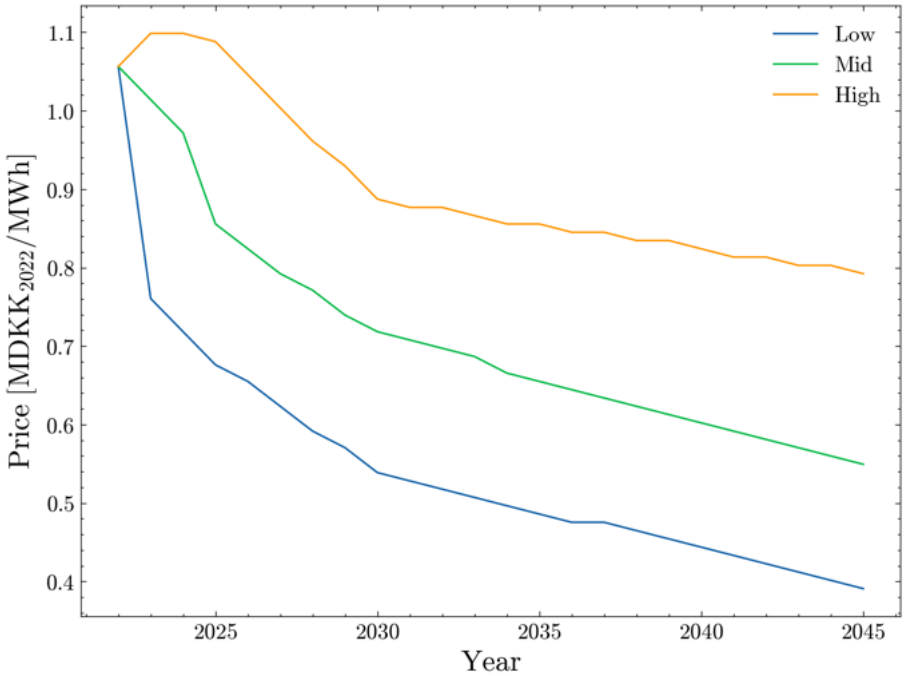

Figure 3.29: Battery prices

3.5.10 Electric grid data

Figure 3.30: Electric grid

The electric grid data is provided by Utiligize in the form of a pandapower net object. The raw data that is fed into the model is provided by NKE-Elnet and the transformation steps from the raw data to the pandapower object are similar to the ones described in [67].

The grid of NKE-Elnet, shown in figure 3.30 starts at the connection points with the DSO Cerius in the form of four 50/10kV transformer stations. The medium voltage grid, which spreads over 110km is then connected by 186 10/0.4kV transformer stations to the low voltage grid which has a total length of 158km. Grid data is available between the 2,700 cabinets and the house connections is not considered, so the individual smart meters are aggregated on these cabinets.

The grid has a typical distribution grid layout in the sense that it is operated in a radial way at both MV and LV levels.

3.5.11 Smart meter data

The smart meter data can be split into two different categories, due to the two types of smart meters cohabitating. 18,522 meters are installed in total, with 18,303 with an hourly resolution and 219 with a 15-minute time resolution. The smart meter values with an hourly resolution are interpolated linearly to get a 15-minute resolution.

In 2022, the peak load in the system happened on January 10$^{\text{th}}$ at 17:00, with a value of 15.751MW.

4 Results

4.1 Base power flow

When running the yearly power flow on the existing grid with the forecasted load and PV production increase, the loading of assets increases steadily. Figure 4.1 displays that the first transformer starts to be overloaded by the year 2028, and by 2045 30% of all transformers experience an overload. The share of cables that experience an overload is smaller but starts earlier. The first cable is overloaded in 2024 and by 2045 10% of all cables experience an overload. A historic simulation based on the 2022 smart meter data show that no thermal overloads are experienced in the grid that year.

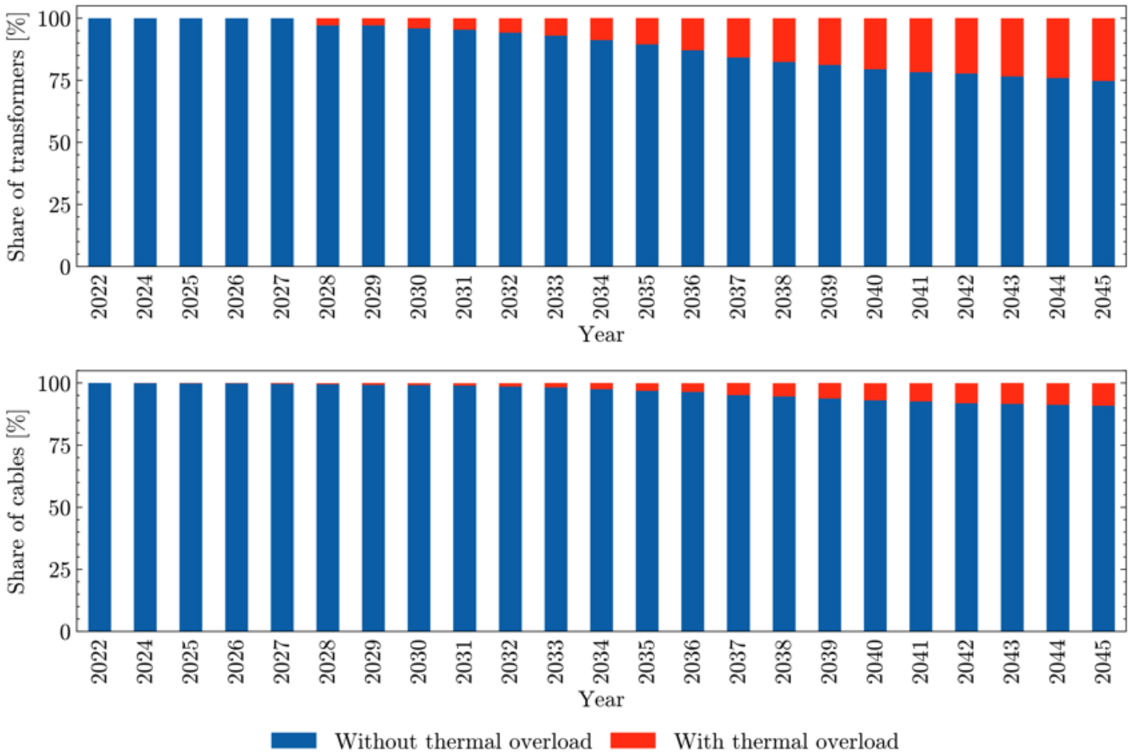

Figure 4.1: Share of overloaded assets per year

Based on the loading distribution over different voltage levels shown in figure 4.2, it can be noted that thermal overloads happen primarily at the low voltage level. Only 18 MV cables are overloaded in 2045 and no MV transformer is, whereas most of the overloads and the most severe ones happen at low voltage cables and transformers, with loadings up to 800% for cables (with most of them laying below 200%) and 300% for transformers. It can be deduced that the MV grid is dimensioned for a significantly higher capacity than the LV grid.

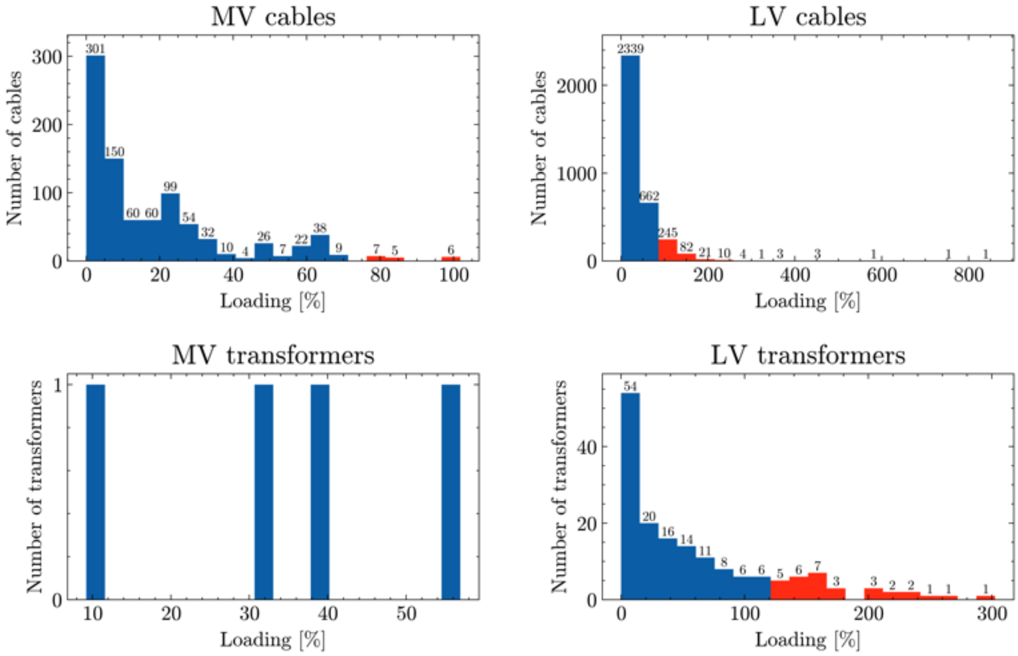

Figure 4.2: Distribution of asset loading in 2045

In terms of voltage issues, the situation is more critical than thermal overloads as shown in figure 4.3. The historic power flow based on the 2022 smart meter data shows that no issues were found for that year. Issues happen from 2024 on and the situation worsens over the years until 70% of cabinets experience voltage issues by 2045.

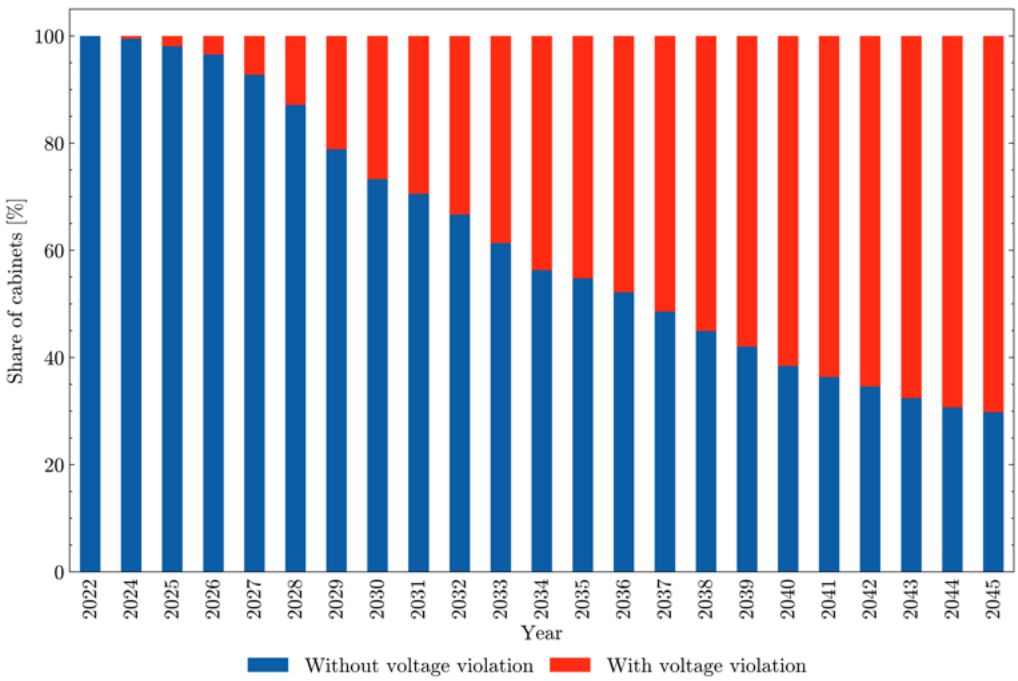

Figure 4.3: Share of cabinets with voltage violation per year

The distribution of this voltage by 2045 shown in figure 4.4 displays that undervoltages spread over a larger range than overvoltages, with 99% of undervoltages laying between

0.78 and 0.95 p.u. (range of 0.17 p.u.) and 99% of overvoltages between 1.025 and 1.116 p.u. (range of 0.089 p.u.). Only 1% of undervoltages and overvoltages happen respectively below 0.8 p.u. and above 1.116 p.u.

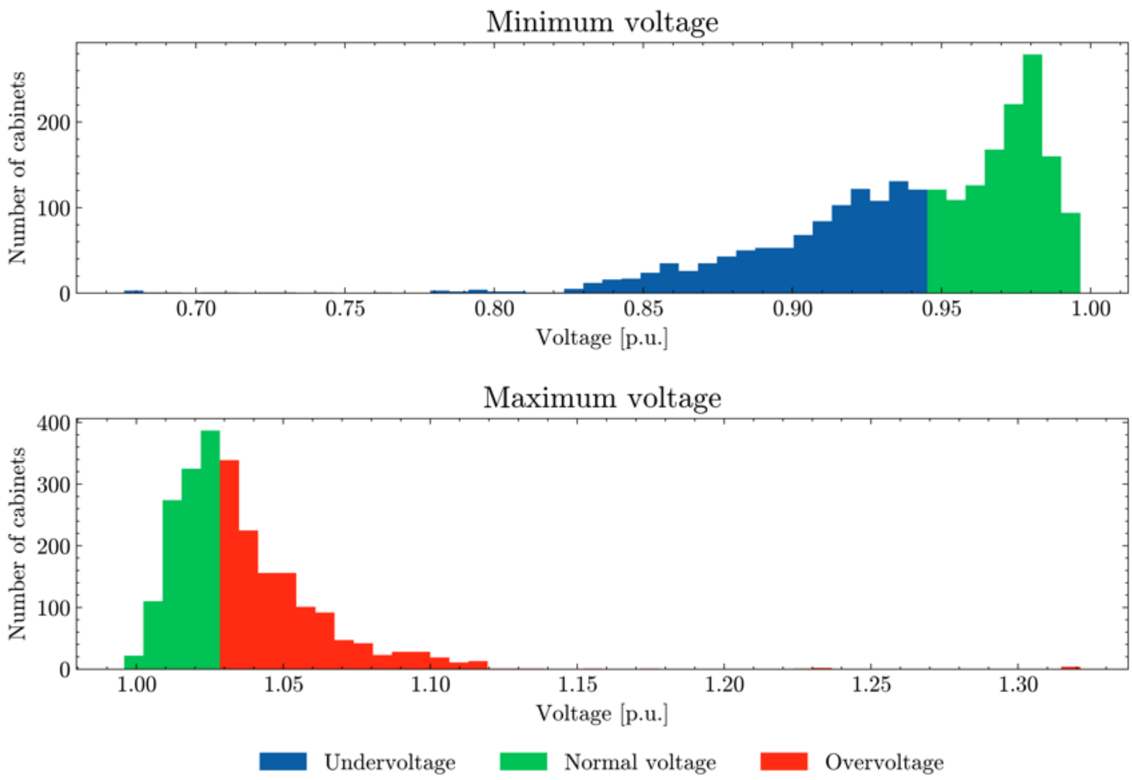

Figure 4.4: Distribution of minimum and maximum voltage at cabinets in 2045

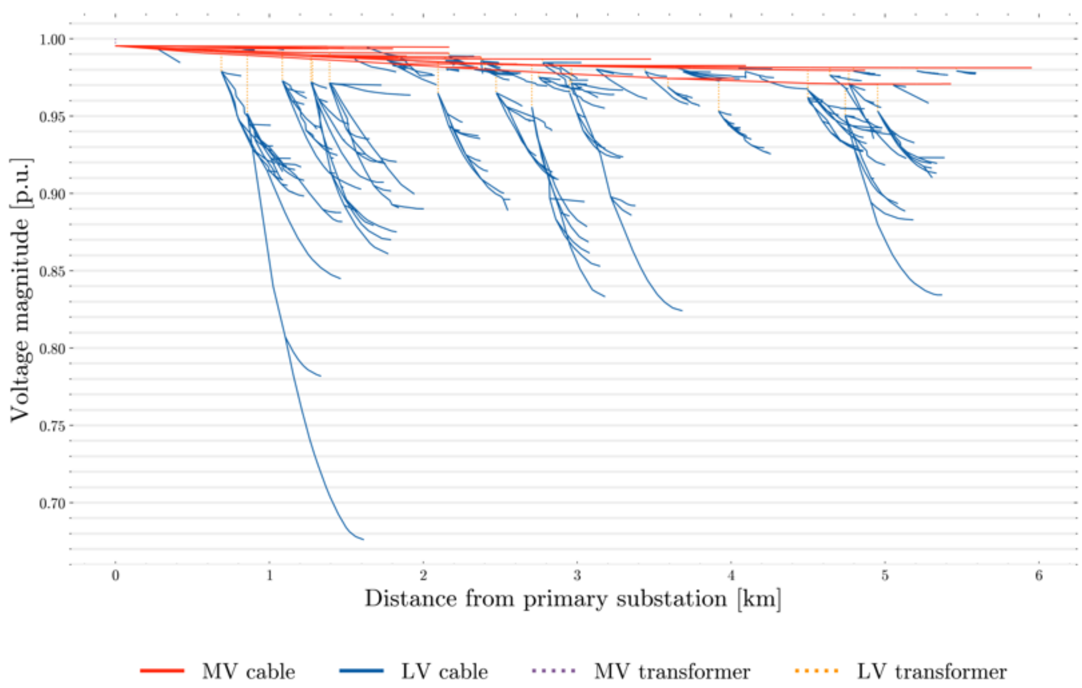

Figure 4.5: Minimum voltage drop plot from one primary substation in 2045

Figure 4.5 gives a different overview of the minimum voltage in 2045 from the primary substation experiencing the largest voltage drop. It can be observed that, similarly to thermal overloads, most issues happen in the LV part of the grid. The voltage drop from the primary substation to the last MV cable is 0.029 p.u., whereas it is 0.304 p.u. between the secondary substation and the last LV cable where the largest drop happens, due to higher currents. The most severe drop to 0.68 p.u., significantly superior to the other can be explained by the large number of DERs connected between the secondary substation and the last cabinet. 290 EV home chargers are connected to this feeder, whereas the average one only has 41 connected.

In terms of maximum voltage as shown in figure 4.6 from the primary substation experiencing the largest voltage increase, similar observations as for the minimum voltage can be made. Most issues happen in the LV part of the grid. Three feeders stand out with voltages going up to more than 1.15 p.u. These feeders are marked by a combination of a higher PV penetration and cables with a smaller dimension than the rest of the grid, with from left to right 1,184kW, 1,996kW and 226kW installed vs. on average 333kW per transformer station. The first feeder, with a lower installed capacity than the second one, experiences a larger voltage increase due to the cable dimensions, being on average 100mm^2 in the first feeder vs. 150mm^2 in the second one. The larger voltage increase in the third feeder over 1.15 p.u. can be explained by the cables with an average dimension of 96mm^2 vs. 148mm^2 across the rest of the grid. The high PV penetration in the LV part of the grid has an impact on the MV part of it as well, since a slight voltage increase can be observed through MV cables the further away they are located from the primary substation.

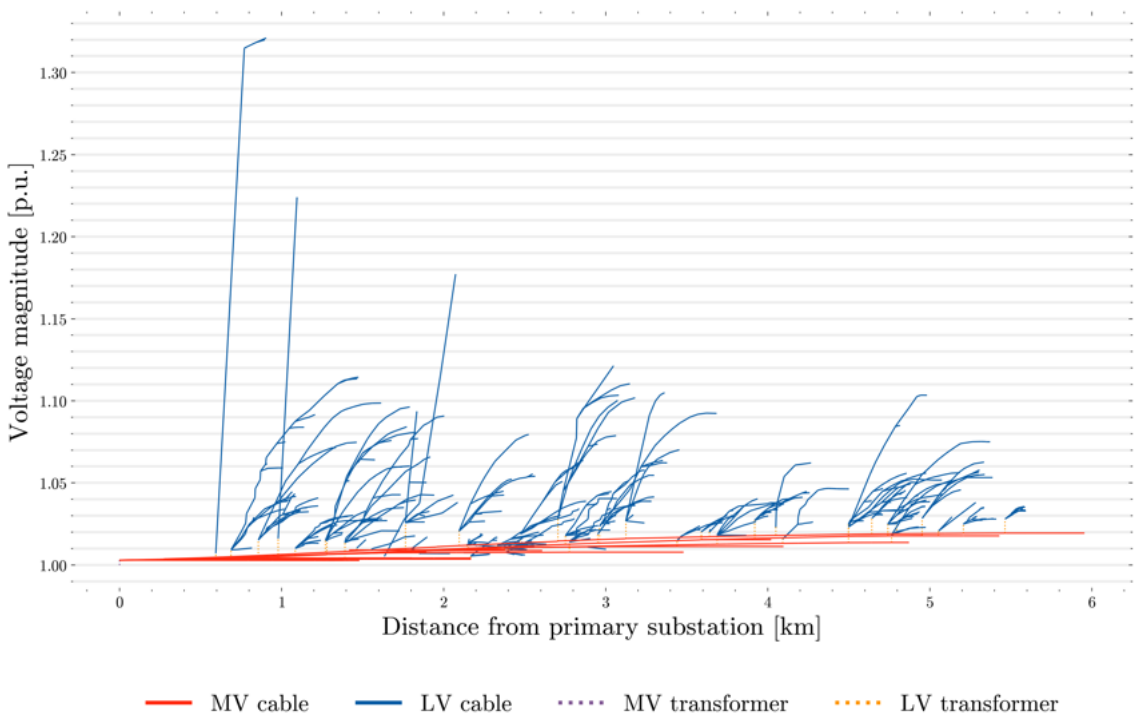

Figure 4.6: Maximum voltage drop plot from one primary substation in 2045

4.2 Power flow with conventional grid upgrade

Once the thermal overload-based upgrade has been applied, the loading across all assets satisfies the overload limits, as shown in figure 4.7.

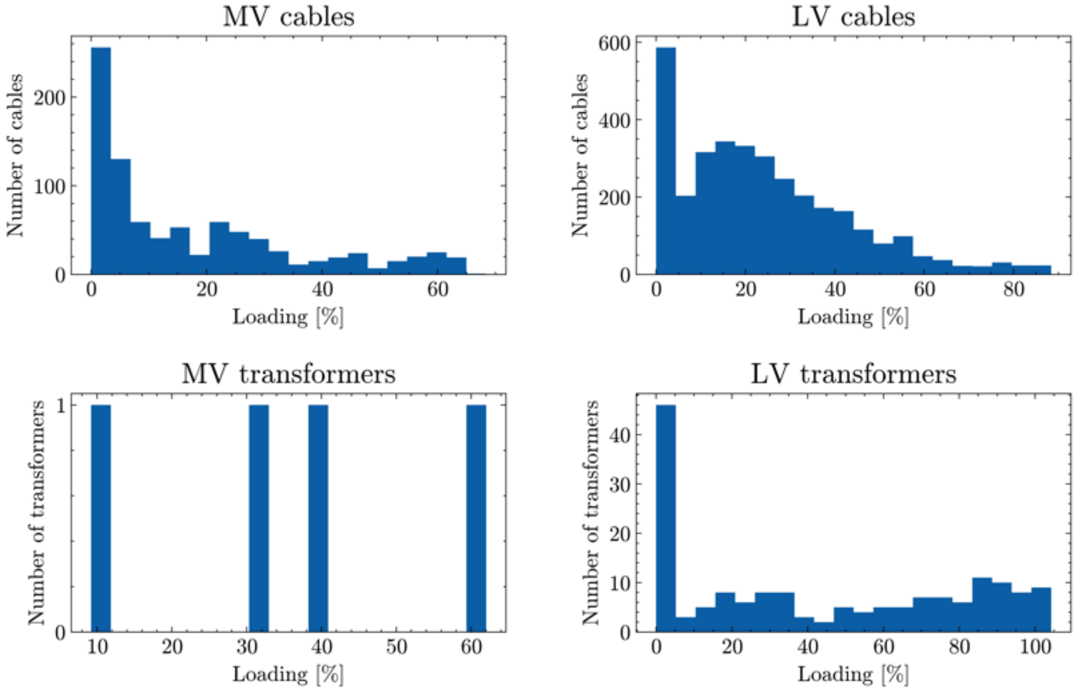

Figure 4.7: Distribution of asset loading in 2045 after overload-related investments

The voltage issues are also mitigated, both due to the reactive power compensation by the PV inverters and to the upgrade where cables with higher ratings also have lower internal resistance, therefore solving some of the voltage issues and minimising overall undervoltages and overvoltages. The voltage issues reduction is shown in table 4.1. The overload-related investments reduce the number of cabinets experiencing undervoltages by 91% and overvoltages by 99.6%.

	Cabinets with undervoltage	**Cabinets with overvoltage**	**Average min voltage [p.u.]**	**Average max voltage [p.u.]**
Without investments	1225	1518	0.957	1.027
With overload investments	109	6	0.972	1.001

Table 4.1: Voltage comparison in 2045

Figure 4.8 displaying the minimum voltage situation shows a pattern where a voltage increase can be observed both in some MV and LV parts of the grid. This is due to the reactive power consumption at PV inverters. This outlines that the minimum voltage situation doesn't happen in all cases when the load is at its highest, which, in a residential grid, is usually in the mornings and evenings when PV production is low or zero. In this case, however, a PV production triggering a reactive power consumption happens during the same time as the load is high, resulting in a minimum voltage situation with an increase from the primary substation.

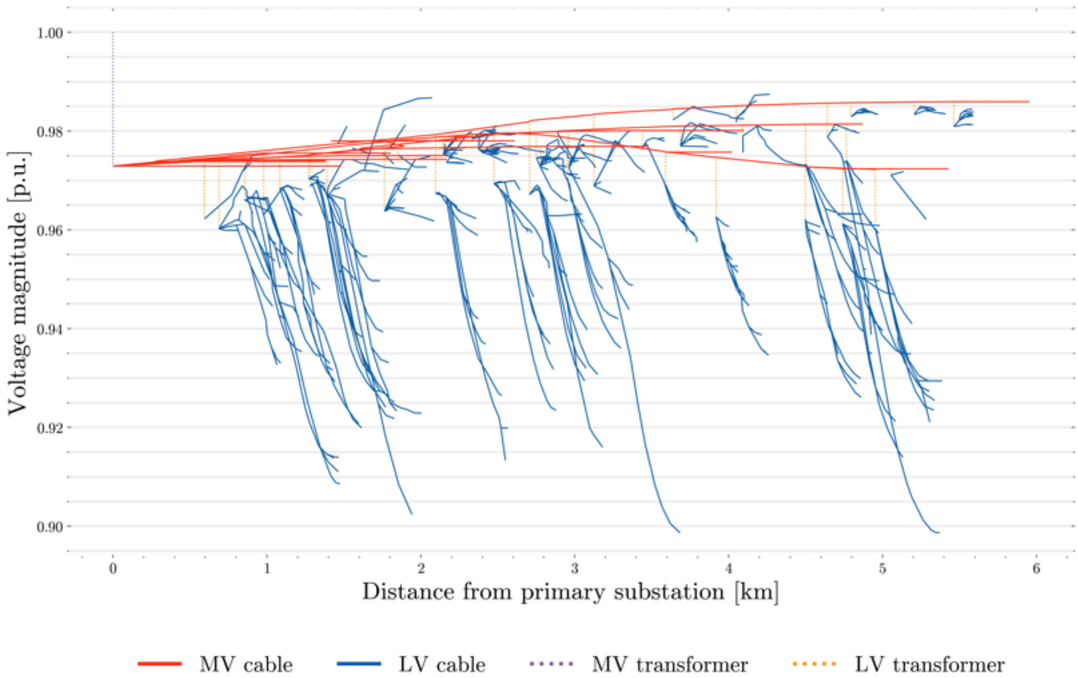

Figure 4.8: Minimum voltage drop plot from one primary substation in 2045 after overload-related investments

Figure 4.9 displays the maximum voltage situation, where only four feeders remain over the maximum voltage limit.

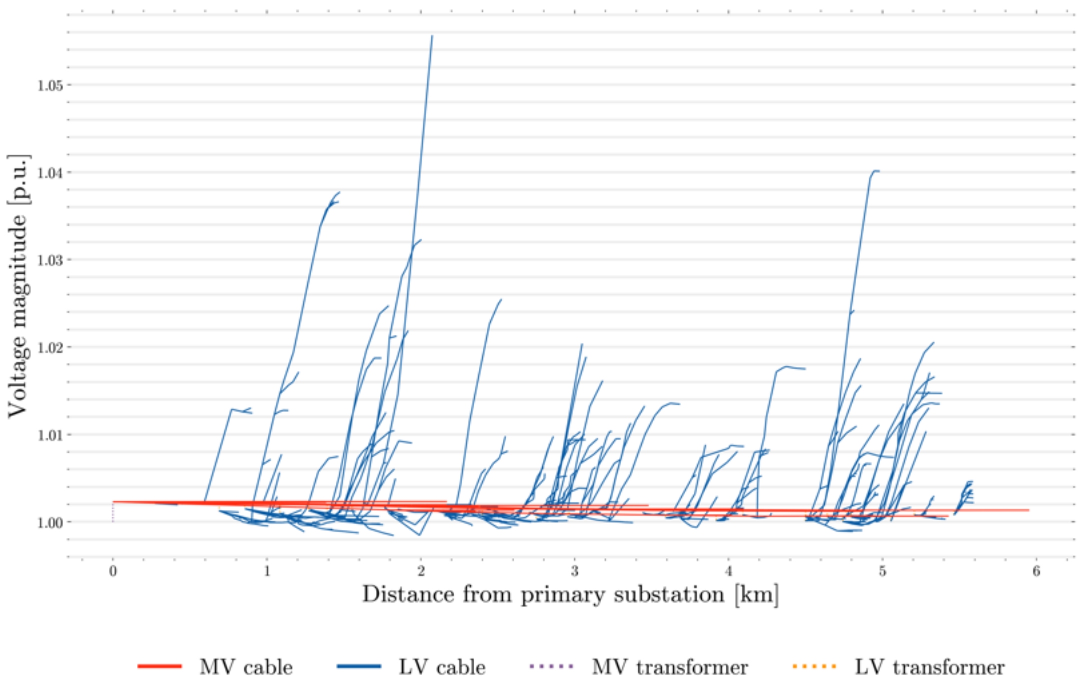

Figure 4.9: Maximum voltage drop plot from one primary substation in 2045 after overload-related investments

Once the voltage issues-related upgrade is also applied to the grid, all voltage issues are solved. Cabinets experience both a minimum and a maximum voltage that satisfies the limits, as outlined in figure 4.10.

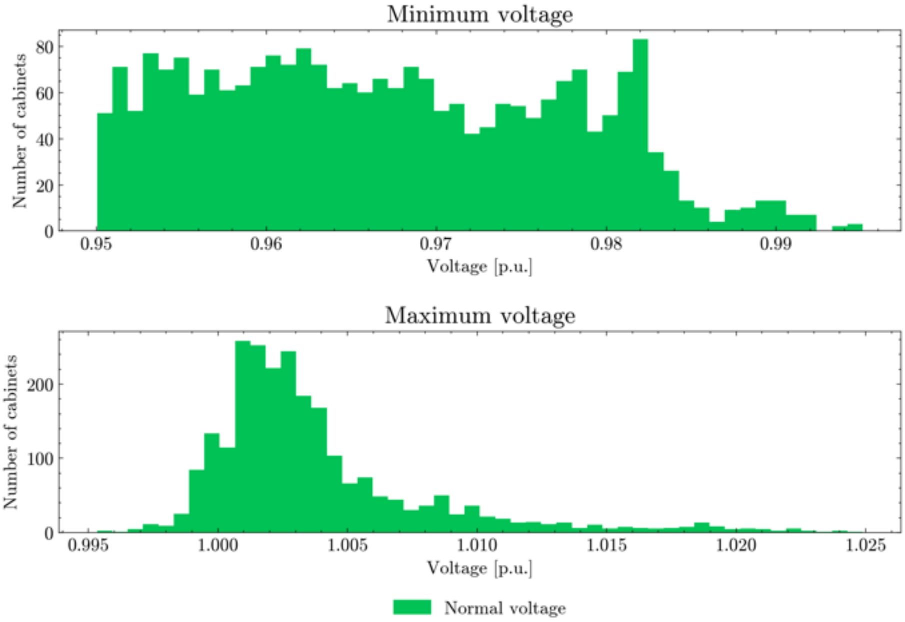

Figure 4.10: Distribution of minimum and maximum voltage at cabinets in 2045 after overload and voltage-related investments

A similar image to 4.8 can be observed in 4.11 where a voltage increase is observed in a minimum voltage situation. The cable upgrade, however, allows all cabinets to lay above the minimum voltage limit by reducing the voltage drops in the LV part of the grid.

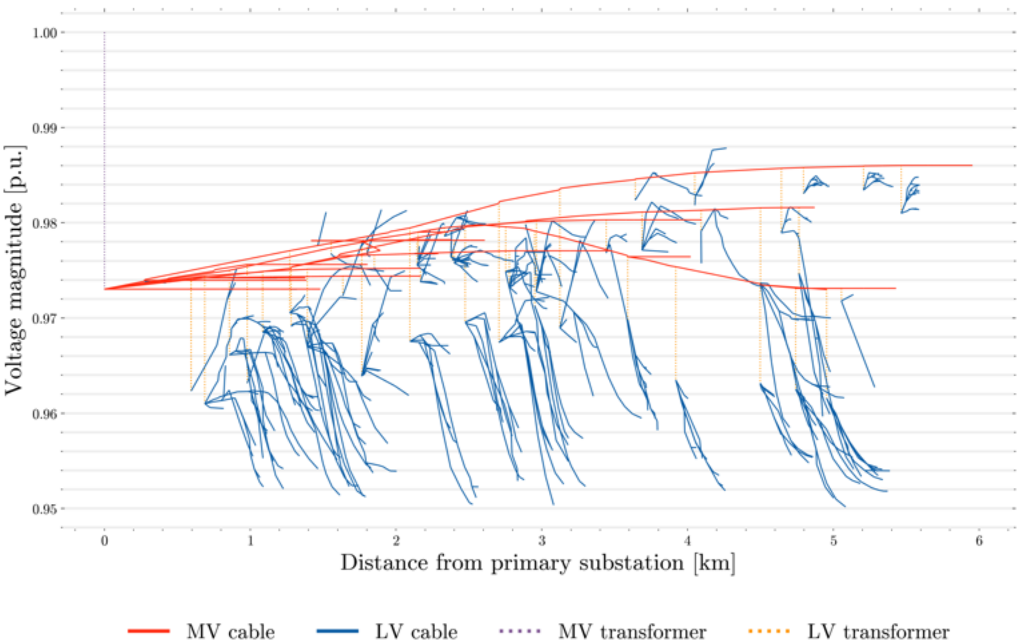

Figure 4.11: Minimum voltage drop plot from one primary substation in 2045 after overload and voltage-related investments

The cable upgrade also solves all issues in the maximum voltage situation, shown in table 4.12.

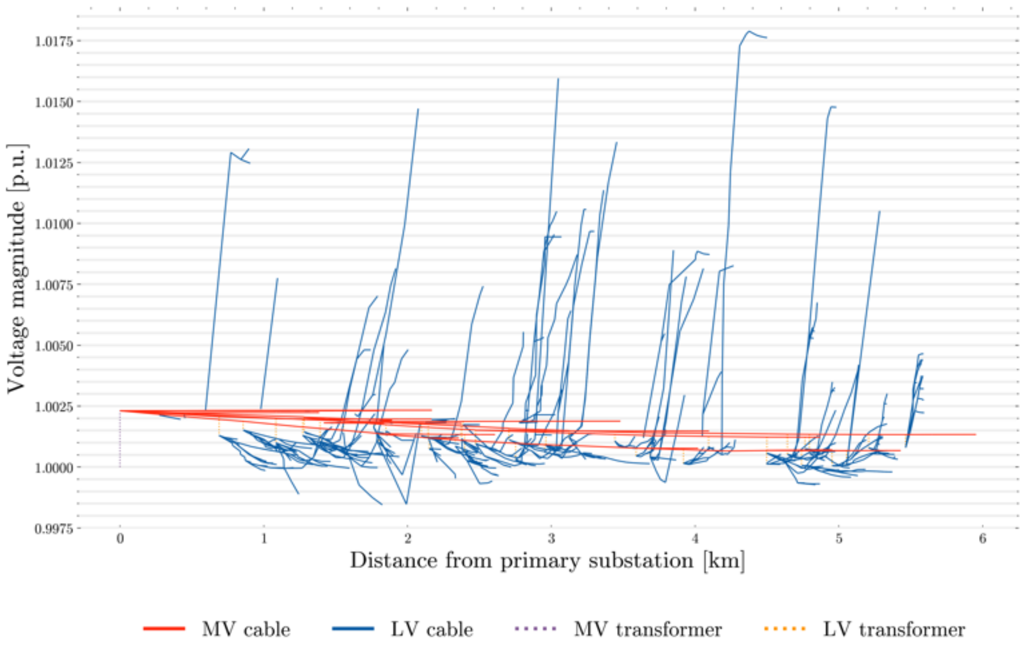

Figure 4.12: Maximum voltage drop plot from one primary substation in 2045 after overload and voltage-related investments

In terms of upgrade costs, figure 4.13 shows that most of the replacement happen at the LV level, corresponding to the experienced overload and voltage issues in the previous section.

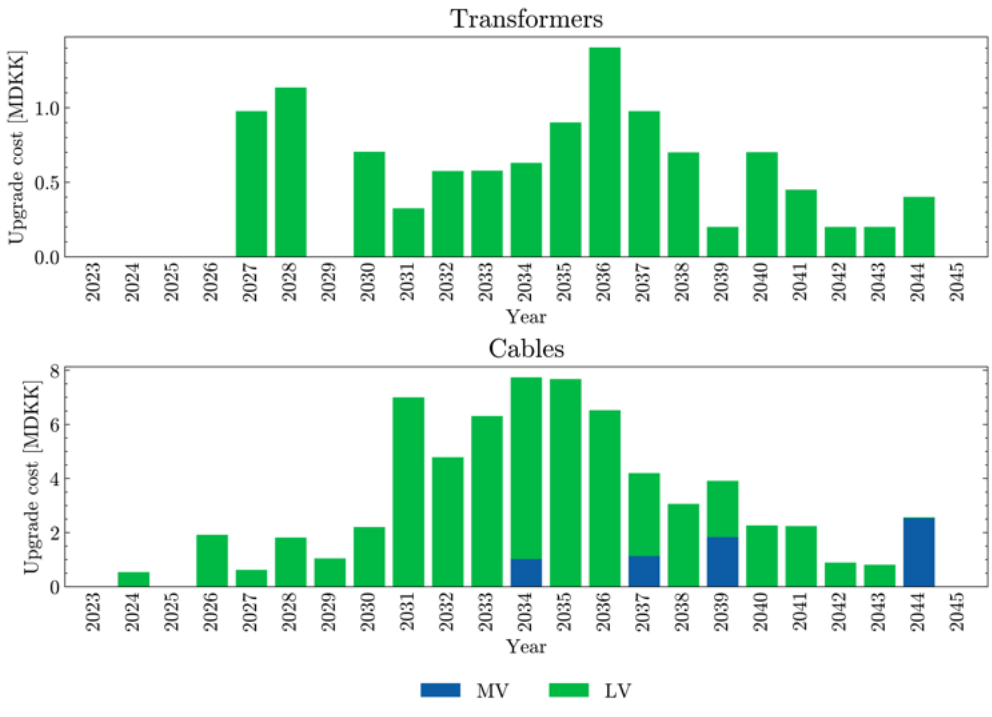

Figure 4.13: Upgrade costs by asset type per year

Only LV transformers are upgraded, most of the upgraded cables are on the LV side as well with only a few MV cables being upgraded towards the middle and end of the simulation. Generally, fewer upgrades are required at the beginning of the simulation due to spare capacity in the grid.

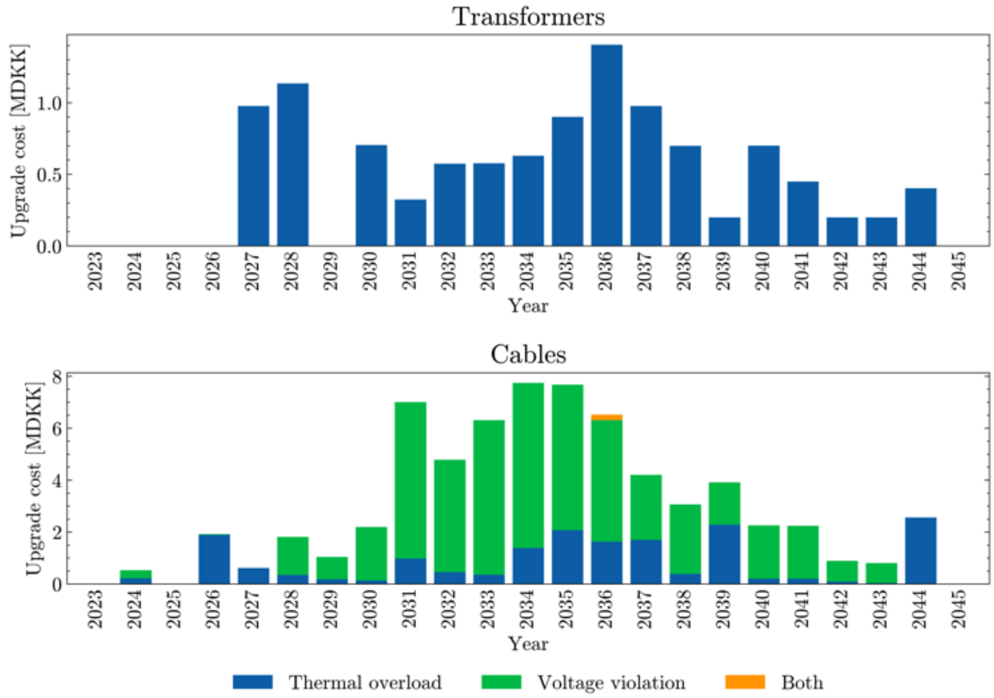

Figure 4.14: Upgrade costs by replacement reason per year

In terms of the upgrade reason displayed in figure 4.14, it can be noted that most of the costs (66%) for cable upgrades are related to solving voltage issues. This can be explained by the need to install parallel cables in some situations to obtain an equivalent internal resistance low enough to satisfy the voltage limits.

It has to be noted that figures displaying upgrade costs only take into account the costs of solving thermal overloads and voltage issues. End-of-life and the resulting replacement costs for assets not impacted to an extent where an upgrade is required due to the rollout of DERs are neither considered nor plotted.

4.3 Power flow with fast charging stations

Connecting the fast charging stations to the grid results in loading and voltage changes at the MV level. The MV transformers and cables get impacted while the LV part of the grid is not due to the new fast charging stations being connected to new secondary substations which are themselves connected to the HV side of existing ones.

Primary Substation	Number of fast chargers	Max loading [%] w/o fast chargers	Max loading [%] with fast chargers	Average loading [%] w/o fast chargers	Average loading [%] with fast chargers
1	1	30.48	31.57	10.26	10.36
2	14	38.51	42.92	15.21	16.39
3	4	9.19	11.80	3.57	3.92
4	8	62.02	60.06	21.63	22.17

Table 4.2: Load change at primary substations due to fast charging stations in 2045

Since all four of the primary substations are modelled as 25MVA and their base thermal loading (i.e. historical consumption and DER rollout) has enough remaining capacity to accommodate for the additional loading, fast charging stations do not have a significant negative impact as specified in table 4.2. The observed maximum loading increase for 2045 lays at 4.41%, representing 1.1MVA for the primary substation to which 14 fast charging stations are connected. Interestingly, the maximum loading at the primary substation number four decreased when installing fast charging stations. The time series show that during the months with little to no sun, the loading at this primary substation shows an increase, whereas it decreases when PV produces a larger amount of electricity. What is happening is that the fast charging stations consume some of the locally produced PV electricity, reducing the feeding back to higher voltage levels and therefore supporting the grid at its highest loading.

Regarding MV cables, a more significant loading increase in comparison to primary substations is observed. Table 4.3 summarizes the average loading over all MV cables connecting a primary substation with a fast charging station.

Max loading [%] w/o fast chargers	Max loading [%] with fast chargers	Average loading [%] w/o fast chargers	Average loading [%] with fast chargers
55.83	70.73	23.66	32.35

Table 4.3: Average load across MV cables connected to fast charging stations in 2045

Overloads are identified at five MV cables. These cables connect a primary substation to a fast charging station and usually experience a single or a few additional peaks due to the combined power of multiple EVs charging at the same time. Figure 4.15 displays such a situation where the power transmitted through a cable experiences a sharp peak at a single timestamp due to 862kW being requested from the fast charging station.

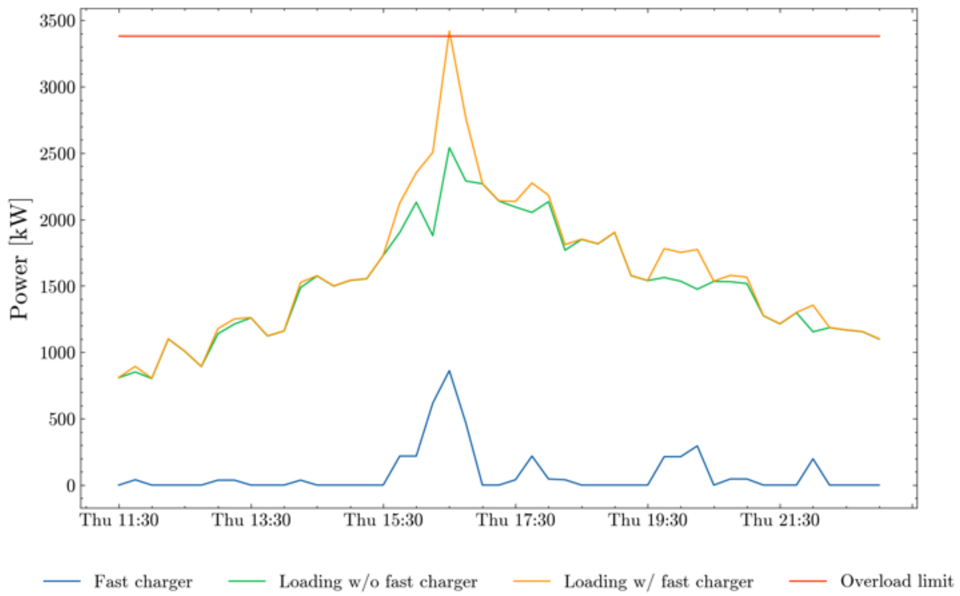

Figure 4.15: Cable loading comparison with and without fast charging station in 2045

In terms of voltage, a minimal decrease can be observed. When comparing the minimum voltage at buses connected to a fast charging station in table 4.4, a voltage decrease of 0.04% for the average minimum voltage and 0.22% for the average mean voltage is observed. This decrease at the HV side of secondary transformers doesn't trigger further undervoltage issues in the LV part of the grid.

Min voltage [p.u.]		**Average voltage [p.u.]**	
w/o fast chargers	**with fast chargers**	**w/o fast chargers**	**with fast chargers**
0.9757	0.9753	0.9853	0.9831

Table 4.4: Average voltage across buses connected to fast charging stations in 2045

4.4 Power flow with fast charging stations and conventional grid upgrade

In figure 4.16 is plotted the upgrade and extension costs for installing fast charging stations in the grid. As outlined in the previous section, only a few MV cable sections need to be upgraded towards the end of the simulation in 2038 due to thermal overloads caused by the number of new fast charging stations and their utilisation due to the higher EV penetration.

Most of the costs (91%) are related to installing the infrastructure, i.e. new transformer station and their connection to the existing grid to accommodate for the fast charging stations.

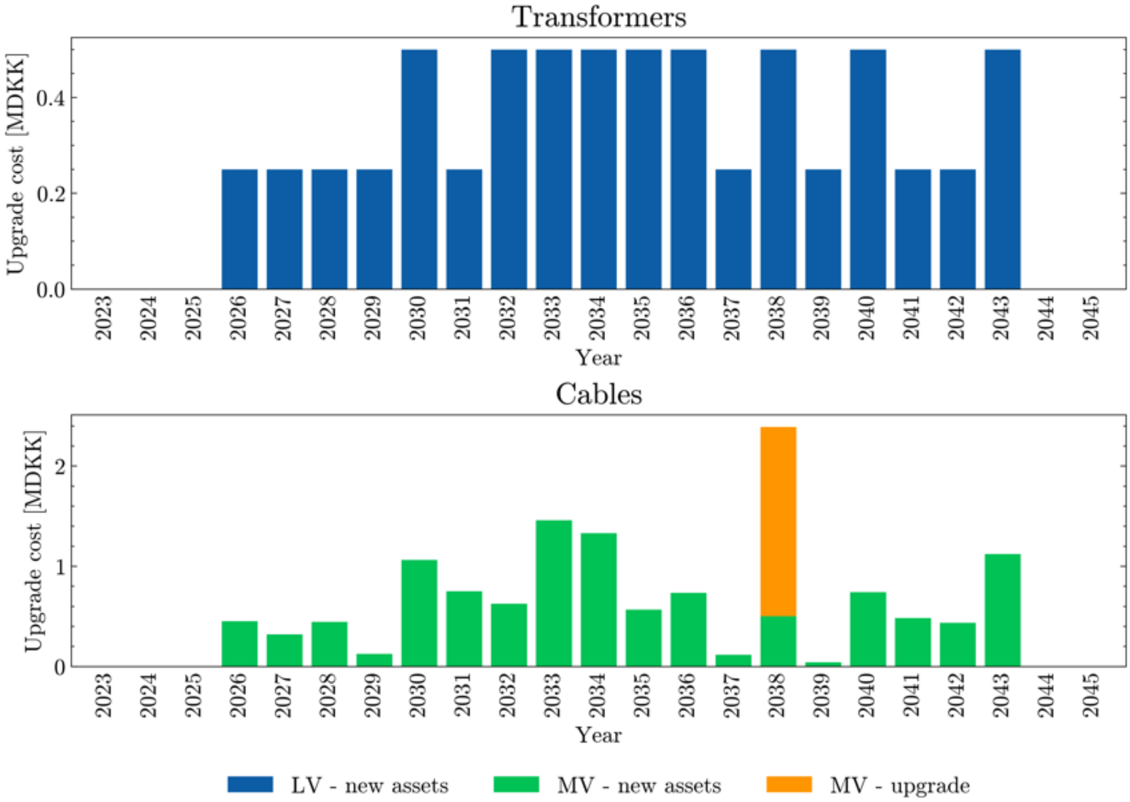

Figure 4.16: Upgrade and extension costs by replacement reason and asset type per year

The grid upgrade on the previously overloaded MV cables removes the overload by reducing the loading over these cables as specified in table 4.5.

Max loading [%]		**Average loading [%]**	
w/o investment	**w/ investment**	**w/o investment**	**w/ investment**
70.73	68.00	32.35	32.08

Table 4.5: Average load across overloaded MV cables connecting to fast charging stations in 2045

4.5 Battery sizing

The results of the optimisation algorithm presented in section 3.3.1 are shown in table 4.6. These results are based on the individually generated fast charging station profiles and an equal weight factor of 0.5 on the maximum charging power and the capacity is applied. It can be noted that the distribution between minimum and maximum charging power and capacity are relatively spread out, with the minimum and maximum values being respectively 64% and 146% of the mean value for the maximum charging power, and similarly 70% and 154% for the capacity. The boxplots in figure 4.17 show the median as the green line and the upper and lower whiskers represent the minimum and maximum values. The standard deviation is 20.05kW for the maximum charging power and 149.48kWh for the capacity.

Fast charger	Max charging power [kW]	Capacity [kWh]	Fast charger	Max charging power [kW]	Capacity [kWh]
1	73.73	1,010.24	15	92.66	754.87
2	79.25	826.97	16	108.92	572.26
3	130.48	557.92	17	93.77	743.92
4	150.53	461.27	18	106.46	679.07
5	129.66	478.72	19	115.45	507.58
6	96.81	789.30	20	109.92	510.80
7	88.02	665.94	21	66.06	888.57
8	120.00	557.92	22	120.48	485.55
9	102.29	653.59	23	77.12	823.33
10	93.94	708.59	24	81.84	787.81
11	77.46	882.54	25	104.18	621.14
12	116.08	484.60	26	119.99	538.19
13	127.95	505.13	27	94.42	726.28
14	97.46	534.55			

Table 4.6: Individual profiles battery sizes

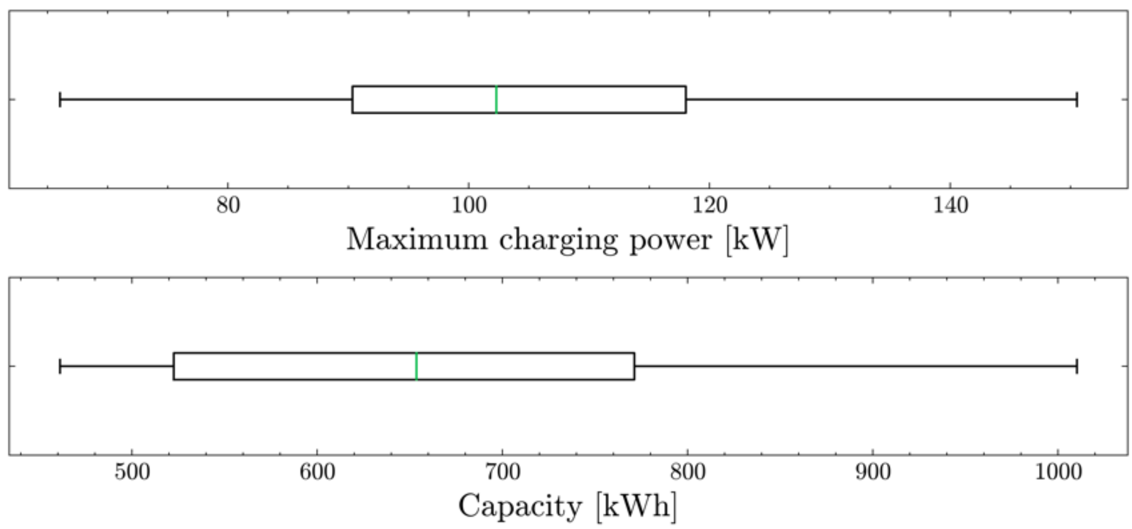

Figure 4.17: Battery parameters distribution

To explain the differences between the different combinations of maximum charging power and capacity, the section of the profiles of the battery with the largest capacity (FC-1) and the one with the largest charging power (FC-4) where the SOC reaches the minimum value are shown respectively in figures 4.18 and 4.19. The profile of FC-1 is characterised by six medium charging peaks of around 250kW, followed by three large peaks of around 400kW, followed again by four medium peaks during the recharging phase. A total of 1.075MWh is consumed over a period of 15 hours, duration between the last SOC of 90% and when the lower limit of 10% is reached. To minimise equally charging power and capacity, the optimum combination tends therefore towards a larger capacity that can be slowly recharged.

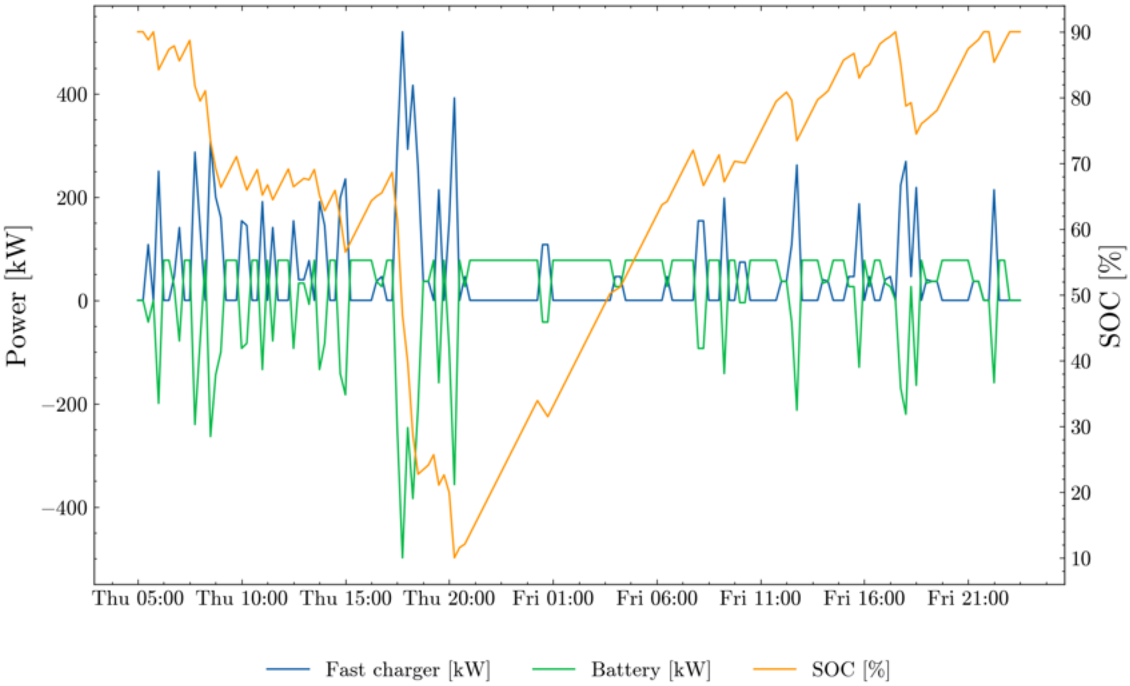

Figure 4.18: Profile of FC-1 at the lowest SOC in 2045

Regarding the battery with the largest charging power, the profile from the fast charging station shows one peak reaching 500kW with multiple charging sessions spreading over 1h30. These 350kWh require a much smaller capacity than in the previous case and the relatively large charging power of 150.53kW is the optimum for minimising the battery capacity at the same weight factor.

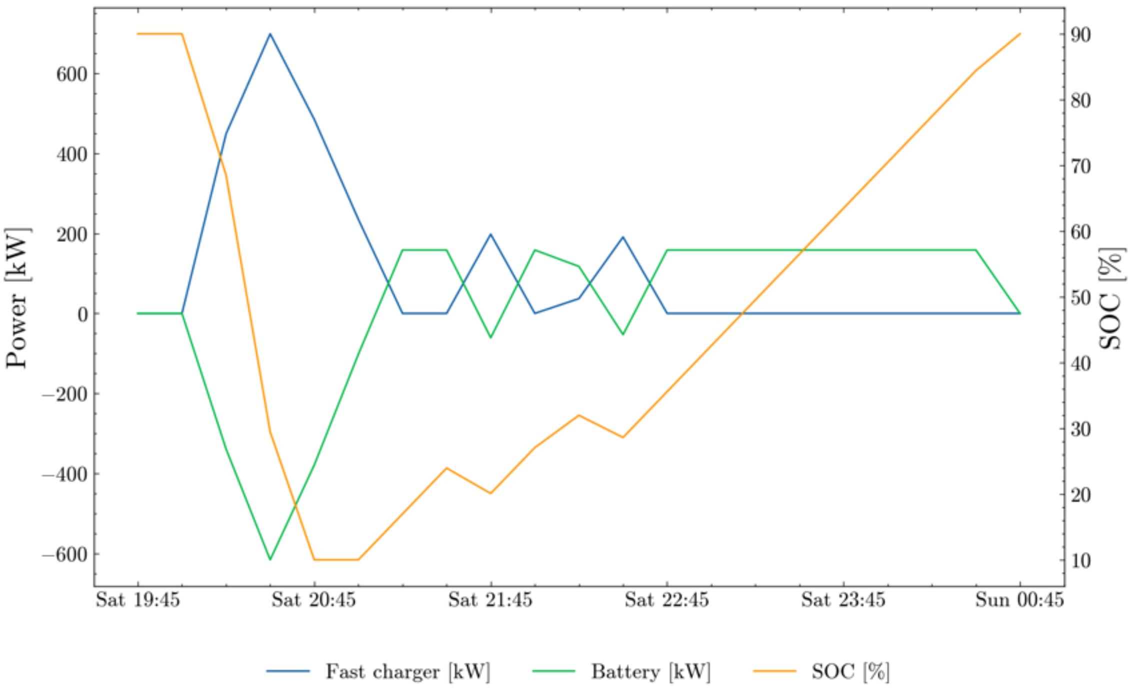

Figure 4.19: Profile of FC-4 at the lowest SOC in 2045

The larger the capacity, the smaller the maximum charging power requirement as the graph in figure 4.20 where weight factors are applied on both capacity and maximum charging power, starting with respectively 0.1 and 0.9 on the left of the x-axis and going to 0.9 and 0.1 in 0.1 increments to the right of the x-axis.

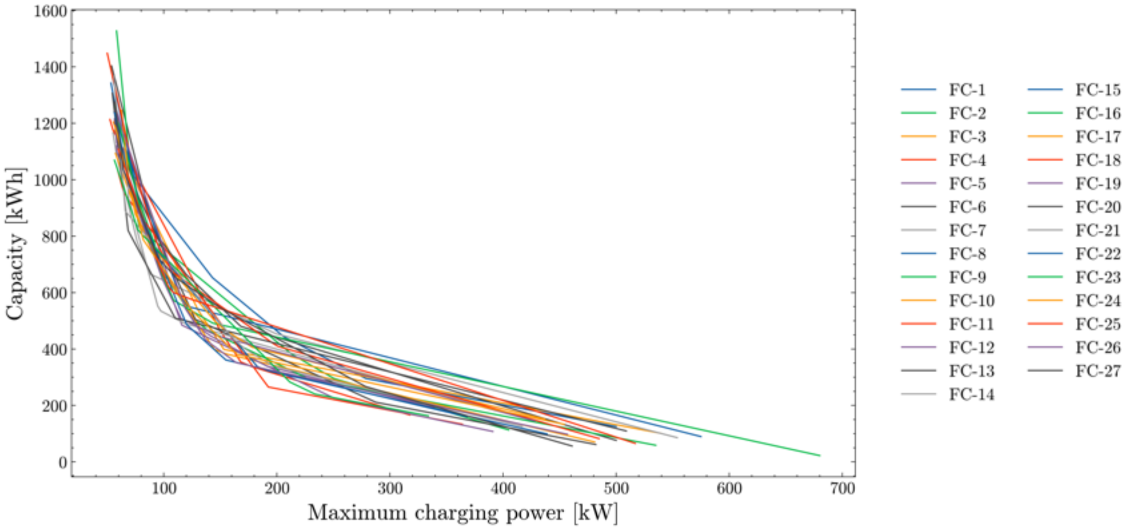

Figure 4.20: Individual profile battery sizes based on weight factors

4.6 Power flow with fast charging stations and battery-based grid upgrade

Since the batteries dimensioned in the previous section are based on a unique load profile, it means that they could not be able to provide support for a slightly different profile. This is the reason why the optimisation algorithm is run with multiple profiles. To take this uncertainty into account, one common size parameter needs to be chosen. In table 4.7 are shown power flow results based on which set of parameters are chosen.

	Sizing based on largest charging power	**Sizing based on largest capacity**	**Sizing based on largest charging power and capacity**
Number of fast chargers violating the grid connection power	4	14	0
Number of timesteps with violation	6	30	0
Maximum power above grid connection allowance [kW/%]	73.14 / 85	315.52 / 179	0
Mean power above grid connection allowance [kW/%]	12.19 / 14	6.28 / 4	0

Table 4.7: Battery sizing common parameters

By selecting the set of parameters with the largest charging power (i.e. 150.53kW &

461.27kWh) or with the largest capacity (i.e. 73.73kW & 1,010.24kWh), thermal overloads happen in the grid. Only taking the combination of both largest parameters (i.e. 150.53kW & 1,010.24kWh) removes all of these overloads.

This over-dimensioning, however, results in low utilization of the battery's capacities, making the economic investment less interesting. Using the battery to provide other services (deferral of investment in other assets for thermal overload or voltage issue reasons) is required to minimise these investments. The SOC duration curve in figure 4.21 shows the percentage of timestamps per year where the SOC is equal to or greater than a certain value. For the combination of the largest charging power and capacity, no battery reaches ever the lowest SOC of 10%. Across all batteries, the SOC never reaches below 35% and it is 90% of the time above 85%.

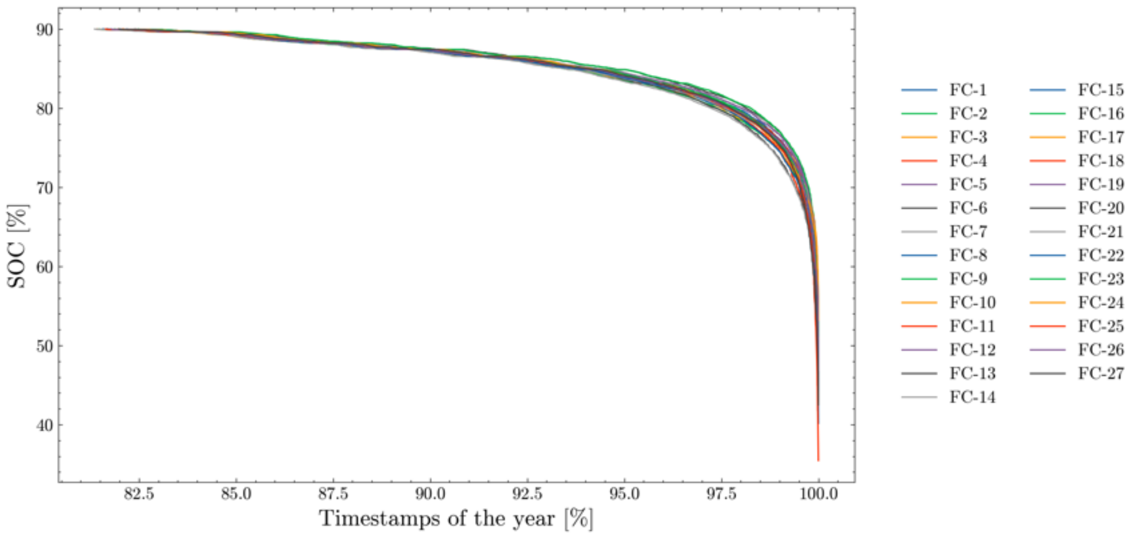

Figure 4.21: SOC duration curve without additional support in 2045

4.6.1 Conventional-like topology

For this topology, the power flow calculation is run on the grid before the investments regarding overloads caused by fast charging stations. The installed batteries are used to remove these overloads by compensating and injecting more power into the grid if required. The batteries charge at the fixed power of 150.53kW as calculated in section 4.6 and inject their power back if the demand at the fast charging station is above this power limit.

Fast charging station-caused thermal overloads

The results show that the overloads happening in the five MV cables after connecting fast charging stations can be resolved by using the battery's active power controller. Due to the low number of newly overloaded assets and the low number of timestamps in which these overloads happen, the batteries' sizing gives enough spare capacity in addition to supplying power to the fast charging stations.

The graph in figure 4.22 shows a section of the time series results of one of the overloaded cables. It can be observed that during the highest peak resulting in an overload, the battery provides 83% of the required power at the fast charging station and only 150.53kW comes from the grid. This removes the overload and significantly decreases the peak loading. After this peak, the cable loading is slightly higher in the situation with batteries than without due to the recharging power being drawn from the grid.

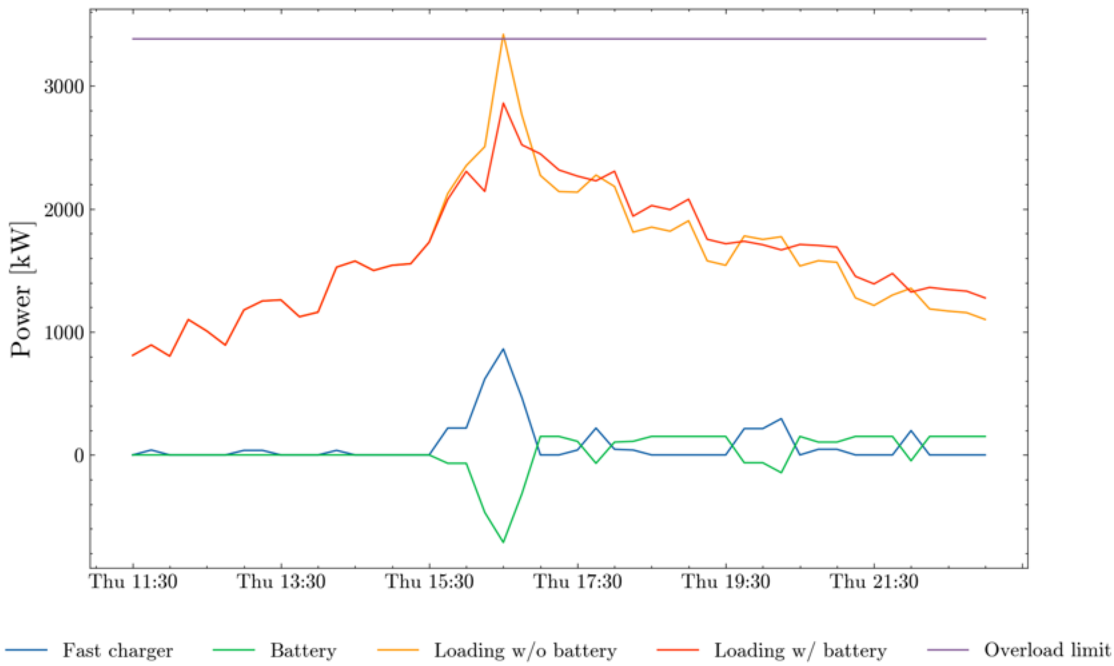

Figure 4.22: fast charging station-related overloaded cable loading with and without battery in 2045

DER-caused thermal overloads
The installed batteries can also provide support to solve thermal loading issues for cables that got overloaded due to the DER rollout and required an upgrade in the first iteration described in section 4.2. To analyse this potential, a power flow is run on the original grid without any investments at MV level and the battery controllers are set to adapt their power setpoint based on the loading of the MV cables between the primary substations and the batteries. The results in table 4.8 show that for the 18 secondary substations to which batteries are connected (some stations have two to three batteries connected), thermal overloads happen in the upstream cables at three stations and can be completely removed for one station. The severity of overloads can be decreased for the two other secondary substations, but the number of overloaded cables remains the same.

	Without batteries		**With batteries**	
Transformer station	**Thermal overloads**	**Average overload [%]**	**Thermal overloads**	**Average overload [%]**
1	14	19.00	14	12.57
13	4	15.43	0	-
14	11	21.18	11	15.87

Table 4.8: Number of MV cables with thermal overload issues per secondary substation with a fast charging station

The reason why the number of overloaded cables can't be decreased for the secondary substations 1 and 14 is shown in figure 4.23. The overloaded cables upstream of these two secondary substations connect a total of three fast charging stations. For visualisation purposes, the sum of the fast charging stations and batteries power as well as the average SOC are plotted. The time series section of one of the cables shows that it starts to be overloaded and the batteries act in the expected manner by injecting more power into the grid. The cable loading is brought back to an acceptable level, until all three batteries reach their minimum SOC, therefore not being able to support the grid anymore. At the same time, there is a demand at two of the fast charging stations, resulting in an additional overload. This situation happens multiple times over the year, resulting in an overall lower number of overloaded timestamps (from 2.8% to 0.7% of the year) and a lower severity, but still requiring a conventional cable upgrade.

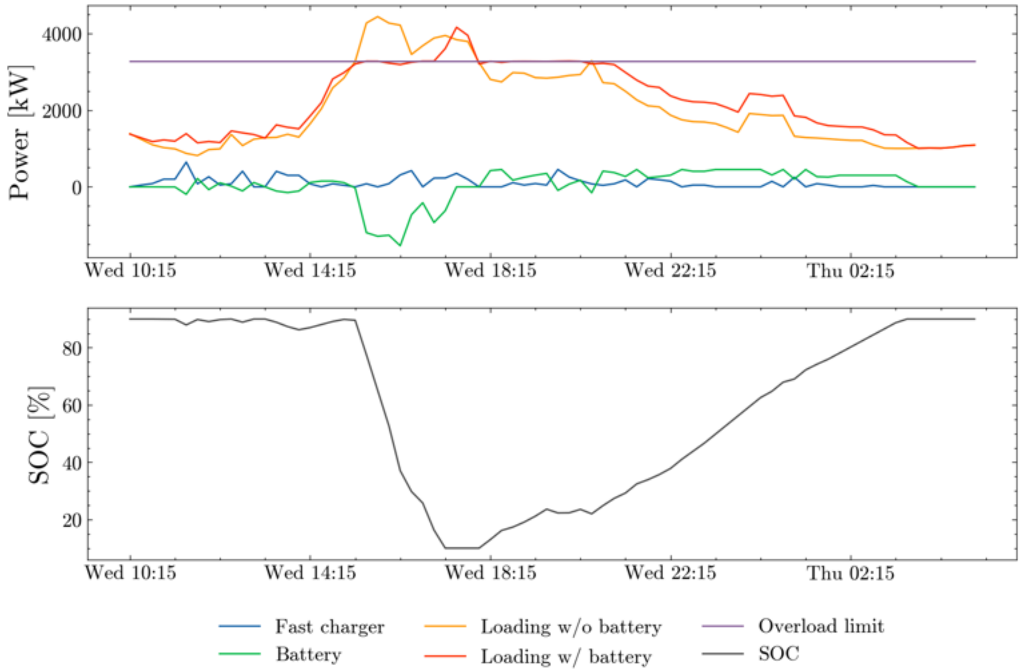

Figure 4.23: DER-related overloaded cable loading with and without battery in 2045

Figure 4.24 displays a time series section of the battery's action on one of the overloaded cables from secondary substation 13 where the issues are solved.

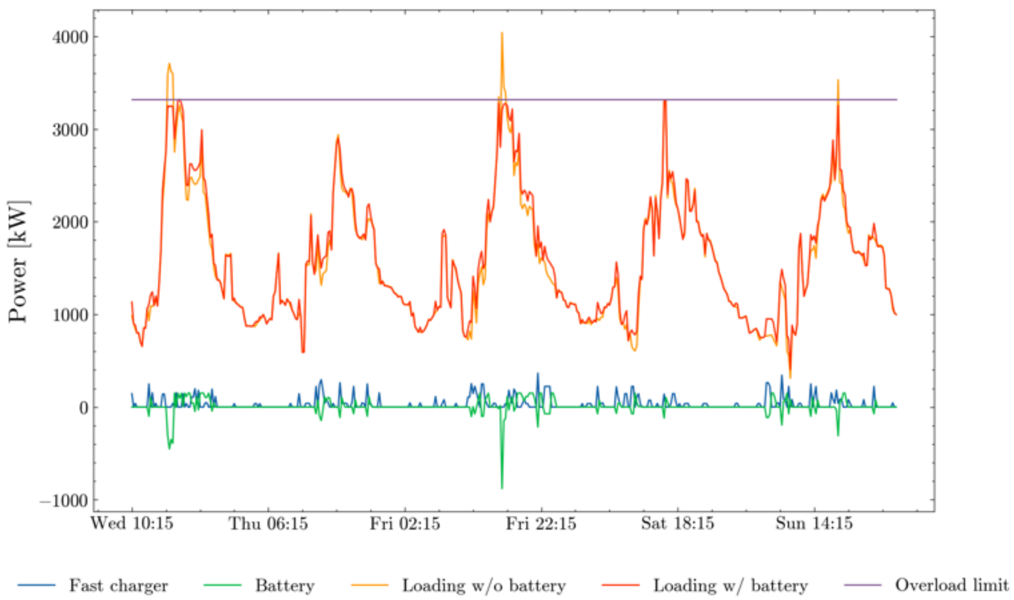

Figure 4.24: DER-related overloaded cable loading with and without battery

It can be observed that for the three overload peaks, the battery injects active power in the grid that is not required by the fast charging station and is therefore directed at relieving the cable loading. The other differences between the two cable time series are that neither the battery nor the fast charging station is connected during the power flow resulting in the orange curve.

In terms of battery utilisation, figure 4.25 shows the SOC duration curve of one of the batteries providing additional support. This support results in a higher utilisation but doesn't have a major impact as the lowest SOC during the year drops from 44% to 40%.

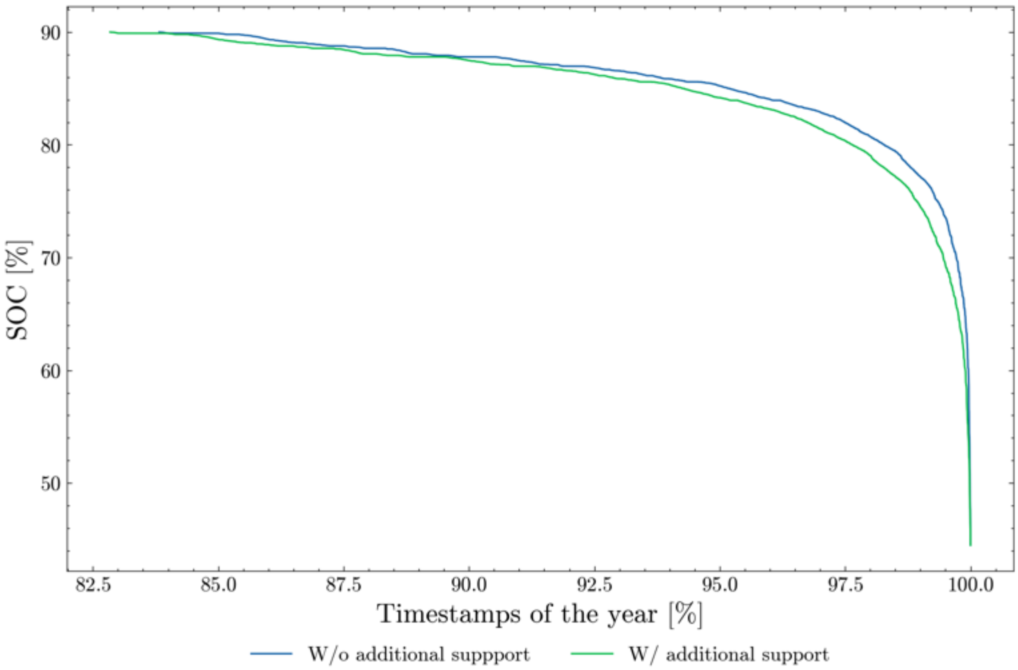

Figure 4.25: SOC duration curve for battery 1 with and without additional support under the conventional-like topology in 2045

4.6.2 Transformer LV-side topology

In this topology, the power flow is run on the grid with overload-related but not voltage-related investments due to the rollout of DERs. It is also to be noted that the reactive power consumption from the PV inverters is set to zero and they operate at a unity power factor. The reactive power controller is then used to inject or consume reactive power and reduce voltage issues.

When connecting the batteries to the LV side of the closest existing secondary substation, they cannot charge at the fixed rate of 150.53kW, or otherwise, they might induce overloads in the transformer. For this reason, if there are no overloads at a specific timestamp, the smallest remaining grid capacity across all components between the primary substation and the fast charging station is calculated and sets the maximum charging power. Similarly, batteries are not discharged at the power demand at the fast charging station minus 150.53kW as it was the case in the previous topology, but they are discharged at the required level to avoid thermal overloads in the upstream part of the grid. This results in varying battery utilisation based on the size and the base load of the secondary substations as figure 4.26 shows. Three batteries reach the lowest SOC of 10% and are active (i.e. have a SOC lower than 90%) during 72% of the year while 17 batteries are active less than 10% of the year. These three batteries are connected to a transformer that experiences a high base load, and due to the charging power being distributed over three batteries and three fast charging stations connected to the same secondary substation, the batteries' utilisation is high compared to the other ones.

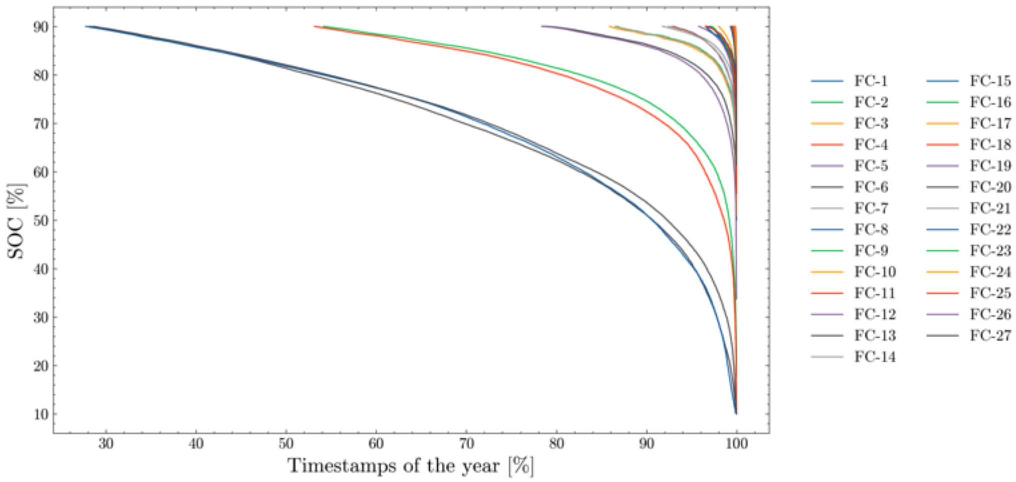

Figure 4.26: SOC duration curve under the transformer LV-side topology in 2045

With this topology, no additional thermal overloads are induced, especially at the existing secondary substations where the fast charging stations are connected. These were not upgraded due to the DER rollout either, so no additional active power support than the one presented in the previous section is required. The overloads at MV cables that were found due to the installation of fast charging stations are solved in the same manner as presented in the previous section, however, the overloads that were induced by the rollout of DERs cannot be solved anymore due to not enough remaining capacity at the transformer to feed power back in the MV grid if required.

On the other side, reactive power support is provided due to voltage issues being identified in the LV feeders connected to the transformer stations. Table 4.9 lists the number of cabinets for the four out of 18 secondary substations with a battery concerned with undervoltage issues (after cable and transformer upgrades due to thermal overloads) before and after the batteries' installation.

	Without batteries		**With batteries**	
Secondary substation	**Voltage issues**	**Average V_{min} [p.u.]**	**Voltage issues**	**Average V_{min} [p.u.]**
1	2	0.946	0	-
2	2	0.946	0	-
8	7	0.942	0	-
12	6	0.944	0	-

Table 4.9: Voltage impact per secondary substation under the LV-side topology

The results show that the batteries can remove all remaining voltage issues.

The graphs in figure 4.27 show the voltage at one of the cabinets connected to secondary substation 2, in purple before the battery is connected and in green after. Two fast charging stations and batteries are connected to this substation, so their power is summed. A time series section where reactive power is used to solve voltage issues is shown. During the time of the voltage drop, the batteries inject reactive power into the grid, therefore relieving the situation and bringing the voltage back within authorised values.

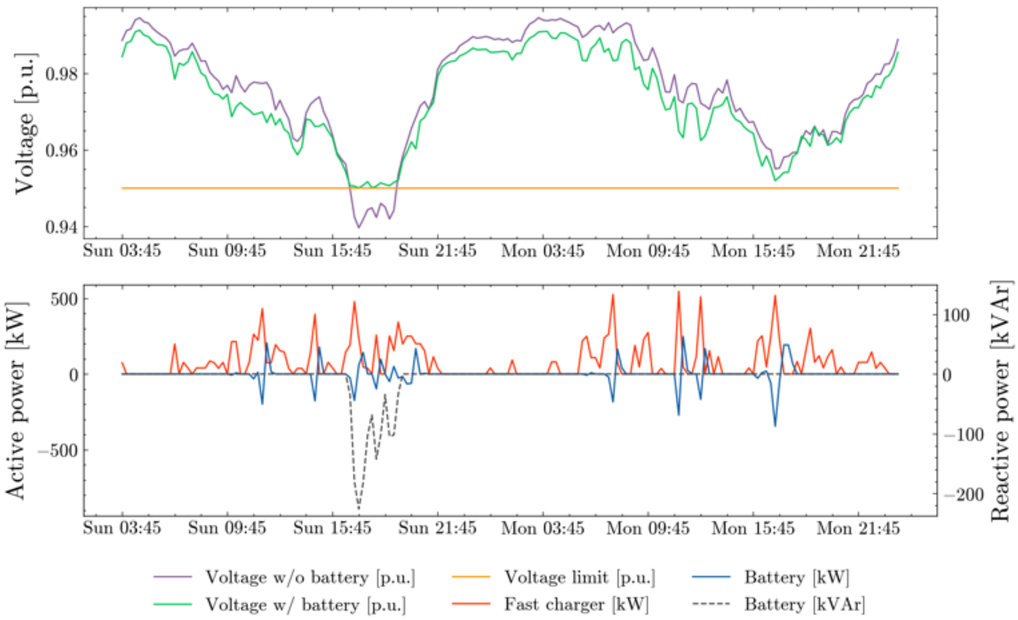

Figure 4.27: Voltage regulation through battery reactive power compensation

4.6.3 LV topology

Similar to the previous topology, a fixed charging power for the battery can't be set due to the variable remaining capacity through the grid. Connecting fast charging stations down the LV feeder creates the issue that not enough remaining capacity is available in the LV cables to charge the battery and therefore provide enough energy to the fast charging station.

This battery topology is run on two different grids: one without any investments and one with overload-related but not voltage-related investments. In both cases, reactive power consumption from PV inverters is set to zero.

The results show that batteries and fast charging stations end up causing more thermal overloads than the DER rollout in the grid without any investments. The remaining spare capacity at LV level is not enough to accommodate for the additional load of the fast charging station and the battery doesn't get enough power to charge and support it. It creates a larger number of thermal overloads both in LV cables and secondary substation transformers which cannot be mitigated. In the thermal overload-related investment case, the results are more mitigated and vary from battery to battery. Only four batteries do not create additional overload when being connected. The remaining ones, in addition to the overload-related upgrades due to the DER rollout, do require supplementary upgrades to distribute the fast charging stations' and batteries' power.

One situation is shown in figure 4.28, where the loading of a transformer is shown in the first graph additionally to the fast charging station time series. The section is from the beginning of the simulation, where the SOC is initialised at 50%. The transformer has a low loading, but LV cables don't have enough spare capacity to charge the battery. Therefore, the SOC often reaches its minimal value, resulting in transformer overloads.

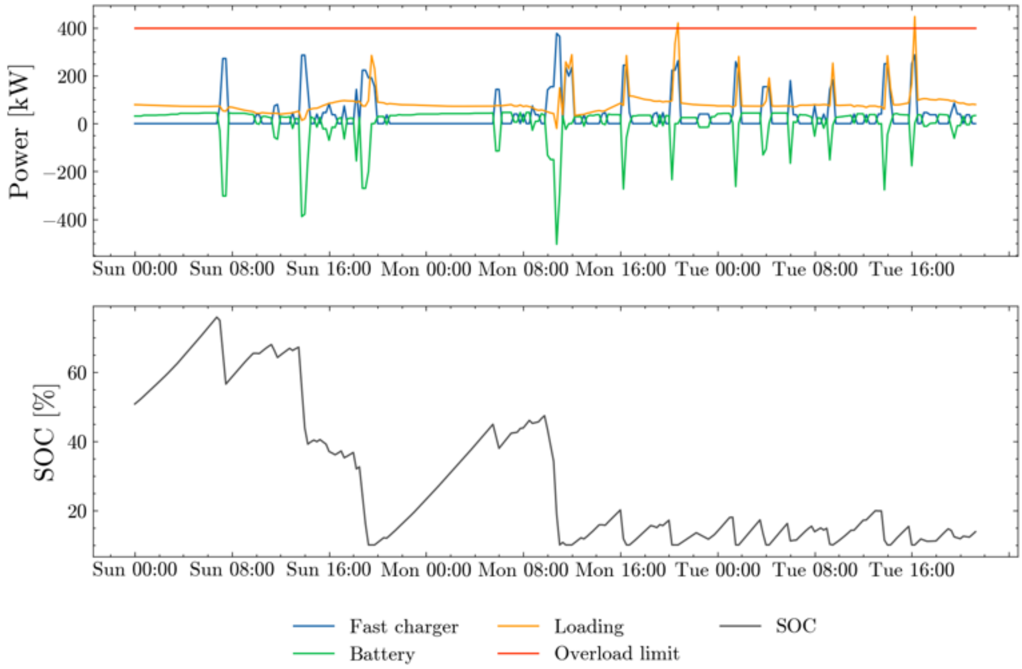

Figure 4.28: fast charging station-related overloaded transformer

Figure 4.29 displays an overview by showing the number of overloaded cables downstream of a secondary substation where a fast charging station and battery are connected. Some of the additional thermal overloads can also be partly explained by the larger and centralised share of reactive power compensation by the batteries to mitigate voltage issues since no reactive power from PV inverters or conventional upgrades mitigate these.

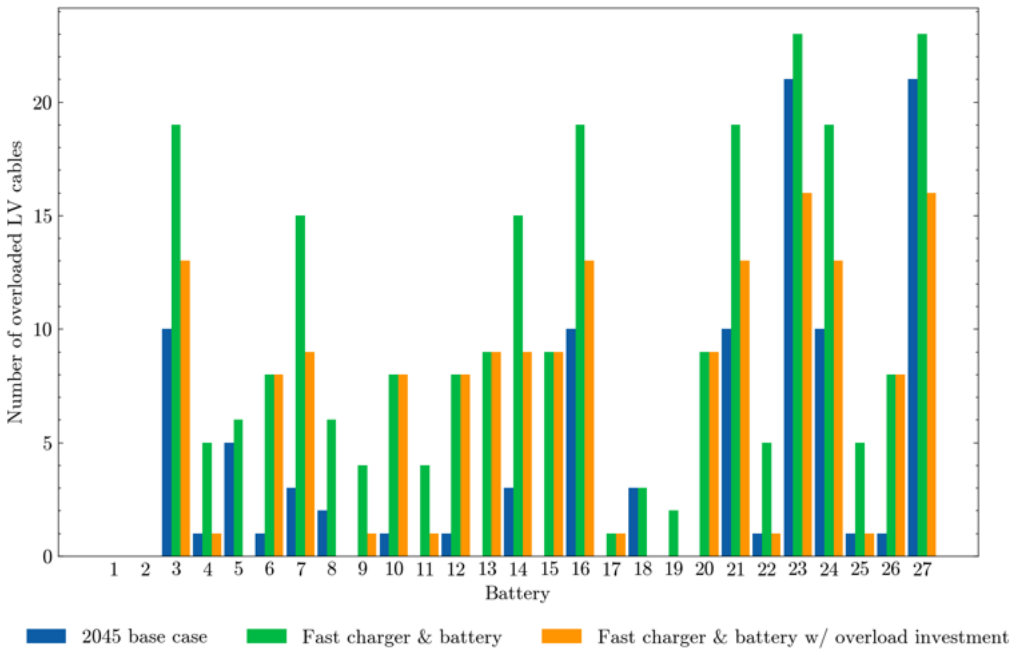

Figure 4.29: Number of overloaded LV cables in 2045 with and without fast charging stations in a grid without investments

Figure 4.30 shows the situation regarding voltage issues, which is less critical than the thermal overloads since only eight of the 27 batteries' grids experience more voltage issues than the original ones. In the case of nine batteries, voltage issues that happened in the original grid can be solved by the battery, even when considering the additional fast charging station load.

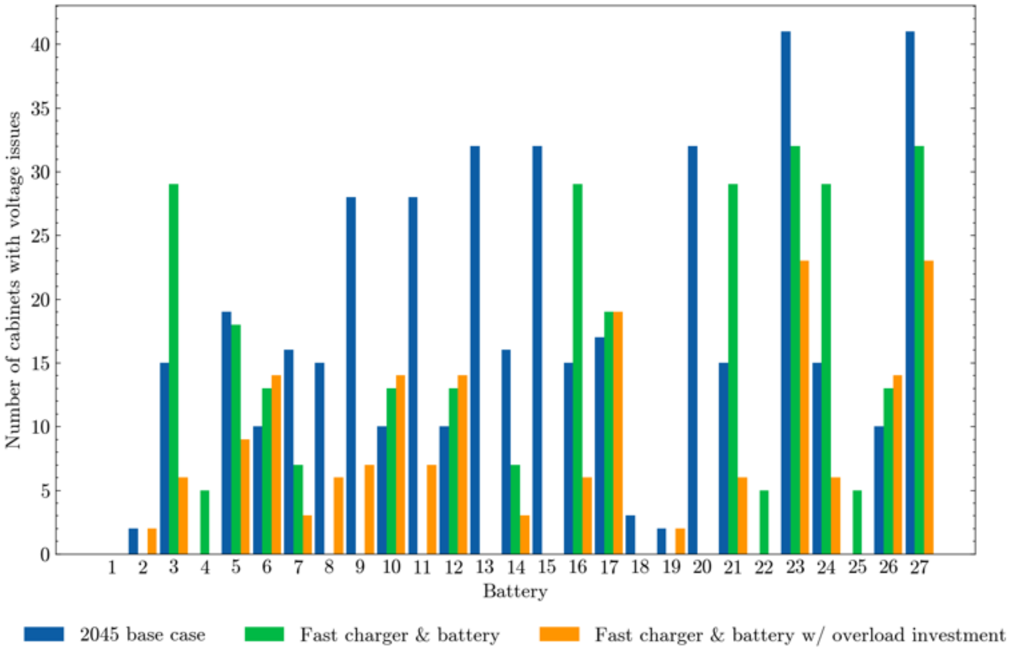

Figure 4.30: Number of cabinets with voltage issues in 2045 with and without fast charging stations in a grid without investments

The reason for the number of voltage issues increase compared to the original grid can be explained through the example in figure 4.31.

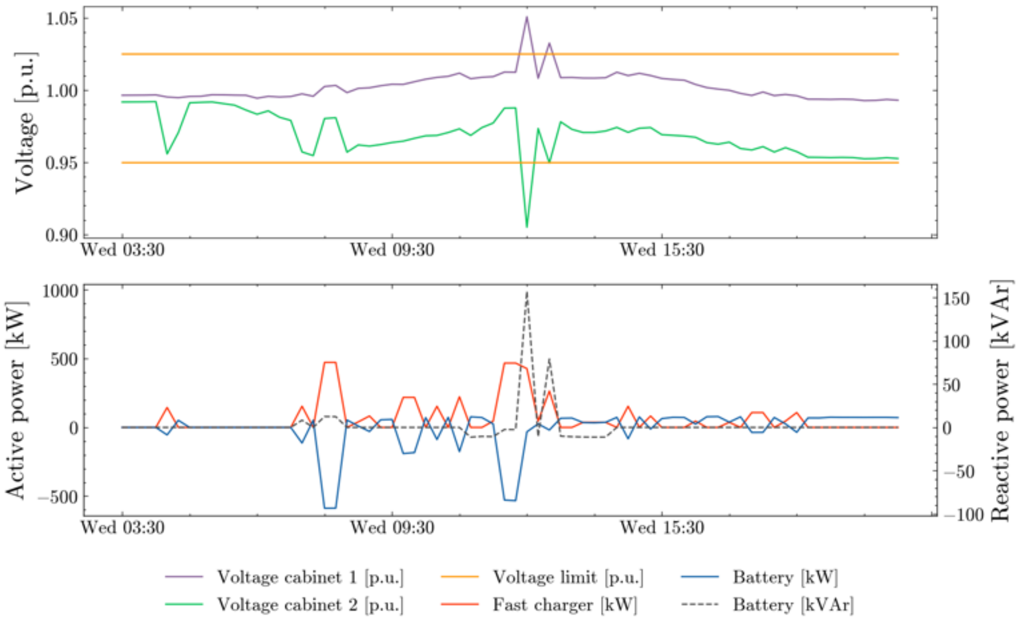

Figure 4.31: Voltage regulation through battery reactive power compensation

The plot shows a time series section of the power output of battery 24 as well as the voltage at two cabinets: cabinet 1, the purple curve, experiencing an overvoltage and cabinet 2, the green curve, to which the battery is connected. In this case, an overvoltage situation is identified in the grid. The battery starts to absorb reactive power to mitigate it (dashed line in the second graph). However, the cabinet experiencing an overvoltage is not the one to which the battery is connected but is placed in a different feeder. This cabinet wasn't experiencing voltage issues, but due to the reactive power absorption, the voltage there starts to decrease and ends up laying below the lower voltage limit. The undervoltage at the cabinet with the battery is, therefore, a consequence of the regulation action. A different control strategy wouldn't yield different results, since the root cause of the induced undervoltage is the reactive power absorption location, which is dependent on the battery, and not the way the reactive power is absorbed. A slightly different control algorithm would be not to track the voltage at all cabinets in a grid but only at the one to which the battery is connected or the ones in that feeder. In this case, the controller would not react to the overvoltage at cabinet 1, therefore not changing the battery's reactive power output and inducing the undervoltage at cabinet 2. When running the simulation with these parameters, however, no significant changes to the results presented in figures 4.29 and 4.30 are observed.

This is not an issue in the previous topology since the batteries are connected to the LV secondary substation bus, which typically has a more stable voltage than the one at cabinets further downstream. In the previous topology, reactive power injection does not cause issues at the transformer's LV bus.

Due to the limited grid capacity at LV level, the batteries are significantly more utilised than in the previous topologies. The SOC duration curve in figure 4.32 shows that a group of six batteries reach the lowest SOC during 6% of the year and 8 other reach it at least for one timestamp, resulting in the additional thermal overloads previously observed. The higher utilisation has an impact on losses and therefore the economic assessment.

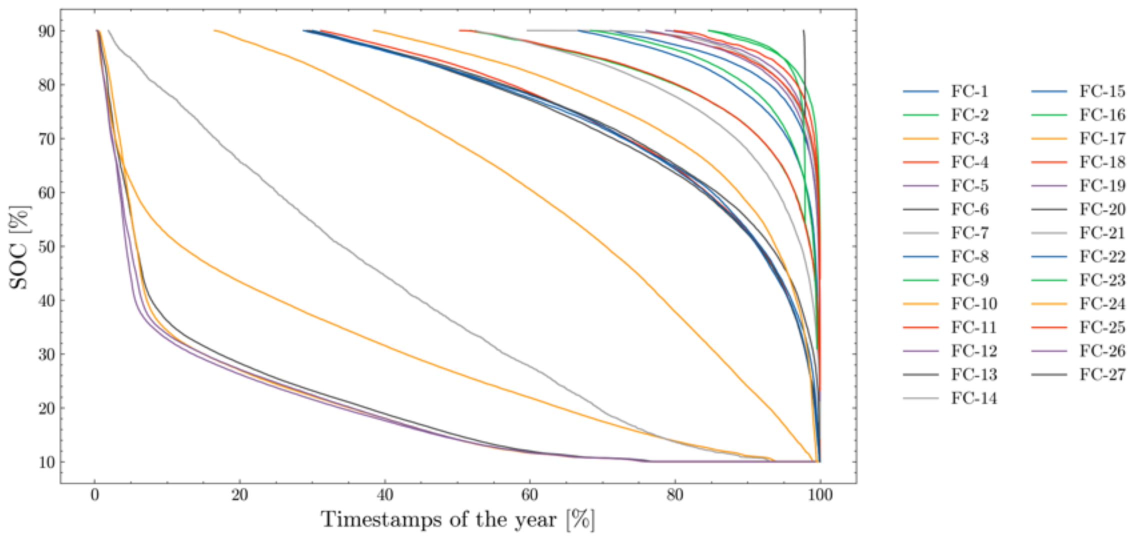

Figure 4.32: SOC duration curve under the LV topology in 2045

4.7 Economic comparison

The cost of a transformer station to connect the fast charging station in a conventional manner serves as the benchmark and is therefore identical across all battery topology options. The cost of connecting the fast charging station to the closest existing transformer station HV side is the one of laying down a 10kV cable with a dimension of 150 mm^2. The total resulting costs per fast charging station are detailed in table 4.10, including CAPEX, O&M costs for transformers, and calculated losses by pandapower. The costs are based on constant CAPEX and O&M costs and varying losses based on utilisation.

Station	**Yearly costs [kDKK/year]**	**Station**	**Yearly costs [kDKK/year]**	**Station**	**Yearly costs [kDKK/year]**
1	19.99	10	27.53	19	18.6
2	18.55	11	17.66	20	15.43
3	19.56	12	26.3	21	21.28
4	16.38	13	18.02	22	16.15
5	21.5	14	17.86	23	19.97
6	23.35	15	17.96	24	19.44
7	19.59	16	20.16	25	18.7
8	17.34	17	16.26	26	22.95
9	18.67	18	16.16	27	20.32

Table 4.10: Conventional connection costs of fast charging stations

All the battery prices used in this section follow the medium price development scenario presented in figure 3.29.

4.7.1 Conventional-like topology

The costs of the batteries under the conventional-like topology are shown in table 4.11. These costs are calculated as the batteries' and cables' CAPEX, O&M costs and losses, minus the transformer costs of table 4.10 since they wouldn't be required. Due to technology costs and higher losses, battery prices are between 212% and 491% more expensive than a connection with transformers, except for battery 1 which benefits from additional savings and is 113% more expensive. Generally, batteries' costs tend to decrease over time with the CAPEX and therefore O&M costs reduction. Variations between the years depend on the batteries' utilisation and the resulting losses.

Battery	**Yearly costs [kDKK/year]**	**Battery**	**Yearly costs [kDKK/year]**	**Battery**	**Yearly costs [kDKK/year]**
1	42.63	10	86.13	19	88.86
2	105.43	11	89.35	20	89.81
3	103.22	12	85.37	21	85.38
4	99.89	13	89.93	22	92.53
5	94.18	14	96.2	23	118.06
6	123.29	15	89.14	24	85.89
7	92.15	16	89.66	25	86.73
8	95.29	17	92.15	26	117.69
9	85.5	18	93.46	27	93.88

Table 4.11: Costs of batteries under the conventional-like topology

Since batteries are connected in the same way as a new transformer station would be, the costs of cables are discarded in the following comparison.

It happens that battery 1 is the same unit that provides active power support to relieve the grid from thermal overloads caused by both the DER rollout and the fast charging station connection. Therefore, its cost-benefit analysis (CBA) will benefit from both the savings on the four MV cables that would have needed to be upgraded because of DERs and the five MV cables because of the fast charging station connection.

Figure 4.33 shows the detailed breakdown of the cost-benefit analysis of battery 1 in the form of a waterfall chart.

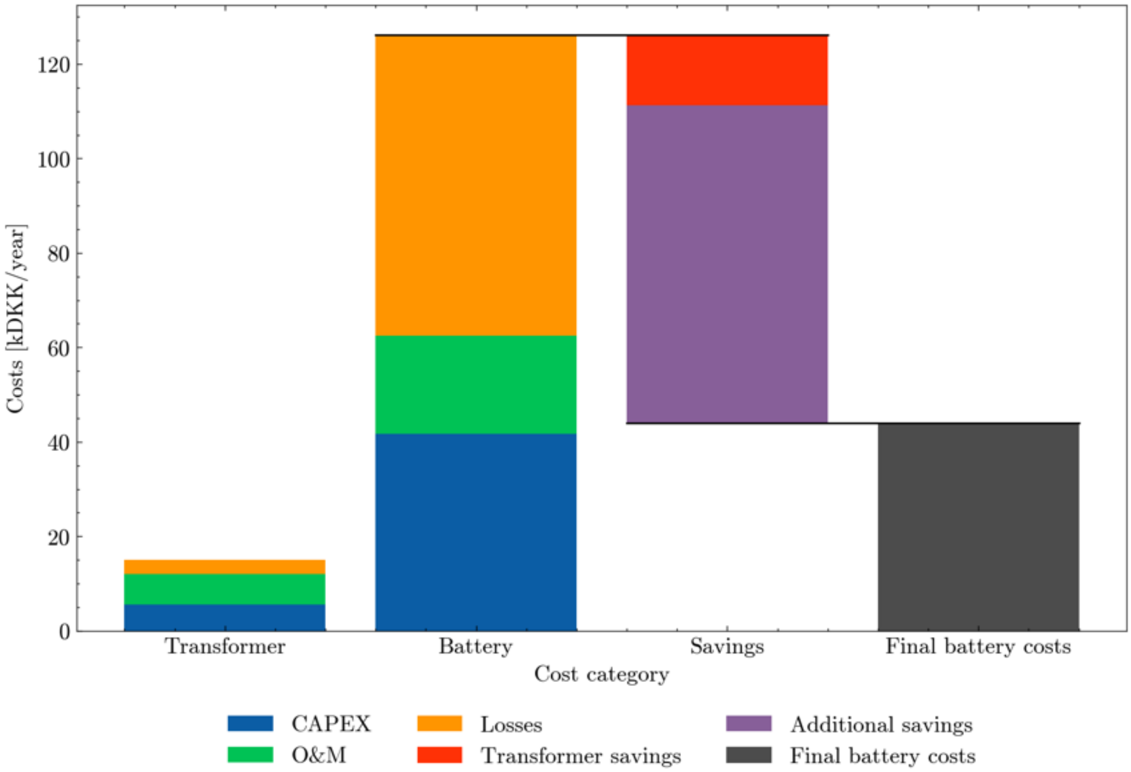

Figure 4.33: CBA breakdown of battery 1 under the conventional-like topology

The first and second bars from the left show the cost breakdown of respectively transformer and battery over CAPEX, O&M and losses. For the transformer, 37% of the yearly costs are due to CAPEX, 43% to O&M and 20% to losses. For the battery, the same distribution is respectively 34%, 18% and 48%. The third bar represents the potential savings with the battery option. First, the transformer costs (left bar) would be completely avoided. Second, the CAPEX costs over the lifetime of the in total nine MV cables not requiring an upgrade since the battery would solve the thermal overloads would also be saved. The battery costs minus the potential savings give the total battery costs. These savings help the battery reduce its yearly costs by 65%, yet the transformer-based solution remains 66% cheaper than the battery one.

Regarding the cables where the average overload values are decreased but not solved, the CBA of one of the three concerned batteries is shown in figure 4.34. In this case, the overload reduction still requires the same upgrade, as the additional savings are equal to the additional CAPEX, meaning that the cable costs saved on with the battery are equal to the cable costs to solve remaining issues after the battery is installed. In this case, the battery's final costs only benefit from the transformer savings, representing a cost reduction of 10% and leaving the transformer as an option 89% cheaper than the battery.

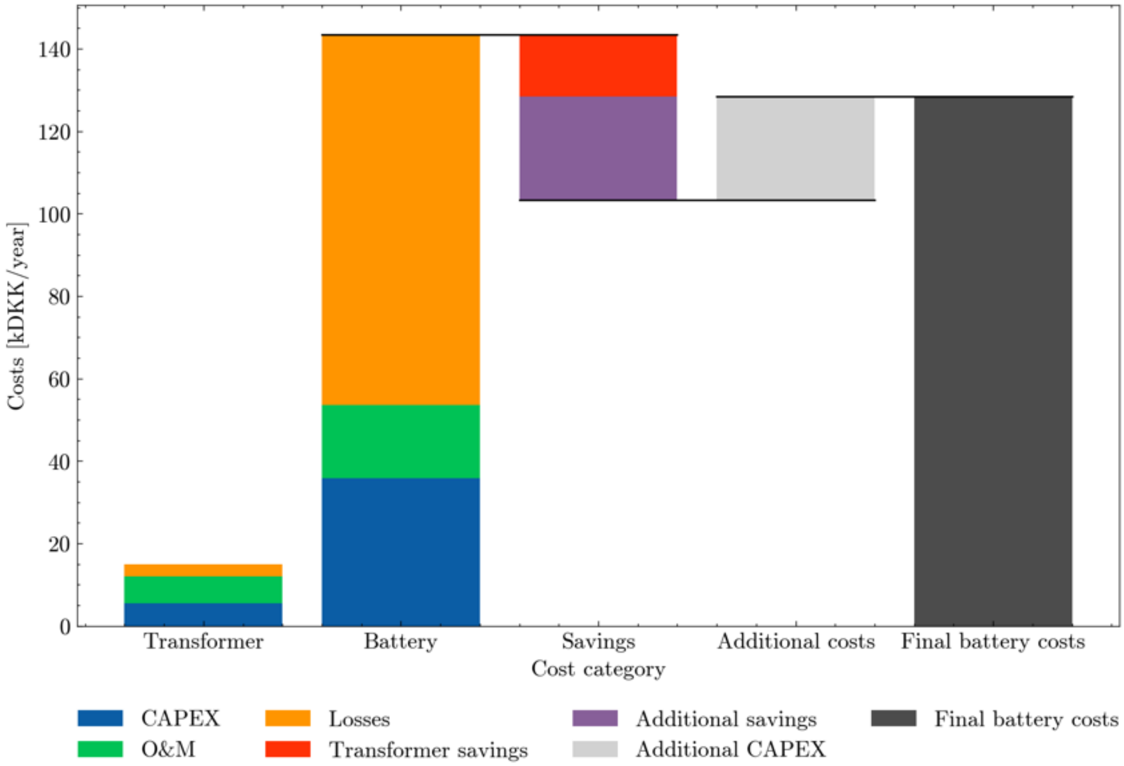

Figure 4.34: CBA breakdown of battery 6 under the conventional-like topology

4.7.2 Transformer LV-side topology

For this topology and the following one, cable costs are included in the comparison. This is because the transformer solution is connected to the existing grid with a 10kV 150 mm^2 cable, while the batteries and the fast charging stations are connected to the LV part of the grid, with a 300 mm^2 0.4kV cable.

It is also to be noted that voltage issues are mitigated conventionally by reactive power compensation from PV inverters (which solves 76% of issues) and through thermal overload-caused upgrades (which solves 12% of issues). This reactive power compensation is assumed here to have no costs and the costs induced by thermal overload-related investments are not used as benchmarks since they only mitigate voltage issues as a consequence, not a primary goal. Therefore, the economic benefit of the batteries might be underestimated in that regard.

Due to the varying power output of the battery not based on a fixed rate but on the thermal loading situation, the batteries' price distribution is significantly different than in the previous topology. Some batteries connected to a low-loaded secondary substation result in low utilisation and therefore lower losses (which is the case for batteries 1 and 19 e.g.), while the opposite happens for other batteries (such as batteries 13, 15 and 20 e.g.). This is also outlined in the SOC duration curve in figure 4.26. The costs of batteries, including LV cable connection costs are shown in table 4.12. In the case where conventional upgrades are differed due to the action of multiple batteries, e.g. when two batteries are connected to the same secondary substation that needed a conventional upgrade due to voltage issues, then the savings are distributed equally over the two batteries.

Battery	Yearly costs [kDKK/year]	Battery	Yearly costs [kDKK/year]	Battery	Yearly costs [kDKK/year]
1	21.41	10	67.07	19	31.1
2	45.65	11	182.47	20	218.18
3	100.11	12	65.37	21	83.81
4	42.31	13	220.05	22	45.31
5	58.08	14	63.81	23	37.42
6	118.2	15	219.95	24	28.48
7	62.53	16	86.35	25	41.75
8	44.88	17	43.97	26	112.91
9	177.98	18	35.29	27	42.12

Table 4.12: Costs of batteries under the transformer LV-side topology

The batteries' costs end up laying between 7% and 1,121% more than the transformer connection costs, with an average decrease of 63% for 22 batteries and an average increase of 43% for the remaining batteries compared to the previous topology.

The most competitive battery to the conventional connection way is battery 1. It benefits from the same savings on the five MV cables that got overloaded when connecting the fast charging stations and it additionally decreases its losses by 66% as the secondary substation it is connected to shows enough spare capacity to provide power to the fast charging station during most of the time, therefore reducing the battery's utilisation. The transformers' loss difference between the power flow results with and without fast charging stations is taken into account.

Figure 4.35 shows the CBA breakdown of battery 23. This battery benefits from total savings of 41% and reduces its final costs from 329% to 193% of the transformer's costs.

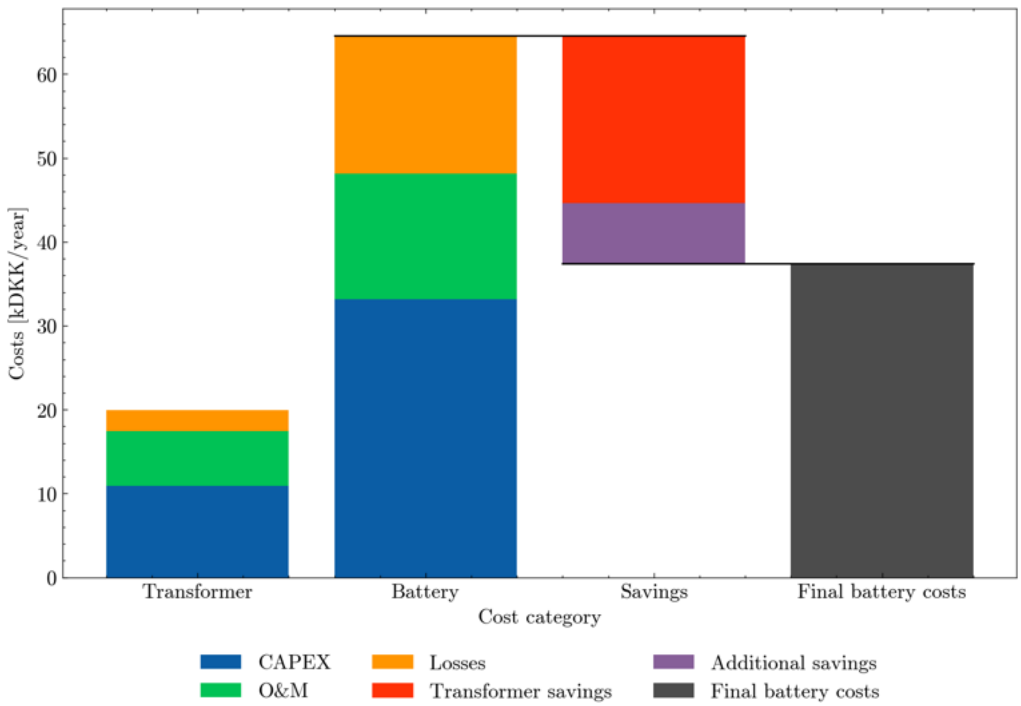

Figure 4.35: CBA breakdown of battery 23 under the transformer LV-side topology

Additional savings can also be reached on batteries 7, 14 (5,951 DKK/year each), 9, 11 (4,770 DKK/year each) and 19 (3,544 DKK/year), resulting in a cost reduction of respectively 9%, 9%, 3% 3% and 10% additionally to the transformer savings. It can be observed that more batteries contribute to solving issues than in the previous topology, however, due to LV cables being cheaper than MV cables, these savings are lower than previously.

4.7.3 LV topology

Table 4.13 displays the batteries' costs under the low voltage topology. The higher prices are mostly due to the higher losses resulting from the frequent utilisation to remove overloads compared to the previous topologies, as well as the upgrade required for newly overloaded cables and transformers.

Battery	Yearly costs [kDKK/year]	Battery	Yearly costs [kDKK/year]	Battery	Yearly costs [kDKK/year]
1	97.53	10	141.78	19	107.19
2	98.09	11	159.57	20	186.05
3	224.96	12	141.87	21	81.42
4	205.6	13	186.08	22	199.03
5	153.19	14	169.64	23	99.76
6	148.43	15	185.94	24	193.81
7	108.73	16	133.49	25	104.66
8	143.37	17	205.58	26	138.3
9	161.04	18	112.81	27	74.93

Table 4.13: Costs of batteries under the LV topology

Figure 4.36 shows the CBA breakdown of battery 7.

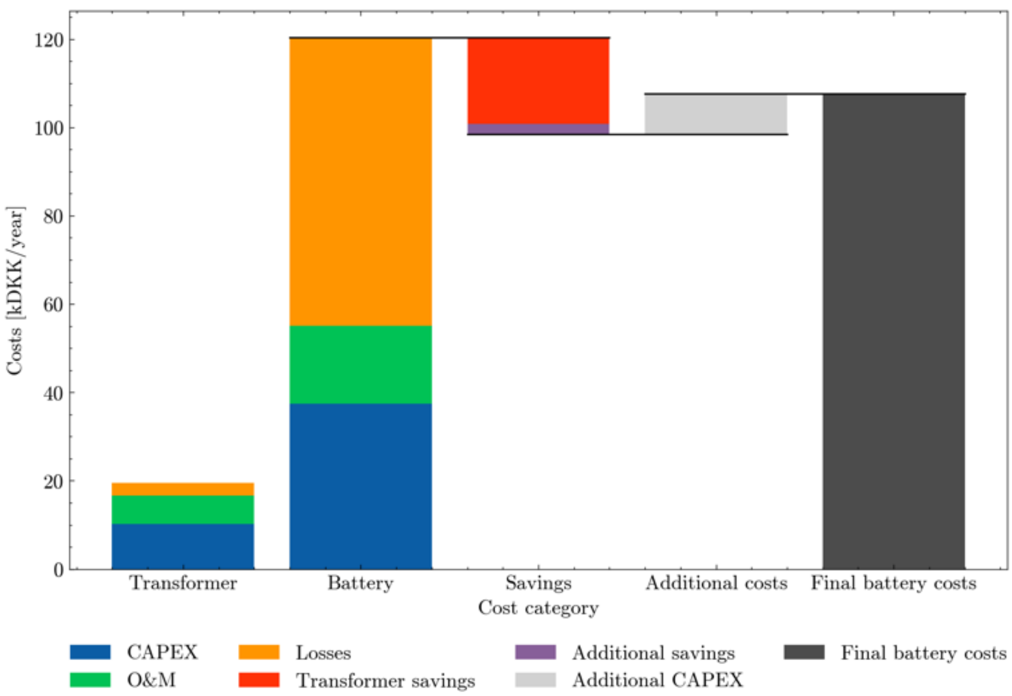

Figure 4.36: CBA breakdown of battery 7 under the LV topology

In this case, the deferral of some voltage-related investments is compensated by higher costs due to newly induced thermal overloads and higher losses. The same situation happens for multiple other batteries.

The prices lay between 206% and 1,109% of the conventional transformer costs and are more expensive than under the transformer LV-side topology for 21 batteries by 41% and less expensive for the remaining batteries by 88% on average. This configuration is also more expensive than the conventional-like topology in 23 cases, by 58%.

4.7.4 Summary

Figure 4.37 displays a summary of the price per installation across the conventional upgrade and the three battery topologies. It outlines that the conventional upgrade is always superior in terms of costs, with a few cases where the transformer LV-side topology is a close competitor but is far off in most of them. The LV topology is the most expensive of all options in most cases, except in some situations where the transformer LV-side topology is more expensive due to high losses at secondary substations.

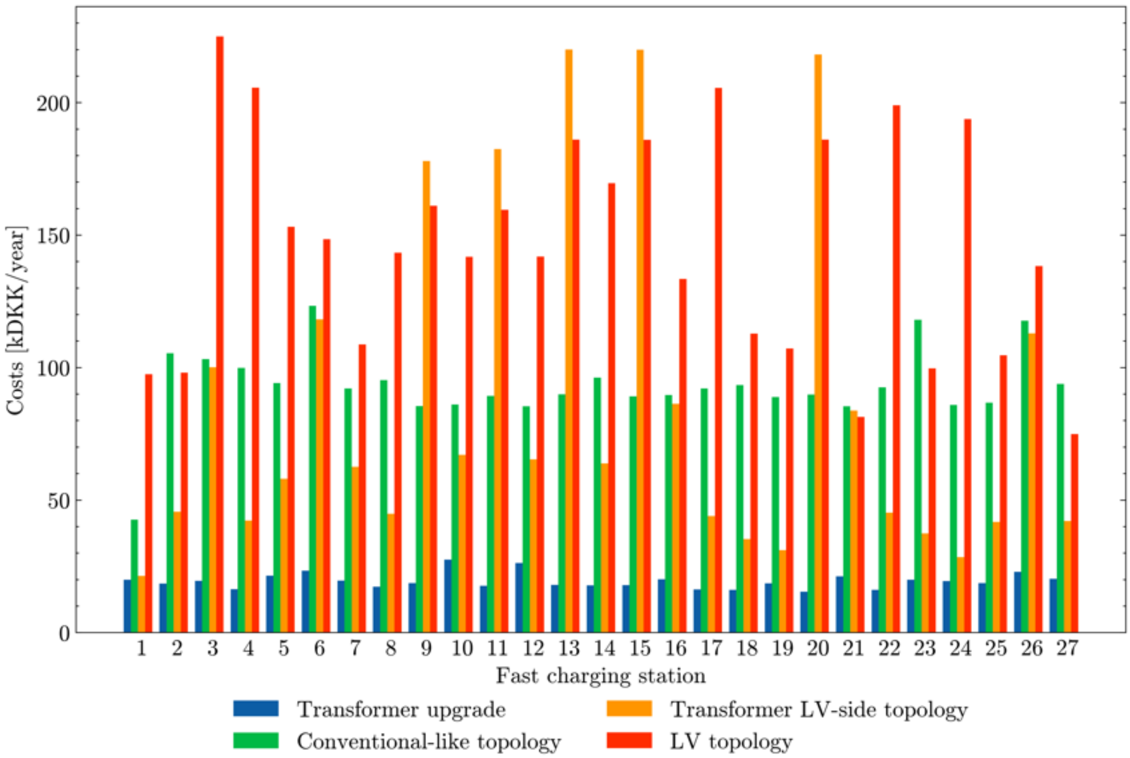

Figure 4.37: Summary of installation costs under the different topologies

4.8 Sensitivity analysis

4.8.1 Hybrid upgrade

Another variant of the transformer LV-side topology is to install a new transformer, similar to the conventional method, but with a smaller rating and a battery supporting it. I.e., instead of installing an 800kVA transformer, a 400kVA with a battery connected to its LV side to supply power during peak times could be chosen. The battery sizing optimisation algorithm is rerun with the maximum charging power constraint set to 400kW and capacity to 250kWh. The largest sizing that satisfies all profiles is 237.77kWh.

The simulation is rerun with an updated topology shown in figure 4.38. The charging power of the battery is set by the controller based on the remaining capacity through the transformer. The transformer and battery sizings allow for the fast charging station to be supplied with the required power at any time, and no thermal overload issues are induced compared to the transformer LV-side topology.

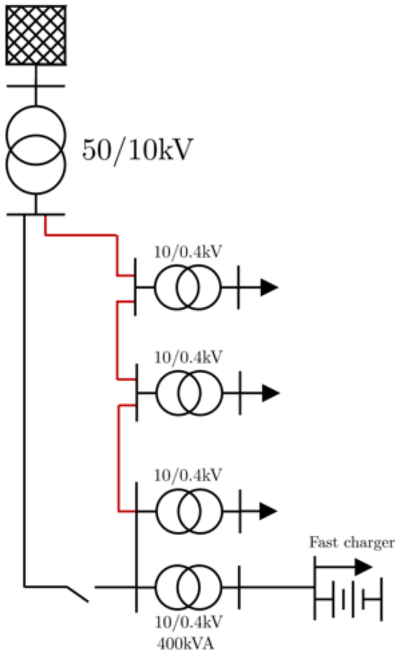

Figure 4.38: Hybrid upgrade topology

This method removes the additional loading on the existing transformer in comparison to the transformer LV-side topology but also removes the possibility for reactive power support on the existing LV grid. The advantage of this topology is the lower battery costs due to the reduced size, which are shown in table 4.14. Here, the battery-option costs are composed of the addition of the CAPEX, O&M and losses costs from the 400kVA transformer and the battery, and the conventional transformer costs are the ones from the 800kVA transformer.

Battery	**Yearly costs [kDKK/year]**	**Battery**	**Yearly costs [kDKK/year]**	**Battery**	**Yearly costs [kDKK/year]**
1	13.93	10	2.89	19	11.64
2	15.08	11	13.19	20	14.84
3	13.4	12	4.58	21	8.72
4	15.32	13	12.79	22	13.97
5	9.96	14	13.32	23	9.8
6	7.49	15	12.99	24	10.31
7	11.14	16	10.2	25	11.35
8	13.62	17	14.06	26	6.74
9	11.84	18	13.92	27	10.58

Table 4.14: Costs of connection (battery + 400kVA transformer) under the hybrid topology

The resulting costs are lower than the conventional connection costs in every case, with being on average 62% more cost-efficient. The reduced battery losses due to its low utilisation as it is only activated for peaks over 400kW combined with a transformer CAPEX being 48% cheaper than the 800kVA one result in interesting savings. Optimising the battery sizing algorithm to take this into account might give a battery and transformer combination that results in even higher savings.

4.8.2 Grouping batteries

In this grid model, 27 batteries are distributed over 18 different secondary substations in the conventional-like and transformer LV-side topologies. It is therefore possible to combine batteries per secondary station as figure 4.39 shows, which could result in a cumulated smaller capacity required than two or three individual batteries. For this purpose, the fast charging station profiles of the batteries to combine are summed and the battery sizing optimisation problem is run on this new input data. The resulting calculated sizes with an equal weight coefficient on the charging power and capacity are shown in table 4.15.

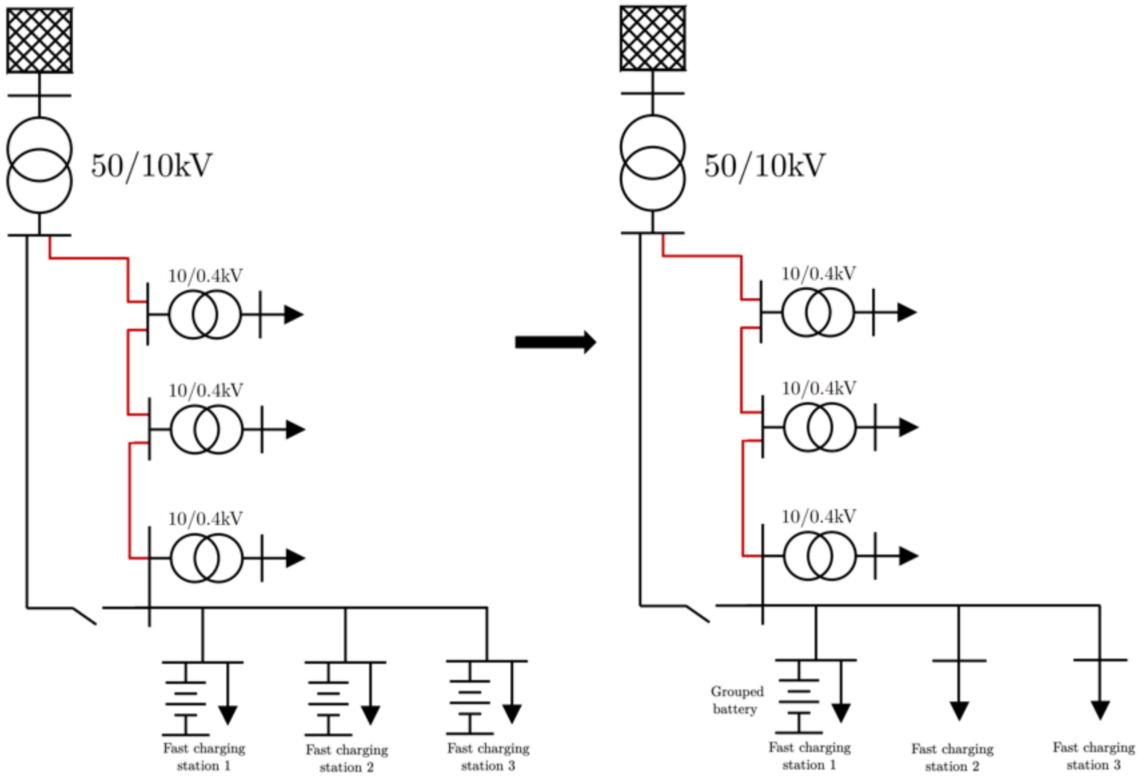

Figure 4.39: Grouping battery per secondary substation

Grouped battery	Initial number of batteries	Max charging power [kW]	Capacity [kWh]
1	2	97.45	1,833.55
2	2	96.84	2,505.23
3	2	93.91	2,266.05
4	2	95.41	2,085.06
5	2	95.30	1,931.95
6	3	141.24	2,626.07
7	3	145.60	2,167.93

Table 4.15: Grouped profile battery sizes

The optimisation results for grouping two batteries show that the optimal combination of charging power and capacity lies at a significantly lower maximum charging power for all batteries (previously 150.53kW). This results in a larger capacity requirement than the one that could be achieved with a larger charging power, therefore more than doubling costs compared to the individual battery per fast charging station. The optimisation problem is therefore rerun but instead of optimising both charging power and capacity, the charging power is set at an upper bound of 150.53kW and removed from the objective function. The updated results are shown in table 4.16.

Grouped battery	**Initial number of batteries**	**Max charging power [kW]**	**Capacity [kWh]**
1	2	150.53	961.22
2	2	150.53	874.76
3	2	150.53	1,099.35
4	2	150.53	1,111.31
5	2	150.53	1,007.69
6	3	150.53	2,089.79
7	3	150.53	2,081.34

Table 4.16: Grouped profile battery sizes with fixed charging power

Based on the similar approach as in section 4.5, the minimum working combination to cover uncertainties is a battery with 1,111.31kWh capacity when grouping two batteries, and 2,089.79kWh capacity when grouping three batteries. It needs to be noted that the uncertainty in this calculation is greater than in the individual one, where 27 different profiles were used. Here, only five and two profiles are used. The cost reduction on CAPEX and O&M compared to individual batteries with 1,010.24kWh capacity is 55% for grouping two batteries and 31% for grouping three. When adding the costs of one secondary substation per fast charging station in the conventional upgrade way, the cost reduction is even greater.

Implementing this solution for the LV topology would require laying a parallel network to the existing one that would connect the battery with all fast charging stations since the spare capacity in the LV grid is not large enough to transport the power required by fast charging stations in most cases.

When running an updated power flow simulation, the grouped batteries are able to supply the required power at the fast charging stations. None of the grouped batteries can be used for active power support since they are not located downstream of thermal overload issues, so no additional savings can be made in the conventional-like topology. However, four of the batteries now grouped into two provide reactive power support in the transformer LV-side topology. Table 4.17 compares the yearly costs (including potential savings) of the conventional transformer upgrade, and the individual and grouped battery costs.

Grouped battery	Initial number of batteries	Transformer costs (conventional) [kDKK/year]	Individual battery costs [kDKK/year]	Grouped battery costs [kDKK/year]
1	2	43.3	236.46	101.67
2	2	41.21	234.88	38.52
3	2	35	232.7	194.16
4	2	53.83	137.78	55.15
5	2	34.85	92.42	26.77
6	3	59.99	223.92	104.08
7	3	51.43	728.58	371.9

Table 4.17: Costs of grouped batteries under the transformer LV-side topology

The battery grouping reduces overall costs by 17% to 84% compared to individual batteries. Two of the combinations, grouped batteries 2 and 5 end up being more competitive than the transformer solution. It is to be noted that this process of grouping batteries requires coordination since two of the batteries that might be connected to the same existing transformer station might be installed with a 10 or 15-year difference due to the fast charging station penetration curve, therefore reducing the coordination potential.

Figure 4.40 displays the CBA breakdown when combining the costs of two conventional secondary substations and the cumulated savings. In this case, the additional savings on the two transformers and the cables that were upgraded for voltage issues reason make the battery option 7% cheaper than the transformer option.

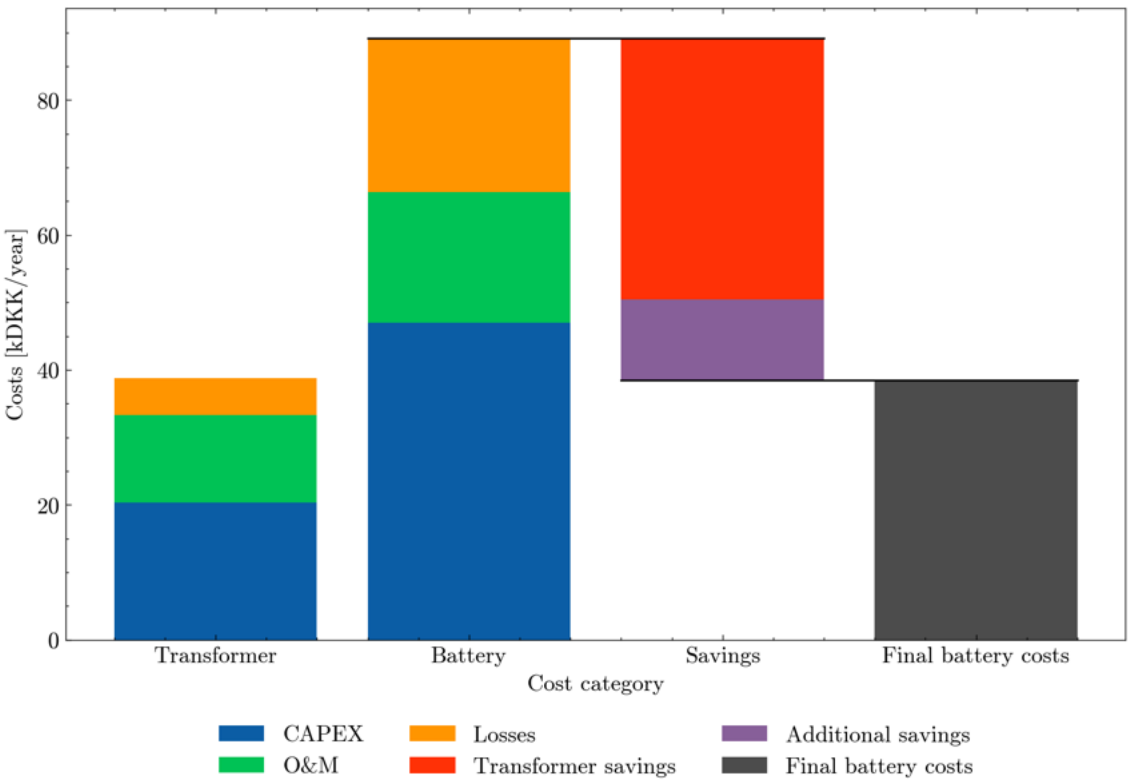

Figure 4.40: CBA breakdown of grouped battery 2 under the conventional-like topology

4.8.3 Asset prices

The economic analysis presented in the previous section was based on medium scenarios for conventional components and battery prices. Here, two additional price scenarios, low and high will be investigated both for conventional assets and batteries. The low and high price scenarios for batteries are shown in figure 3.29 and for conventional assets, they are respectively 50% lower and higher than the previously used prices.

Overview

The economic results of the different scenarios are shown in the sensitivity matrix in table 4.18. The combination of each price scenario for conventional assets and batteries is calculated and the most cost-efficient option is stated for each of these combinations. The percentage value represents the number of cases (each battery under each topology) in which the most cost-efficient method is superior. The results show that the conventional solution is the most cost-effective one in most cases even in extreme scenarios, with high conventional component prices and low battery prices e.g., where batteries are superior in only 11% of all cases. The total cost differences are so high that the model isn't very sensitive to price variations.

		Battery Low	Battery Medium	Battery High
Conventional assets	**Low**	Transformer 100.0%	Transformer 100.0%	Transformer 100.0%
	Medium	Transformer 98.0%	Transformer 100.0%	Transformer 100.0%
	High	Transformer 89.0%	Transformer 96.0%	Transformer 100.0%

Table 4.18: Asset price sensitivity matrix across all topologies

When considering only the most competitive topology, i.e. the transformer LV-side one, the results shift towards batteries becoming more competitive, as outlined in the sensitivity matrix 4.19, but again, only up to 30% of all cases are competitive.

		Battery Low	Battery Medium	Battery High
Conventional assets	**Low**	Transformer 100.0%	Transformer 100.0%	Transformer 100.0%
	Medium	Transformer 93.0%	Transformer 100.0%	Transformer 100.0%
	High	Transformer 70.0%	Transformer 89.0%	Transformer 100.0%

Table 4.19: Asset price sensitivity matrix under the transformer LV-side topology

Changing the battery size doesn't significantly impact the results either. Until now, a 1,010.24kWh battery was considered, due to the common sizing across all profiles chosen in section 4.6. When specifying 150.53kW charging power as a constraint and rerunning the optimisation algorithm, the larger battery capacity is 625.07kWh (38% decrease) and is still able to provide the active and reactive power support previously mentioned. Running the sensitivity analysis over all topologies gives the sensitivity matrix 4.20.

		Battery		
		Low	**Medium**	**High**
Conventional assets	**Low**	Transformer 99.0%	Transformer 99.0%	Transformer 100.0%
	Medium	Transformer 86.0%	Transformer 95.0%	Transformer 99.0%
	High	Transformer 79.0%	Transformer 80.0%	Transformer 90.0%

Table 4.20: Asset price sensitivity matrix under a 625.07kWh battery

Batteries become a superior solution in less favourable economic cases than before (e.g. high battery and medium conventional asset prices), but overall in only between 1% and 10% more cases than with the 1,010.24kWh battery. This can be explained by the losses, which are not size-dependent, making up larger shares of the overall battery prices.

Conventional asset most favourable scenario

The most favourable case for the conventional asset-based solution, shown in figure 4.41 is under a low conventional asset price scenario and a high battery price. In this case, some additional savings are made but these as well as the transformer savings are offset by newly induced overloads and voltage issues since this case happens under the LV topology. This battery is also concerned with massive losses due to a high utilisation.

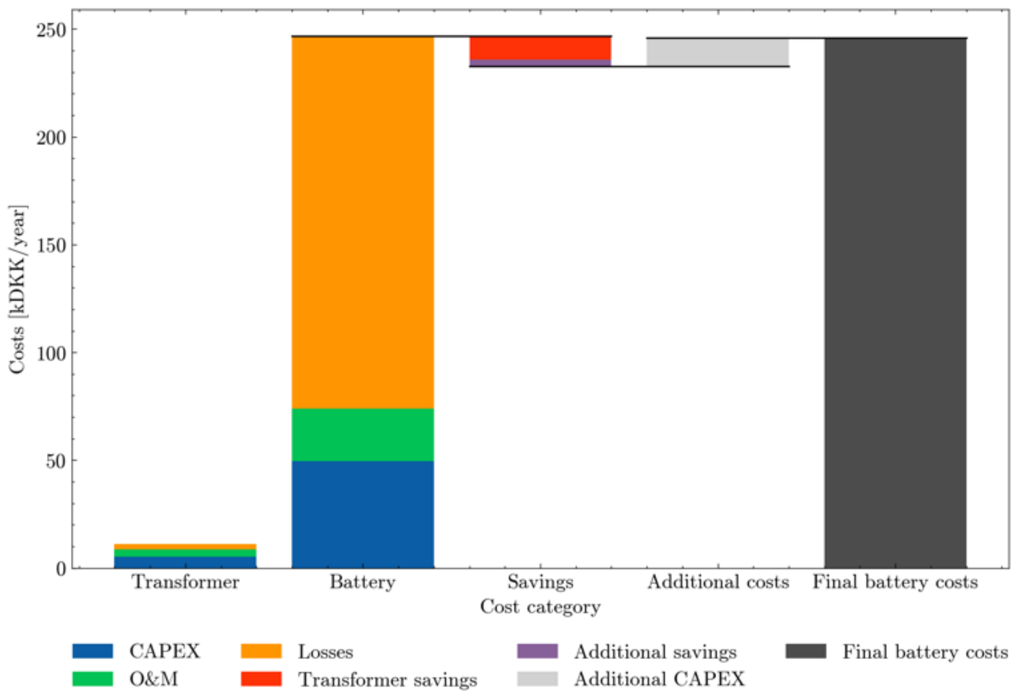

Figure 4.41: CBA breakdown the most competitive conventional option

Battery most favourable scenario

The battery's most competitive case is one of the edge cases, where the final battery's costs are close to zero, as shown in figure 4.42. This case, under the transformer LV-side topology, benefits from savings on MV cables due to active power support. It happens during the conventional asset high price and battery low price scenario.

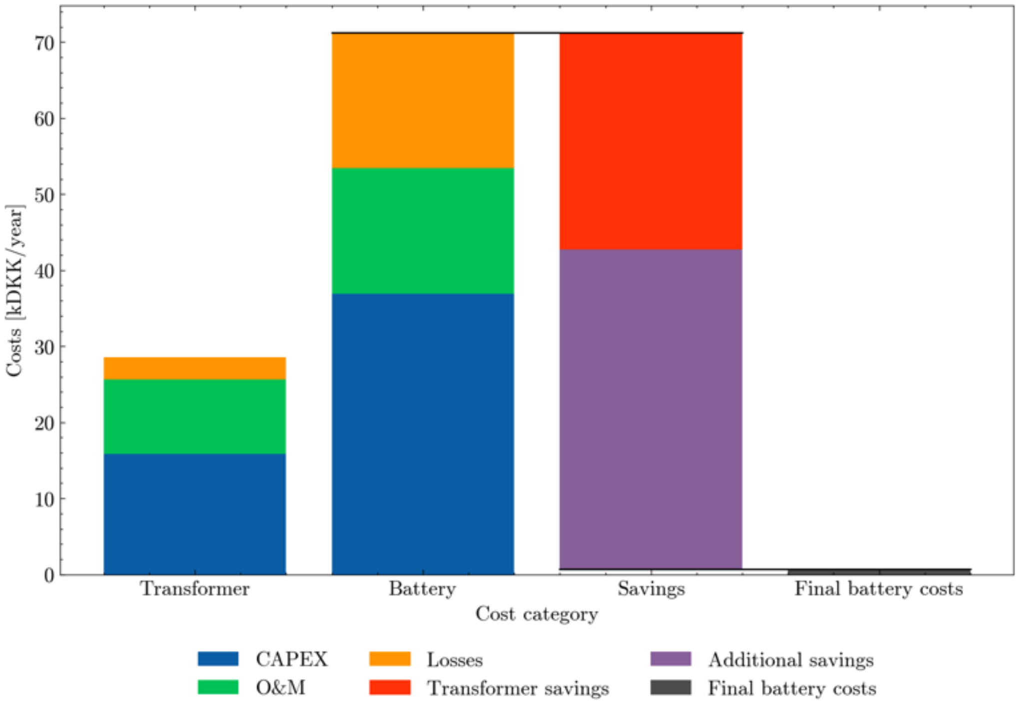

Figure 4.42: CBA breakdown the most competitive conventional battery

4.8.4 Electricity prices

The electricity price, used for losses in the CBA calculation, is the 2021 average day-ahead spot price for the bidding area DK2. For the sensitivity analysis, this will be assumed as the medium scenario and a low scenario (2020 price, 211.73 DKK/MWh, 68% lower) and a high scenario (2022 price, 1,563.34 DKK/MWh, 239% higher) are assessed [23].

The results in the sensitivity matrix 4.21 show for each topology and electricity price the option which is the most cost-efficient one and the percentage of cases (i.e. across all 27 batteries) under which it is more cost-efficient.

		Electricity price scenario		
		Low	**Medium**	**High**
Topology configuration	**Conventional-like**	Transformer 96.0%	Transformer 100.0%	Transformer 100.0%
	Transformer LV-side	Transformer 96.0%	Transformer 100.0%	Transformer 100.0%
	LV	Transformer 100.0%	Transformer 100.0%	Transformer 100.0%

Table 4.21: Electricity price sensitivity matrix

Similar to the asset prices, the electricity price doesn't significantly impact the competitiveness of one solution over the other. Only under the low electricity price scenario, 4% of the battery cases are cheaper than the conventional upgrade for two topologies. The batteries with the lowest losses pass under the threshold of the conventional upgrade costs.

5 Discussion

5.1 Technical assessment

5.1.1 Battery topologies

The three battery connection topologies presented here allow for different contributions of these on the grid. These contributions can be split between active and reactive power support and are limited by the chosen topology. The conventional-like topology, where the battery is connected at the LV side of the closest secondary substation requires MV power electronics. Additionally, this topology can only provide active power support on MV cables and primary substations. However, since these assets are generally more expensive than the LV ones, in the case of a battery being able to differ some of these investments, its economic assessment will be significantly impacted for the better. Reactive power support is not provided here, since voltage issues appear only in the LV part of the grid and there is not enough transformer capacity to distribute reactive power without inducing thermal overloads.

The transformer LV-side topology allows to solve some of the thermal overloads happening at the MV part of the grid, under the limitation of the transformer's capacity. Active power support can also be provided to this transformer but is not required here. Additionally, reactive power support to the LV grid can be provided. Voltage issues that would need to be solved by upgrading existing cables can therefore be avoided. This reactive power support doesn't impact the batteries' SOC or state of health (SOH) since it is completely emulated by the inverters.

The final topology connects the batteries and the fast charging stations to the closest cabinet. This downstream connection creates challenges since the required power to charge the batteries and supply the fast charging stations needs to be distributed through the LV grid which already faces issues due to the DER rollout. In theory, the battery could provide active power support to upstream cables and substations on both MV and LV levels, additionally to reactive power support. In practice, the required power for the additional load from the fast charging stations creates new thermal overloads and voltage issues, which makes this topology configuration not a suitable solution.

5.1.2 Battery sizing

The optimisation problem which sizes batteries based on a fast charging station load profile has demonstrated its accuracy when looking at individual profiles. However, when choosing a common size for all batteries that would satisfy all generated profiles, the only combination which doesn't violate any grid constraint is the one of the largest charging power and capacity, resulting in an over-dimensioned battery for the sole purpose of fast-charging active power support. When using this battery to provide active power support to other assets, some of these batteries start to use their full range of capacity, but until then it results in a large investment need with limited benefits.

The positive aspect of this low utilisation is that the batteries' degradation will be slower and their SOH will remain high for a longer time than for highly utilised batteries.

This results in a longer lifetime and therefore decreases the CAPEX over time. To increase the batteries' utilisation, participation in other regulation markets such as primary frequency control can be considered, especially when grouping all the batteries in a virtual power plant. This needs to be coordinated with the fast charging station demand and the batteries can only be scheduled during hours when the demand is low. The resulting risk, however, is that the batteries induce thermal overloads when being activated for that purpose. This activation would result in value stacking, further discussed in section 5.3.2.

5.1.3 Existing transformer upgrade

The strength of the conventional-like topology is the removal of MV-side thermal overloads through active power support, and therefore consequent additional savings. The transformer LV-side topology can, additionally to voltage support through reactive power, also contribute to removing MV-side thermal overloads. However, this topology is limited by the secondary substation's transformer size and can in this case, only solve the minor thermal overloads. A hybrid solution could be to upgrade the size of the transformer to allow for more power to flow through. This would reduce the battery's costs by allowing for greater savings on cable costs, but the required transformer upgrade would diminish these savings and this drawback needs to be assessed.

5.1.4 Voltage issue mitigation methods

As mentioned in section 3.2.2, several methods can be used to deal with voltage issues. Here, the use of reactive power compensation from the PV inverters in combination with a conventional cable upgrade to reduce the internal resistance is used. Other methods can be used, such as transformer tap changers. It is mentioned that these could not be used due to not being on-load tap changers remotely or sensor-based controlled. However, in a grid with the suited components, simulations using the pandapower transformer tap changer controller [17] could show whether this solution is suited and enough to remove all voltage issues. Three other solutions exist: the use of reactive power compensation units, placed strategically in the grid where reactive power injection or consumption has the most positive effect, could be investigated. Another one is to equip PV inverters with a controller that sets the active power injection to zero when the voltage measured at the connection point is above a certain threshold. The final one is to extend the MV grid in areas where the most severe voltage issues at LV level are identified. Replacing some LV cables with MV ones and installing new transformer stations would help technically but need to be economically assessed first.

5.2 Economic assessment

The economic sensitivity analysis has shown that the model is not very sensitive to asset and battery prices. The cost differences are so significant that price variations in both these categories do not affect the majority of outcomes. Only some edge cases give the economic advantage to the battery-based solution.

The electricity price also plays a role in the economic assessment but to a lower extent. Due to the batteries' higher losses in comparison to transformers, they are more affected both positively in the case of low electricity prices and negatively in the case of high prices. The chosen electricity price here is the 2021 average day-ahead one, significantly higher than the previous years but similar to the 2023 one. A strong future price evolution could move the balance in favour of one or the other option, but only in a minority of cases.

Batteries that benefit from the highest additional savings are the ones able to differ investments in the MV part of the grid. However, these are also the batteries that will be activated most often to solve these issues. These savings, then come at the cost of higher losses (which are taken into account in the CBA analysis) and at a higher degradation rate, potentially resulting in a lower lifetime which would affect negatively the batteries' costs.

The best economic outcome is reached under different topology variations, such as the hybrid upgrade, which is systematically cheaper than the conventional upgrade, or grouping batteries when the topology allows it, resulting in 29% of cases under which the battery is economically superior.

5.3 Futher considerations

5.3.1 Battery ownership

In this thesis, the ownership of the battery lies in the hands of the grid operators. However, based on current regulations, these are not allowed to own or operate such an asset [68].

When a battery is installed in combination with a fast charging station today, the charge point operator is usually the owner and operator of the battery. This battery can then be used to perform energy arbitrage: the operator charges it when the electricity spot price is low, therefore decoupling the charging sessions from the time when power is drawn from the grid [69]. While this method can be very effective for the charge point operator to reduce both connection and energy costs, the battery is not operated in a grid-supportive way, and could even increase the stress on it if one assumes that owners of EVs charging at home follow similar price signals.

Therefore, the grid-supportive operation of the batteries as presented in this thesis is only possible under the participation of the charge point operator in local congestion or voltage support markets where the financial incentives are higher than the potential savings from energy arbitrage or a change of regulations allowing the grid operators to own and operate these assets (which is currently discussed [68]).

The work in this thesis shows that under the right conditions, grid investment savings can be reached by using batteries. If these batteries could be owned by grid operators, social welfare could be increased and society could benefit from it. Therefore, the regulation framework needs to be adapted to allow this while enforcing rules to ensure that the batteries are not misused to generate additional revenues.

5.3.2 Value stacking

Value stacking is using the battery for multiple purposes and offering its services on multiple markets, therefore maximising its utilisation and increasing the revenue stream. Already mentioned in the previous sections, this is dependent on the battery ownership and the regulation framework around it. Besides congestion management and investment deferral, common battery applications are primary frequency control and energy arbitrage. As of now, these two cannot be performed by grid operators, due to unbundling regulations. From a technical point of view, the remaining battery capacity after its primary objective (here differ grid investments) needs to be assessed first. The average number of cycles per year under different topologies is shown in table 5.1.

Topology	**Average number of cycles per battery per year**
Conventional-like	94
Transformer LV-side	59
LV	50
Hybrid upgrade	8

Table 5.1: Number of cycles per topology

With an assumed average 2,000 cycles lifetime, over a 20-year period as used here, batteries in the conventional-like topology do not have a significant spare capacity. This is mostly due to the control method which uses a fixed charging power, compared to the other ones based on the grid's status. The same method on the conventional-like topology would probably result in a lower number of cycles. On the LV topology, the cycle number is lower than the transformer LV-side topology because of the grid upgrade performed to accommodate the battery and fast charging loads. Before these upgrades, the average number of cycles per battery and year lies at 157, resulting in an estimated lifetime of 13 years. The other topologies and in particular the hybrid upgrade could offer more spare capacity, between 820 and 1,840 cycles for other purposes, over 20 years or more.

From a scheduling point of view, figure 5.1 shows the batteries' minimum remaining capacity for every day of a year after investment deferral activation under the conventional-like topology.

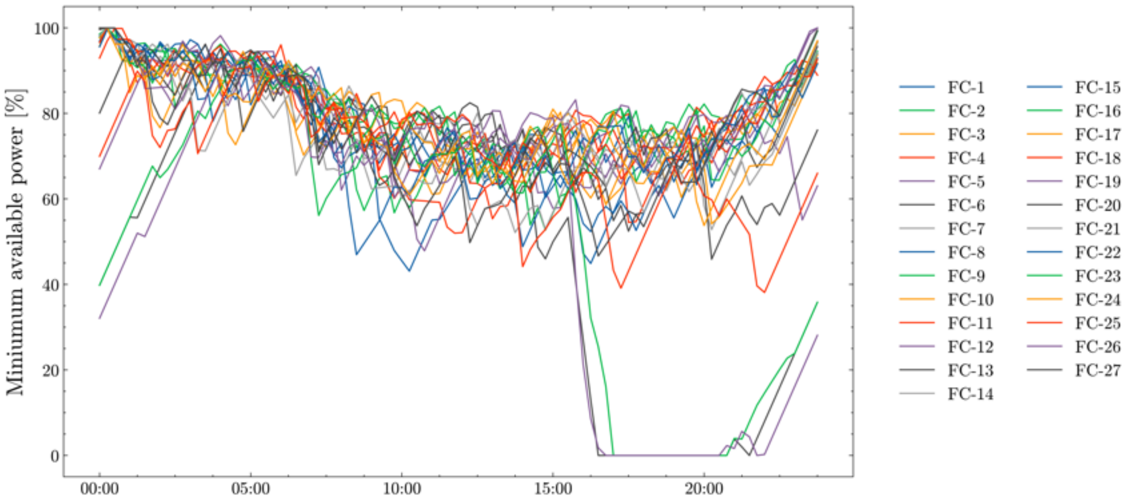

Figure 5.1: Minimum remaining capacity per hour under the conventional-like topology over a year

This topology connects the batteries to the MV part of the grid, therefore making feeding back not dependent on the capacity of the LV grid. It shows that for some hours of the day, the remaining capacity is relatively homogenous across the battery fleet, but still with differences of up to 40% (e.g. from 05:00 to 15:00), and spreads out even more in the evening and night. This shows that each battery needs to be assessed individually before it can be used to do value stacking since not all of them might be available. The other aspect to consider is local congestion at the activation time, to ensure that no new thermal overloads are induced in the distribution grid when using the batteries on other markets.

5.3.3 Battery size footprint

The battery's footprint is another factor that influences its economic impact. When installing a fast charging station in a public parking space, it can be assumed that the space requirements are not as strict as compared to a densely built urban area. However, batteries of the size investigated here still require a larger footprint than a secondary substation that would be built in the conventional option (14.4m^2 for a 1MWh battery vs. 7.41m^2 for a 800kVA secondary substation) [70, 71]. The space for the battery that would otherwise probably be an additional parking spot represents a loss for the parking operator who would ask for some sort of compensation. This cost needs to be added to the batteries' economic impact and might make it a less viable option.

5.3.4 Flexibility

Flexibility is a widely discussed topic in the electric grid and markets as a solution to accommodate high loads in grids that are not dimensioned to withstand these. In this case, as well, flexibility could be a viable solution to reduce some of the investments that represent a significant amount of money and are caused by peaks.

More than 80% of the voltage issues due to the rollout of DERs are solved during the thermal overload-related investments, but 66% of the total upgrade costs are spent on solving the remaining 20%. Similarly, the overload peaks that happen after connecting the fast charging stations only occur during a few timesteps. Savings could be achieved on the cables to upgrade or the battery to install by activating flexibility on other installations (since fast charging stations are not suited for that due to the immediate power expectation from the users). Installing a small-scale battery to handle these peaks might also be a viable solution, as presented under the hybrid topology.

6 Conclusion

The methodology for a grid planning algorithm to assess the impact of DERs and fast charging stations has been developed and tested on the grid and meter data from the Danish DSO NKE-Elnet. Furthermore, a conventional and a battery-based upgrade to accommodate fast charging stations have been compared technically and economically, under different topology configurations.

The impact of DERs results in thermal overloads and voltage issues mostly on the LV side of the grid, requiring investments and the use of other measures such as reactive power compensation. The total investment need due to the additional load and production capacity lies at 79MDKK until 2045, with 92% of these costs caused by issues in the low voltage grid. The voltage issues not being solved by reactive power compensation require a cable upgrade and represent 66% of the total investment.

Fast charging stations mostly impact the MV grid by increasing the loading in primary substations and MV cables. In this case, the MV grid showed enough spare capacity resulting in only a few issues due to additional loading compared to DERs. The alternative solution to the conventional grid extension is to use batteries. These fulfil their role without causing technical issues, but their higher costs and losses make this option 212% to 491% higher than the cost of using transformers.

One advantage of batteries is their additional saving potential that can be achieved by removing the need to replace assets with thermal overloads or voltage issues due to the DER or fast charging station rollout. The developed active and reactive power controllers show that the power output of batteries can be controlled based on the grid's status to reduce thermal loading and voltage issues. Different battery topologies are tested and can target either the MV grid by placing batteries upstream of secondary substations or the LV grid by placing them downstream of these stations. Thermal overloads on the MV grid can be removed and significant savings can be reached due to the high costs of MV cables, resulting in battery savings of up to 65%. Fewer thermal overloads can be removed when connecting the batteries to the LV grid, but this configuration can solve voltage issues. The resulting battery savings lay between 3% and 41%.

However, the battery-based solution is not economically viable even with these savings due to the relatively high costs of batteries compared to conventional grid components and their higher losses. Across all topologies situations, a transformer-based conventional upgrade is between 7% and 1,109% more cost-efficient, the large spread being due to energy losses and battery-induced savings or additional expenses.

This model is not particularly sensitive to price variations. Conventional assets and battery price development as well as electricity prices were investigated and results show that the conventional upgrade method is economically more viable in the large majority of cases. Sensitivity analyses show that batteries are more cost-efficient than conventional upgrades only in up to 11% of the cases depending on the chosen topology and the individual situation. In the most cost-efficient topology, 30% of the investigated cases are less expensive than a conventional upgrade under the right economic situation. Different topology variations yield better results, such as grouping batteries for multiple fast charging stations creates individual situations where batteries are economically superior to transformers. Using a hybrid upgrade where a transformer is built and combined with a smaller capacity battery is the most competitive topology variation, resulting in an average of 62% cost savings compared to a conventional upgrade. This topology shows that a transformer sized at 50% of the connection needed in combination with an optimally sized battery is a reliable and cost-efficient solution, especially when compared to a conventional upgrade.

It can be concluded that using batteries to differ conventional grid investments is sensitive to the chosen topology and while some might not be a universal solution and need to be assessed individually, others give systematic savings. The grid planning algorithm developed and tested on this use case presents a methodology that grid planners can use to assess the technical and economic impact of the two discussed grid upgrade methods. The current and forecasted battery prices are one of the main challenges regarding the competitiveness of this solution compared to conventional assets. In case of major additional decreases in these prices or increases in conventional asset prices, the battery-based solution might significantly gain attractiveness. Further major blockers to getting there are the current regulation not allowing DSOs to own and operate such assets, and the lack of experience of grid operators with these assets.

This analysis was performed from the DSO point of view. For a charge point operator, the battery solution still makes sense, as it allows for a faster and cheaper connection to the grid, and operational savings by decoupling the fast charging station demand from the time the power needs to be drawn from the grid. If not owned by the DSO, the batteries could also be used to perform other grid services, such as primary frequency control. This would result in a higher utilisation and lower costs, but requires coordination with the fast charging station demand and could result in inducing new thermal overloads. These operation modes might, therefore, end up with higher investment needs for the DSO.

Future work

Future investigations can be carried out on multiple aspects touched upon in this thesis. Regarding the generation of fast charging station profiles, differences between stations based on parameters that were not taken into account here can appear: a station located next to a road experiencing a high traffic number will probably be more used than a station seeing less traffic. Charging price is also an important factor, as users will prefer a cheaper operator. Finally, based on the location type of the fast charging station, its peak usage and the time of this peak might vary based on which type of amenities it is close to [72]. Another investigation area is the batteries' charging mode. Here, the batteries are charged either based on a fixed charging power or on the available remaining grid capacity. Another mode could charge the battery based on the upcoming needs. A machine learning algorithm could be trained based on a large number of profiles and it could optimise the charging of the battery based on the forecasted upcoming demand at the fast charging station. As the hybrid topology showed the most interesting economic results, the battery sizing algorithm could be extended to take this parameter into account, and output not only a battery charging power and capacity but also a transformer capacity, where the combination of these two assets would result in the minimum costs. Finally, the value stacking opportunity can be investigated and the combined operation mode of these batteries on multiple markets can be assessed technically and economically, to find where the largest technical impact can be made and social welfare generated.

Bibliography

[1] H. Hõimoja et al. "An Ultrafast EV Charging Station Demonstrator". In: *International Symposium on Power Electronics Power Electronics, Electrical Drives, Automation and Motion* (2012). DOI: https://doi.org/10.1109/SPEEDAM.2012.6264617.

[2] D. Sbordone et al. "EV fast charging stations and energy storage technologies: A real implementation in the smart micro grid paradigm". In: *Electric Power Systems Research* 120 (2015), pp. 96–108. DOI: https://doi.org/10.1016/j.epsr.2014.07.033.

[3] Jan Engelhardt et al. "Energy management of a multi-battery system for renewable-based high power EV charging". In: *eTransportation* 14 (2022), p. 100198. DOI: https://doi.org/10.1016/j.etran.2022.100198.

[4] Huajie Ding, Zechun Hu, and Yonghua Song. "Value of the energy storage system in an electric bus fast charging station". In: *Applied Energy* 157 (2015), pp. 630–639. DOI: https://doi.org/10.1016/j.apenergy.2015.01.058.

[5] Lu Wang et al. "Grid Impact of Electric Vehicle Fast Charging Stations: Trends, Standards, Issues and Mitigation Measures - An Overview". In: *IEEE Open Journal of Power Electronics* 2 (2021), pp. 56–74. DOI: 10.1109/OJPEL.2021.3054601.

[6] Wajahat Khan, Furkan Ahmad, and Mohammad Saad Alam. "Fast EV charging station integration with grid ensuring optimal and quality power exchange". In: *Engineering Science and Technology, an International Journal* 22.1 (2019), pp. 143–152. ISSN: 2215-0986. DOI: https://doi.org/10.1016/j.jestch.2018.08.005. URL: https://www.sciencedirect.com/science/article/pii/S2215098617315057.

[7] Mostafa M. Mahfouz and M. Reza Iravani. "Grid-Integration of Battery-Enabled DC Fast Charging Station for Electric Vehicles". In: *IEEE Transactions on Energy Conversion* 35.1 (2020), pp. 375–385. DOI: 10.1109/TEC.2019.2945293.

[8] L. G. González, E. Siavichay, and J. L. Espinoza. "Impact of EV fast charging stations on the power distribution network of a Latin American intermediate city". In: *Renewable and Sustainable Energy Reviews* 107 (2019), pp. 309–318. DOI: https://doi.org/10.1016/j.rser.2019.03.017.

[9] Kalid Yunus, Hector Zelaya De La Parra, and Muhamad Reza. "Distribution grid impact of Plug-In Electric Vehicles charging at fast charging stations using stochastic charging model". In: *Proceedings of the 2011 14th European Conference on Power Electronics and Applications*. 2011, pp. 1–11.

[10] Niels Leemput et al. "MV and LV Residential Grid Impact of Combined Slow and Fast Charging of Electric Vehicles". In: *Energies* 8.3 (2015), pp. 1760–1783. ISSN: 1996-1073. DOI: 10.3390/en8031760. URL: https://www.mdpi.com/1996-1073/8/3/1760.

[11] Chunyang Zhao et al. "Grid-connected battery energy storage system: a review on application and integration". In: *Renewable and Sustainable Energy Reviews* 182 (2023), p. 113400. DOI: https://doi.org/10.1016/j.rser.2023.113400.

[12] K. Prakash et al. "Planning battery energy storage system in line with grid support parameters enables circular economy aligned ancillary services in low voltage networks". In: *Renewable Energy* 201 (Part 1 2022), pp. 802–820. DOI: https://doi.org/10.1016/j.renene.2022.10.101.

[13] Carlos Mateo et al. "Analysis of the impact of battery storage on power distribution systems". In: (2015).

[14] Carlos Mateo et al. "Cost-benefit analysis of battery storage in medium-voltage distribution networks". In: *IET Generation, Transmission & Distribution* 10 (3 2016), pp. 815–821. ISSN: 1751-8687. DOI: https://doi.org/10.1049/iet-gtd.2015.0389.

[15] Marjan Gjelaj et al. "Optimal infrastructure planning for EV fastcharging stations based on prediction of user behaviour". In: *IET Electrical Systems in Transportation* 10 (1 2020), pp. 1–12. ISSN: 2042-9738. DOI: https://doi.org/10.1049/iet-est.2018.5080.

[16] Jos van der Burgt et al. "Grid impact of charging electric vehicles; study cases in Denmark, Germany and The Netherlands". In: *2015 IEEE Eindhoven PowerTech* (2015), pp. 1–6. DOI: 10.1109/PTC.2015.7232234.

[17] L. Thurner et al. "pandapower — An Open-Source Python Tool for Convenient Modeling, Analysis, and Optimization of Electric Power Systems". In: *IEEE Transactions on Power Systems* 33.6 (Nov. 2018), pp. 6510–6521. ISSN: 0885-8950. DOI: 10.1109/TPWRS.2018.2829021.

[18] Janamejaya Channegowda, Vamsi Krishna Pathipati, and Sheldon S. Williamson. "Comprehensive review and comparison of DC fast charging converter topologies: Improving electric vehicle plug-to-wheels efficiency". In: *2015 IEEE 24th International Symposium on Industrial Electronics (ISIE)*. 2015, pp. 263–268. DOI: 10.1109/ISIE.2015.7281479.

[19] Md Mustafizur Rahman et al. "The development of techno-economic models for the assessment of utility-scale electro-chemical battery storage systems". In: *Applied Energy* 283 (2021), p. 116343. ISSN: 0306-2619. DOI: https://doi.org/10.1016/j.apenergy.2020.116343. URL: https://www.sciencedirect.com/science/article/pii/S0306261920317256.

[20] Wesley Cole and Akash Karmakar. "Cost Projections for Utility-Scale Battery Storage: 2023 Update". In: (2023). URL: https://www.nrel.gov/docs/fy23osti/85332.pdf.

[21] Energi- og Forsyningsministeriet Klima-. *Bekendtgørelse om indtægtsrammer for netvirksomheder*. 2021. URL: https://www.retsinformation.dk/eli/lta/2021/1127.

[22] M. Ravindran. "Transformer life-cycle costing analysis". In: *International Journal of Scientific & Engineering Research* 9.4 (2018). ISSN: 2229-5518. URL: https://www.ijser.org/researchpaper/TRANSFORMER-LIFE-CYCLE-COSTING-ANALYSIS.pdf.

[23] Nord Pool. *Day-ahead prices*. 2023. URL: https://www.nordpoolgroup.com/en/Market-data1/Dayahead/Area-Prices/ALL1/Yearly/?view=table.

[24] Robert J. Hijmans and Berkeley. Museum of Vertebrate Zoology University of California. *Second-level Administrative Divisions, Denmark*. 2015. URL: https://geodata.lib.berkeley.edu/catalog/stanford-zz765fd7706 (visited on 09/13/2023).

[25] Neogeografen N. Darville. *dagi*. 2015. URL: https://github.com/ok-dk/dagi (visited on 09/13/2023).

[26] Klima- Energi- og Forsyningsministeriet. *Sådan hjælper Danmark andre lande til at nå deres klimamål*. 2023. URL: https://kefm.dk/aktuelt/nyheder/2023/apr/saadan-hjaelper-danmark-andre-lande-til-at-naa-deres-klimamaal#:~:text=Klimaloven%20s%C3%A6tter%20bindende%20nationale%20m%C3%A5l,udledninger%20uden%20for%20Danmarks%20gr%C3%A6nser. (visited on 09/12/2023).

[27] DBI IT A/S. *Bilstatistik*. 2023. URL: https://www.bilstatistik.dk/ (visited on 09/12/2023).

[28] Danmark Statistik. *BY1: Folketal 1. januar efter byområder, landdistrikter, alder og køn*. 2023. URL: https://www.statistikbanken.dk/by1 (visited on 09/20/2023).

[29] Næstved Kommune - Plan & Trafik. *Lokalplan C1.1/30-3/E28.1-1/E3.1-1*. 2012. URL: https://dokument.plandata.dk/20_1062219_1473415527517.pdf (visited on 09/26/2023).

[30] Næstved Kommune - Plan & Trafik. *Lokalplan 027*. 2012. URL: https://dokument.plandata.dk/20_1425741_APPROVED_1331201555356.pdf (visited on 09/26/2023).
[31] Søren Jakobsen et al. *Sådan skaber Danmark grøn infrastruktur til én million elbiler: Analyse og anbefalinger fra DEA og DTU, november 2019*. English. Technical University of Denmark, 2020.
[32] Energistyrelsen. *Analyseforudsætninger til Energinet*. 2023. URL: https://ens.dk/service/fremskrivninger-analyser-modeller/analyseforudsaetninger-til-energinet (visited on 09/15/2023).
[33] ChargeFinder. *ChargeFinder*. 2023. URL: https://chargefinder.com/dk/naestved/ladestandere-elbiler/2pj5wy (visited on 09/12/2023).
[34] Vejdirektoratet. *Vejdirektoratet*. 2023. URL: http://vej08.vd.dk/komse/nytui/komse/komSe.html?noegle=2505043944 (visited on 09/12/2023).
[35] Geofabrik GmbH and OpenStreetMap Contributors. *Denmark*. 2018. URL: http://download.geofabrik.de/europe/denmark.html (visited on 09/13/2023).
[36] Google. *Google Maps*. 2023. URL: https://www.google.dk/maps/search/gas+station/@55.2330784,11.7449977,13.19z/data=!4m2!2m1!6e2?entry=ttu (visited on 09/13/2023).
[37] Brandon Cohen. *Open Parking Map App*. 2023. URL: https://parkingreform.org/resources/parking-lot-map/open-parking-map-app/ (visited on 09/13/2023).
[38] EV Database. *EV Database*. 2015. URL: https://ev-database.org/ (visited on 09/13/2023).
[39] Rick Wolbertus and Robert Van Den Hoed. "Fast Charging Systems for Passenger Electric Vehicles". In: *World Electr. Veh. J.* 11 (4 2020), p. 73. DOI: https://doi.org/10.3390/wevj11040073.
[40] Mærk Næstved. *Turismetillæg*. 2018. URL: https://www.naestved.dk/media/ddrbofz3/bilag-a-til-kommuneplanstrategi-2019-turismetillaeg.pdf (visited on 09/13/2023).
[41] ICP A/S. *Detailhandelsanalyse - Næstved kommune*. 2013. URL: https://naestvederhverv.dk/wp-content/uploads/sites/8004/2014/11/ICP-N%C3%A6stved-april-2013.pdf (visited on 09/13/2023).
[42] OpenStreetMap contributors. *Planet dump retrieved from https://planet.osm.org*. 2017. URL: https://www.openstreetmap.org.
[43] Søren Flytkjær and Rasmus Jungersen. *Vores biler bliver større - og nu undersøges det, om p-båsene også burde være det*. 2022. URL: https://www.dr.dk/nyheder/indland/vores-biler-bliver-stoerre-og-nu-undersoeges-det-om-p-baasene-ogsaa-burde-vaere-det (visited on 09/29/2023).
[44] Næstved Kommune. *Varmeplanskort 2030*. 2022. URL: https://naestved.viewer.dkplan.niras.dk/plan/8#/3349 (visited on 09/14/2023).
[45] Klima- Energi- og Forsyningsministeriet. *Aftale om et mere grønt og sikkert Danmark*. 2022. URL: https://kefm.dk/aktuelt/nyheder/2022/jun/aftale-om-et-mere-groent-og-sikkert-danmark- (visited on 09/14/2023).
[46] Vurderingsstyrelsen. *BBR*. 2022. URL: https://bbr.dk/forside (visited on 09/14/2023).
[47] Energinet. *Production per Municipality*. 2023. URL: https://www.energidataservice.dk/tso-electricity/CommunityProduction (visited on 09/15/2023).
[48] Solargis s.r.o. *Global Solar Atlas*. 2023. URL: https://globalsolaratlas.info/map?c=55.230785,11.609802,11&s=55.174554,11.758448&m=site&pv=small,180,40,1 (visited on 09/15/2023).
[49] Næstved Kommune. *Debatoplæg Solcelleanlæg ved Viborggård*. 2023. URL: https://www.naestved.dk/media/0lipuwwt/debatoplaeg_solceller-ved-viborggaard.pdf (visited on 09/15/2023).

[50] Næstved Kommune. *Forslag til Klimaplan 2020-2030*. 2020. URL: https://www.naestvedfjernvarme.dk/media/36719/bilag-61-forslag-til-naestved-kommunes-klimaplan-2020-2030.pdf (visited on 09/15/2023).

[51] Martin Raifer. *overpass turbo*. 2023. URL: https://overpass-turbo.eu/ (visited on 09/15/2023).

[52] Energistyrelsen. *Technology Data - Generation of Electricity and District Heating*. 2016. URL: https://ens.dk/sites/ens.dk/files/Analyser/technology_data_catalogue_for_el_and_dh.pdf (visited on 09/15/2023).

[53] J. Melius, R. Margolis, and S. Ong. *Estimating Rooftop Suitability for PV: A Review of Methods, Patents, and Validation Techniques*. 2013. URL: https://www.nrel.gov/docs/fy14osti/60593.pdf (visited on 09/15/2023).

[54] Skipper Seabold and Josef Perktold. "statsmodels: Econometric and statistical modeling with python". In: *9th Python in Science Conference*. 2010.

[55] Rick Wolbertus and Robert Van Den Hoed. "Electric Vehicle Fast Charging Needs in Cities and along Corridors". In: *World Electr. Veh. J.* 10 (2 2019), p. 45. DOI: https://doi.org/10.3390/wevj10020045.

[56] Christopher Neuman, Andrew Meintz, and Myungsoo Jun. "Workplace Charging Data." In: *NREL Data Catalog* (2022). DOI: https://doi.org/10.7799/1838140. URL: https://data.nrel.gov/submissions/182.

[57] ElaadNL. *Download data van Elaad*. 2020. URL: https://platform.elaad.io/download-data/ (visited on 09/13/2023).

[58] Elisabeth Schneider & Michael Knoop Marlon Schlemminger Tobias Ohrdes. "Dataset on electrical single-family house and heat pump load profiles in Germany". In: *Sci Data* 9 (2022). DOI: https://doi.org/10.1038/s41597-022-01156-1.

[59] DMI. *DMI*. 2023. URL: https://www.dmi.dk/frie-data/ (visited on 09/13/2023).

[60] Statistisches Bundesamt (Destatis). *Von Januar bis November 2020 genehmigte Wohnungen: 59 % in Mehrfamilienhäusern*. 2021. URL: https://www.destatis.de/DE/Presse/Pressemitteilungen/2021/02/PD21_N015_44.html#:~:text=Wohnungen%20in%20neuen%20Einfamilienh%C3%A4usern%20waren,Einfamilienh%C3%A4usern%20betrug%20durchschnittlich%20152%20Quadratmeter. (visited on 09/15/2023).

[61] Energinet. *Production and Consumption - Settlement*. 2023. URL: https://www.energidataservice.dk/tso-electricity/ProductionConsumptionSettlement (visited on 09/13/2023).

[62] Energistyrelsen. *Energistyrelsen lancerer ny solcelleopgørelse over udbygningen med solceller i Danmark*. 2023. URL: https://ens.dk/node/4320/pdf (visited on 09/13/2023).

[63] Raveendhra Dogga and M.K. Pathak. "Recent trends in solar PV inverter topologies". In: *Solar Energy* 183 (2019), pp. 57–73. ISSN: 0038-092X. DOI: https://doi.org/10.1016/j.solener.2019.02.065. URL: https://www.sciencedirect.com/science/article/pii/S0038092X19301999.

[64] Can Karatas, Jasmin Mehmedalic, and Jonas B. B. Hansen. *TEGRA-modellen – Forstærkning*. 2022. URL: https://greenpowerdenmark.dk/files/media/document/RA638-TEGRA-modellen-Forstaerkning.pdf.

[65] Forsyningstilsynet. *Reguleringsregnskaber*. 2023. URL: https://forsyningstilsynet.dk/el/indberet/netvirksomheder/reguleringsregnskaber.

[66] BloombergNEF. *Top 10 Energy Storage Trends in 2023*. 2023. URL: https://about.bnef.com/blog/top-10-energy-storage-trends-in-2023/ (visited on 11/22/2023).

[67] Tim Unterluggauer et al. "Impact of cost-based smart electric vehicle charging on urban low voltage power distribution networks". In: *Sustainable Energy, Grids and Networks* 35 (2023), p. 101085. DOI: https://doi.org/10.1016/j.segan.2023.101085.

[68] Council of European Energy Regulators. *CEER Short paper on the ownership of Storage Facilities in the Electrical Distribution System*. 2023. URL: https://www.ceer.eu/documents/104400/-/-/d87af5f6-794d-ac83-f3f5-c28c26789cfd.

[69] Freewire. *Boost Charger 150*. 2023. URL: https://freewiretech.com/dc-boost-charger/.

[70] Battery Backup Power. *1,144 KWh (1 MWh) Industrial Battery Backup And Energy Storage Systems (ESS) (277/480Y Three Phase)*. 2023. URL: https://www.backupbatterypower.com/products/1-144-kwh-industrial-battery-backup-and-energy-storage-systems-ess-277-480-three-phase?pr_prod_strat=use_description&pr_rec_id=83109ee86&pr_rec_pid=6561192214696&pr_ref_pid=6561191395496&pr_seq=uniform.

[71] ABB. *UniPack-G Product catalog*. 2023. URL: https://library.e.abb.com/public/4da8d0dee20f40a99ed6eb87e9286858/UniPack-G%20Catalog%20Rev%20C.pdf?x-sign=rJTzAR9JjxJJB4L3JbesotOFzk08zcOgNQ+ubqBwAyKhIUAcHyhFvCMBO8sDIhro.

[72] Xiao-Hui Sun, Toshiyuki Yamamoto, and Takayuki Morikawa. "Fast-charging station choice behavior among battery electric vehicle users". In: *Transportation Research Part D: Transport and Environment* 46 (2016), pp. 26–39. ISSN: 1361-9209. DOI: https://doi.org/10.1016/j.trd.2016.03.008. URL: https://www.sciencedirect.com/science/article/pii/S1361920916000377.

A Fast charging station locations

Figure A.1: Traffic data

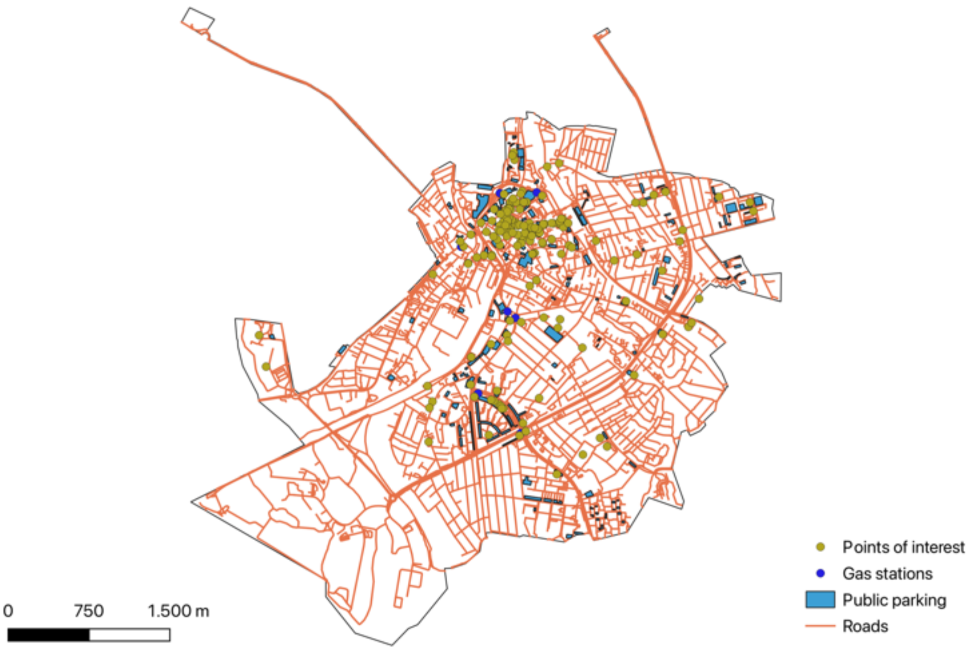

Figure A.2: Points of interest for fast charging stations

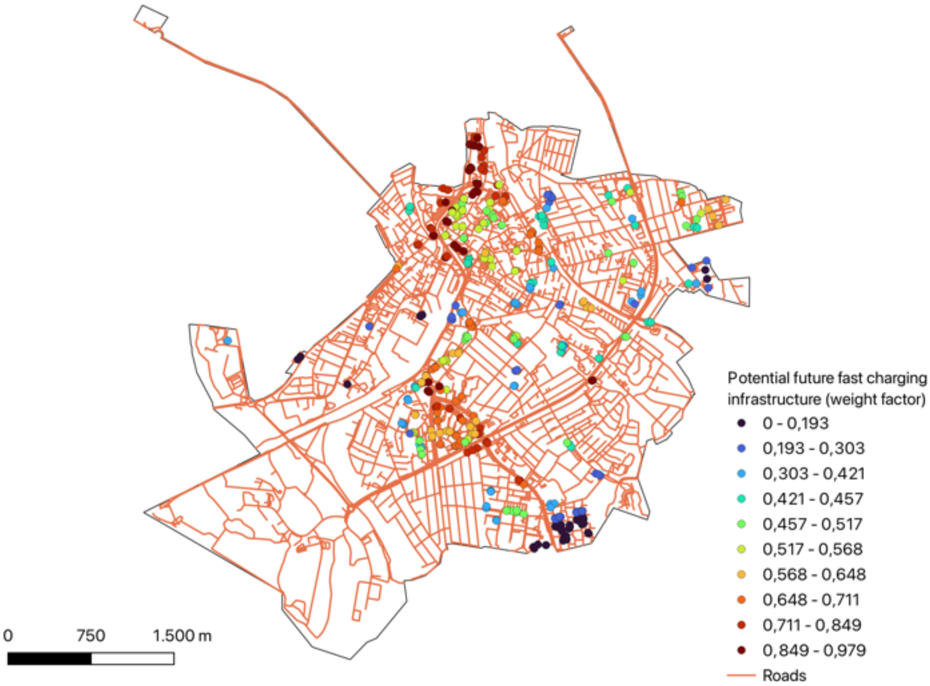

Figure A.3: Potential future fast charging stations

B Fast charging use

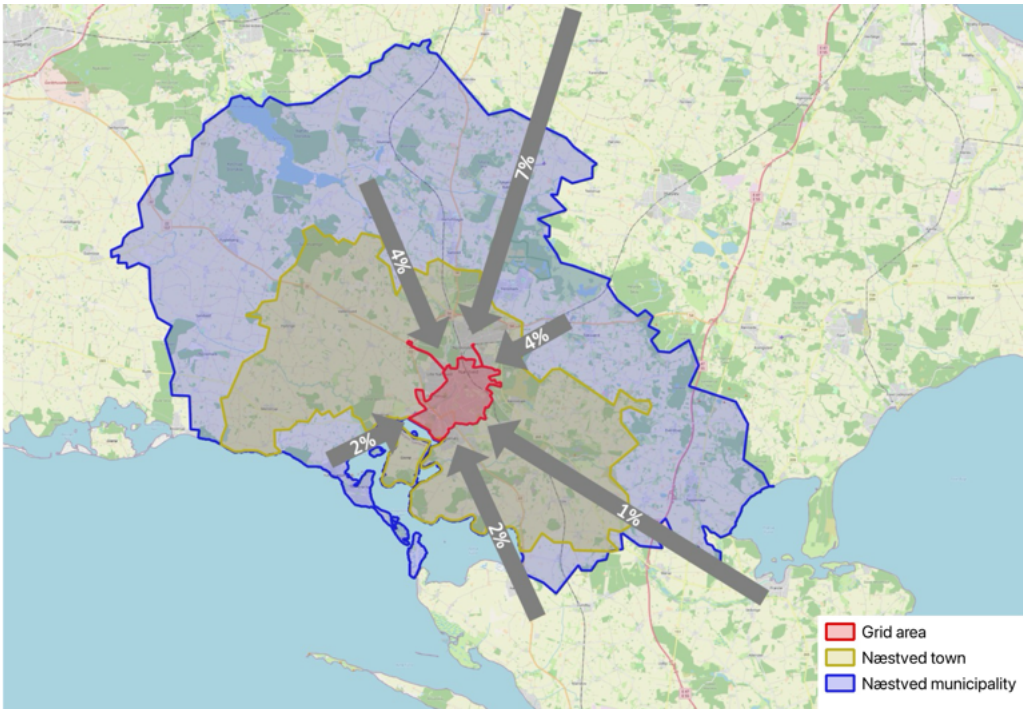

Figure B.1: Day tourists coming outside of Næstved town

C Penetration of other DERs

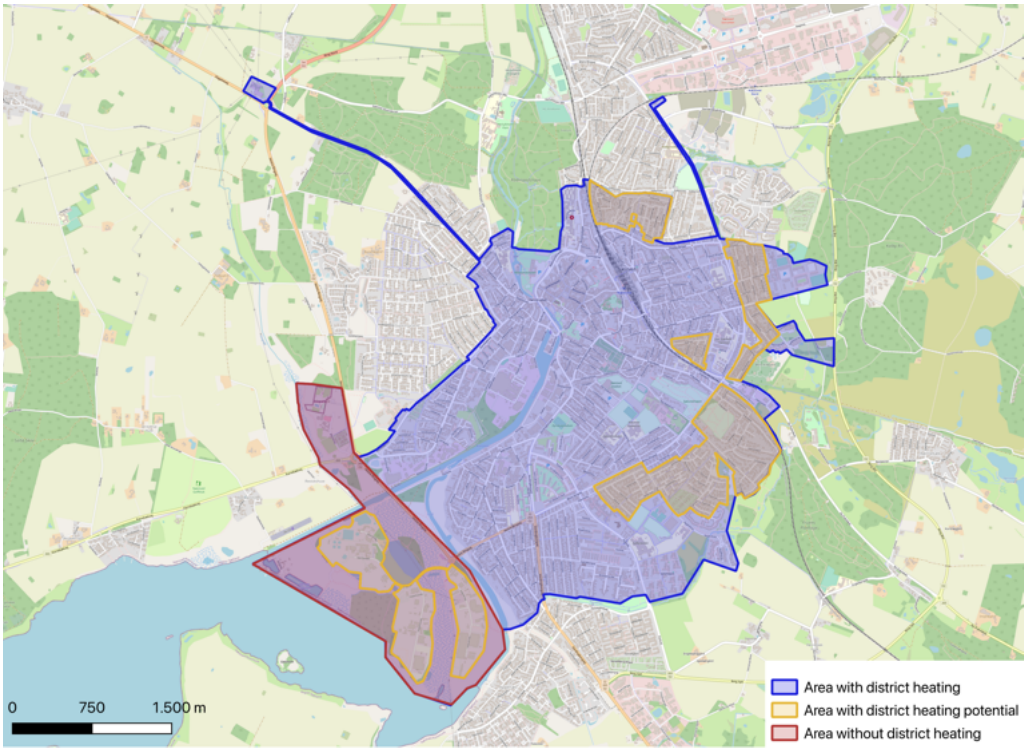

Figure C.1: District heating areas

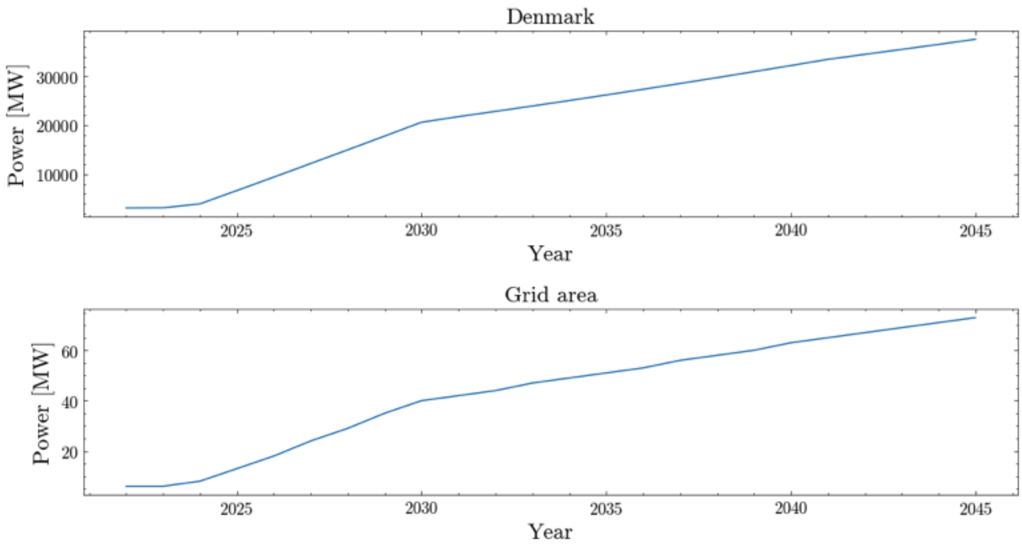

Figure C.2: PV capacity

D Load profiles

Battery size category [kWh]	Battery size [kWh]	Maximum fast charging power [kW]
(30, 50]	32.3	37
	35.8	40
	49	46
(50, 70]	52	46
	54.25	74
	64	141
	64.8	80
	66.25	223
	67.3	214
	67.5	145
	67.5	114
	68.2	143
	68.7	145
	69	218.5
(70, 100]	70.45	154
	70.6	250
	74	37
	76	198
	77	154
	82.6	108
	95	223

Table D.1: EV maximum fast charging power based on battery size

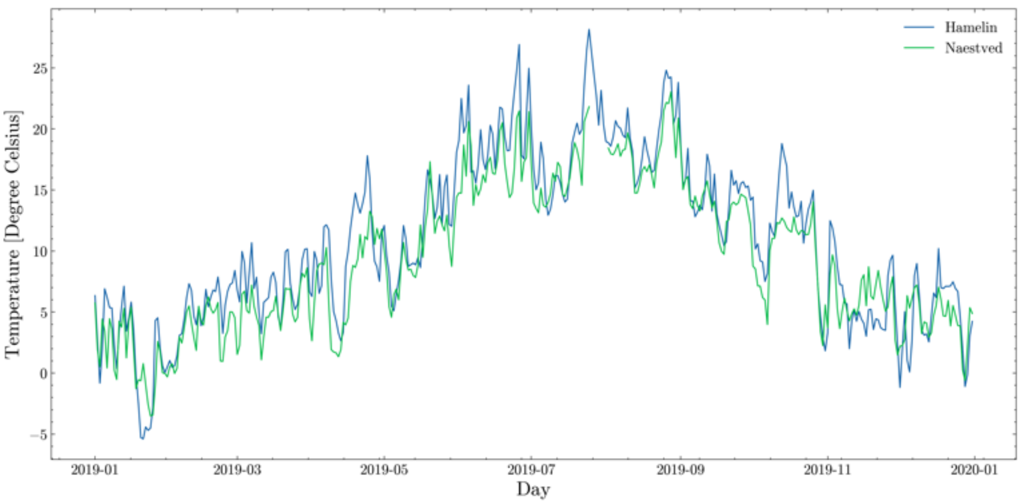

Figure D.1: Temperature in Næstved and Hamelin in 2019

E Conventional grid upgrade model

Dimension [mm^2]	Voltage [kV]	Rated current [A]	R [Ω/km]	X [Ω/km]	C [nF/km]
95	10	222	0.32	0.097	310
120	10	243	0.253	0.099	400
150	10	283	0.206	0.091	360
240	10	373	0.125	0.085	440
300	10	455	0.075	0.089	440
400	10	515	0.083	0.097	560
500	10	570	0.067	0.094	620
95	0.4	213	0.32	0.103	370
120	0.4	240	0.254	0.072	1,000
150	0.4	276	0.206	0.080	1,260
240	0.4	315	0.127	0.072	970
300	0.4	410	0.103	0.072	1,030

Table E.1: Cable electrical parameters

Voltage level [kV]	Rated power [kVA]	Short circuit voltage [%]	Real component of short circuit voltage [%]	Iron losses [kW]	Open loop losses [%]
60/10	16,000	10	0.66	17.9	0.146
60/10	20,000	10	0.65	21.1	0.105
60/10	25,000	10	0.6	24.6	0.06
10/0.4	250	4	1.2	0.82	0.382
10/0.4	400	4	1.075	1.15	0.288
10/0.4	600	4	1.016	1.5	0.238
10/0.4	800	6	0.963	1.7	0.212
10/0.4	1,000	6	0.88	2	0.2
10/0.4	1,250	6	0.84	2.4	0.192
10/0.4	2,500	6	0.76	4.3	0.172

Table E.2: Transformer electrical parameters

Technical University of Denmark
Department of Wind Energy
Frederiksborgvej 339
4000 Roskilde
Denmark

vindenergi.dtu.dk